

Climate4you update August 2024



1

Summary of observations until August 2024:

1: Observed average annual global air temperature change since 1979 (46 years) is $+0.0156^{\circ}\text{C}$ (UAH). If unchanged, additional average global air temperature increase by year 2100 will be about $+1.175^{\circ}\text{C}$.

2: Tide gauges along coasts indicate a typical global sea level increase of about 1-2 mm/yr. Coastal sea level change rate last 100 year has essentially been stable, but with periodic variations. If unchanged, global sea level at coasts will typically increase 8-16 cm by year 2100, although many locations in regions affected by glaciation 20,000 years ago, will experience a relative sea level drop.

3: Since 2004 the global oceans above 1900 m depth on average have warmed about 0.037°C . The maximum warming (about 0.2°C , 0-100 m depth) mainly affects oceans near Equator, where the incoming solar radiation is at maximum.

4: Sources and sinks for CO_2 are many. However, changes in atmospheric CO_2 follow changes in global air temperature, and changes in global air temperature follow changes in ocean surface temperature.

5: There was no perceptible effect on atmospheric CO_2 due to the 2020-21 COVID-related drop in GHG emissions, underlining the fact that natural sinks and sources for atmospheric CO_2 far outweigh human contributions. Therefore, any future reductions in the use of fossil fuels are unlikely to have any significant effect on the amount of atmospheric CO_2 .

Contents:

Page 3:	August 2024 global surface air temperature overview
Page 4:	August 2024 global surface air temperature overview versus August last 10 years
Page 5:	August 2024 global surface air temperature compared to August 2023
Page 6:	Temperature quality class 1: Lower troposphere temperature from satellites
Page 7:	Temperature quality class 2: HadCRUT global surface air temperature
Page 8:	Temperature quality class 3: GISS and NCDC global surface air temperature
Page 11:	Comparing global surface air temperature and satellite-based temperature
Page 12:	Global air temperature linear trends
Page 13:	Global temperatures: All in one, Quality Class 1, 2 and 3
Page 15:	Global sea surface temperature
Page 18:	Ocean temperature in uppermost 100 m
Page 20:	Pacific Decadal Oscillation (PDO)
Page 21:	North Atlantic heat content uppermost 700 m
Page 22:	North Atlantic temperatures 0-800 m depth along 59N, 30-0W
Page 23:	Global ocean temperature 0-1900 m depth summary
Page 24:	Global ocean net temperature change since 2004 at different depths
Page 25:	La Niña and El Niño episodes, Oceanic Niño Index
Page 26:	Zonal lower troposphere temperatures from satellites
Page 27:	Arctic and Antarctic lower troposphere temperatures from satellites
Page 28:	Arctic and Antarctic surface air temperatures
Page 31:	Long Arctic annual surface air temperature series
Page 32:	Long Antarctic annual surface air temperature series
Page 33:	Temperature over land versus over oceans
Page 34:	Troposphere and stratosphere temperatures from satellites
Page 35:	Sea ice; Arctic and Antarctic
Page 39:	Sea level in general
Page 40:	Global sea level from satellite altimetry
Page 41:	Global sea level from tide gauges (extended Holgate-9)
Page 42:	This month's selected sea level station (tide gauge): <i>Nauru, western Pacific Ocean</i>
Page 44:	Snow cover; Northern Hemisphere weekly and seasonal
Page 46:	Greenland Ice Sheet net surface mass balance
Page 47:	Atmospheric relative and specific humidity
Page 49:	Atmospheric CO ₂
Page 50:	Relation between annual change of atm. CO ₂ and La Niña and El Niño episodes
Page 51:	Phase relation between atmospheric CO ₂ and global temperature
Page 52:	Global air temperature and atmospheric CO ₂
Page 56:	Latest 20-year QC1 global monthly air temperature change
Page 57:	Sunspot activity and QC1 average satellite global air temperature
Page 57:	Sunspot activity and average neutron counts
Page 59:	Sunspot activity, ONI, and change rates of atmospheric CO ₂ and specific humidity
Page 60:	Monthly lower troposphere temperature and global cloud cover
Page 61:	Climate and history: 120-114 BC: The Cimbrian flood and the Cimbrian war 113-101 BC

August 2024 global surface air temperature overview

General: This newsletter contains graphs and diagrams showing a selection of key meteorological variables, updated to the most recent past month, if possible. All temperatures are given in degrees Celsius.

Traditionally, a 30-year reference period is often used by various meteorological institutions for comparison purposes and are supposed to be updated through the end of each decade ending in zero (e.g., 1951-1980, 1961-1990, 1971-2000, etc.). The concept of a normal climate goes back to the first part of the 20th century. At that time, lasting to about 1960, it was generally believed that for all practical purpose's climate could be considered constant, no matter how obvious year-to-year fluctuations might have been. On this basis meteorologist decided to operate with an average or normal climate, defined by a 30-year period, called the normal period, assuming that it was of sufficient length to iron out all intervening variations.

3

In fact, using a 30-yr 'normal' period is rather unfortunate, as observations clearly demonstrate that various global climate parameters (see, e.g., page 20) are influenced by periodic changes of 50-70 years duration. The frequently used 30-yr reference period is roughly half this time interval and is therefore highly unsuited as reference period. In the maps on page 4, showing the geographical pattern of surface air temperature anomalies, the last previous 10 years are therefore used as reference period. This decadal approach corresponds well to the typical memory horizon for many people and is also adopted as reference period by other institutions, e.g., the Danish Meteorological Institute (DMI).

In many diagrams shown in this newsletter the thin line represents the monthly global average value, and the thick line indicate a simple running 37-month average, nearly corresponding to a three-year average. The year 1979 has been chosen as starting point in many diagrams, as this approximately corresponds to both the beginning of satellite observations and the onset of the late 20th century warming period. However, most of the data series

have a longer record length, which may be inspected in greater detail on www.climate4you.com.

August 2024 surface air temperature

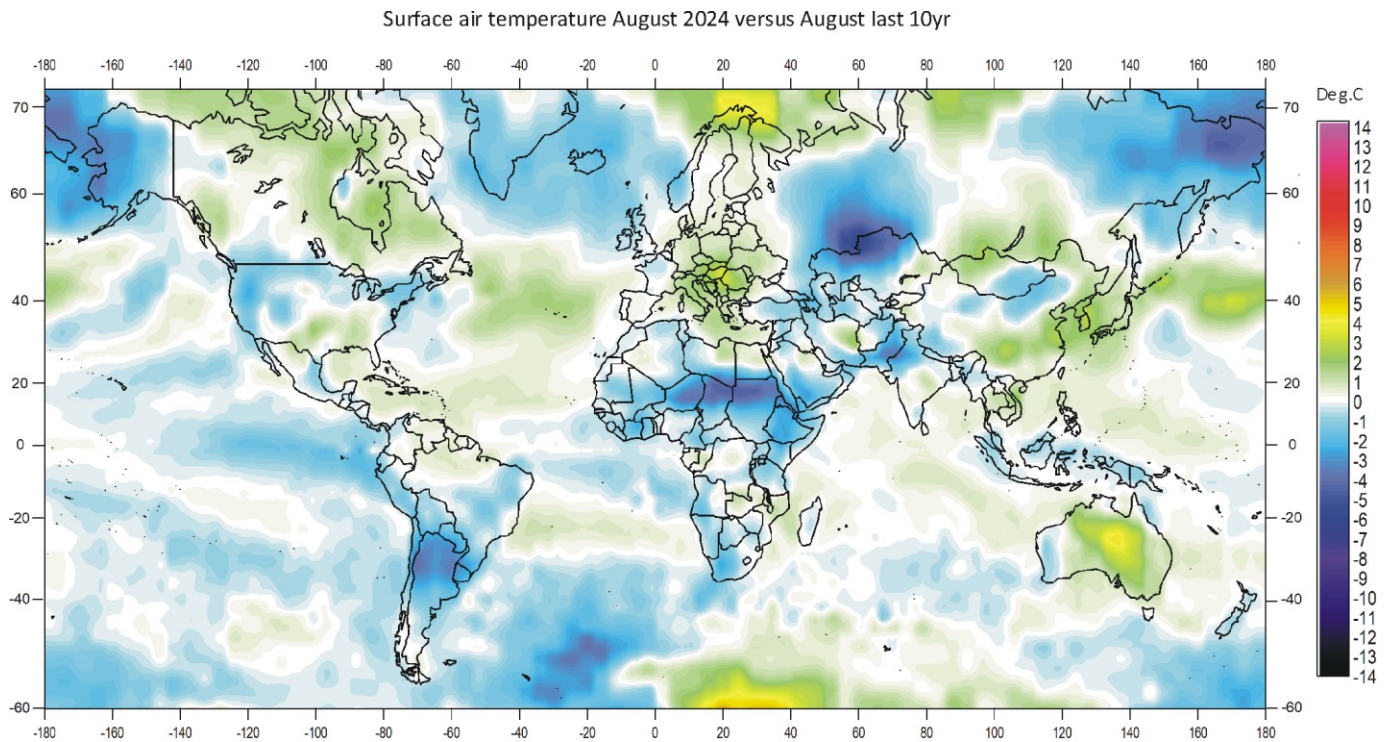
General: For August 2024, the GISS data portal provided AIRS interpolated surface air data, based on satellite observations (p.4-5). According to the GISS and NCDC records, the August global temperature anomaly was slightly higher than the July anomaly. The UAH and RSS lower troposphere satellite series show the August temperature anomaly near the July anomaly. The AIRS v6 August global average temperature anomaly compared to the average for the last 10 years shows little change (diagrams p.4-5) but is slightly cooler than August last year. All the above air temperature records are displaying high August 2024 anomalies, mainly due to Antarctic winter temperature conditions (see below).

The Northern Hemisphere surface temperature anomaly pattern (p.4) was characterised by regional contrasts, mainly controlled by the dominant jet stream position. Especially SE and N Europe were warm relative to the average for the last 10 years. In contrast, parts of S Russia, E Siberia, Alaska and Greenland were relatively cold. Ocean wise, much of the North Atlantic was relatively warm south of 50°N, while the Greenland and Norwegian Seas were cold. The Pacific Ocean was relatively cold, except for a region centred around 40°N. PDO (p.20) remains negative. Arctic Ocean surface air temperatures were near or below the 10-yr average.

Near the Equator temperatures were generally near the 10-year average. Apparently, ocean heat released during the previous warm El Niño episode is now slowly dissipating.

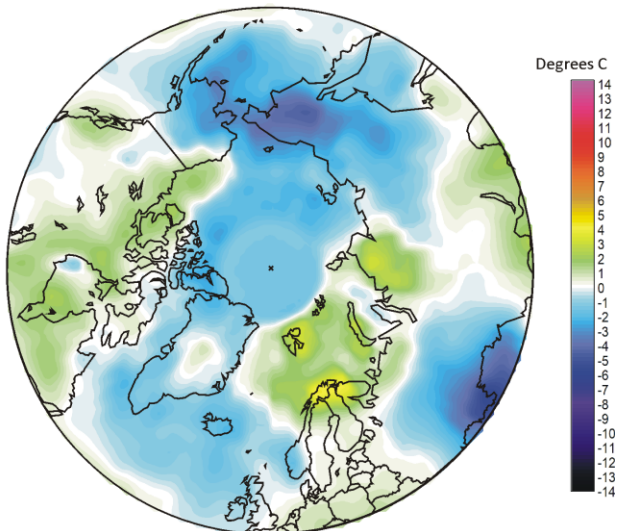
Southern Hemisphere temperatures were near or below the 10-yr average for June. Central Australia was relatively warm, while extensive regions in South America and South Africa were relatively cold. In contrast, most of Antarctic had temperatures much above the 10-yr average. In fact, the still high August 2024 global surface air temperature anomaly is mainly derived from warm conditions in Antarctic (now in mid-winter season, see also diagram p.27).

August 2024 global surface air temperature overview versus average August last 10 years

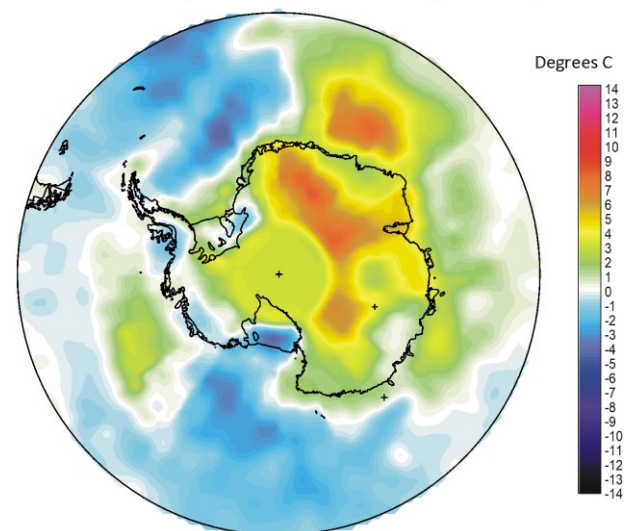


4

Surface air temperature August 2024 versus August last 10 yr

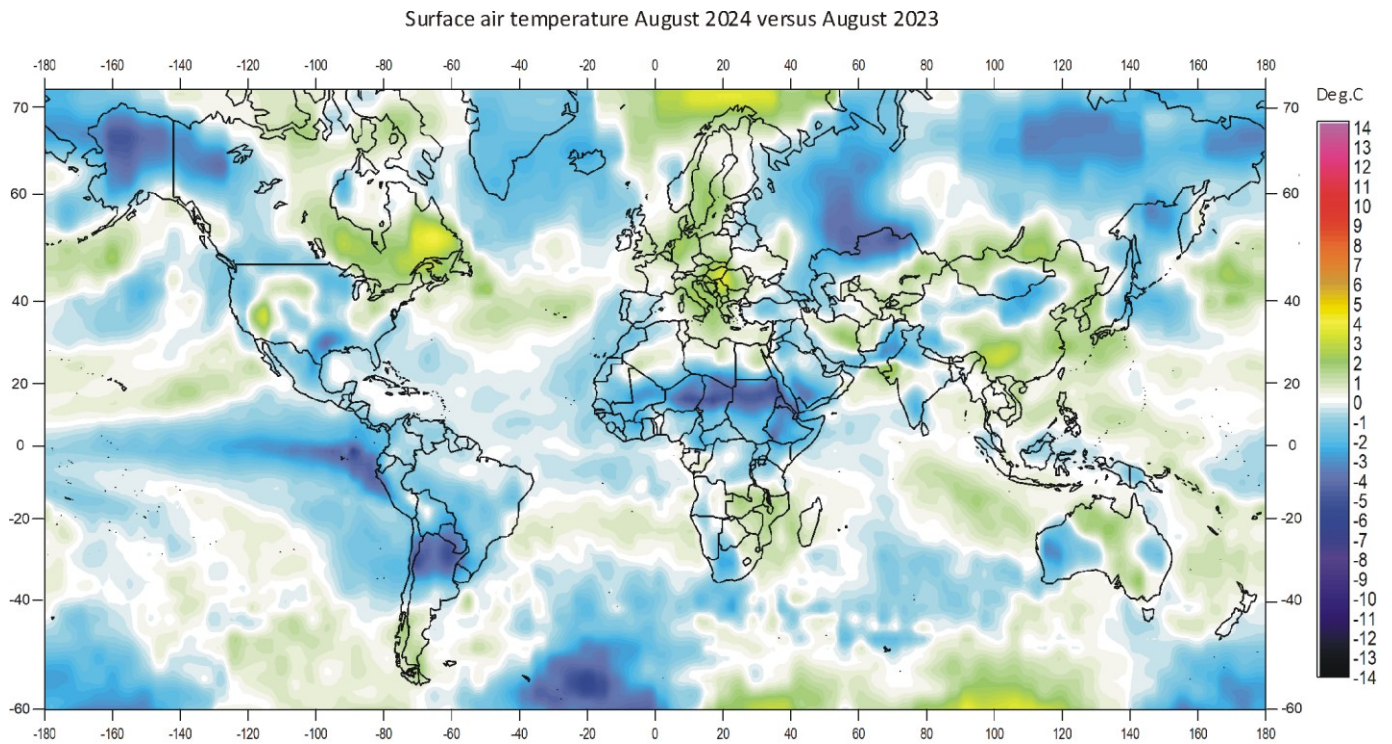


Surface air temperature August 2024 versus August last 10 yr



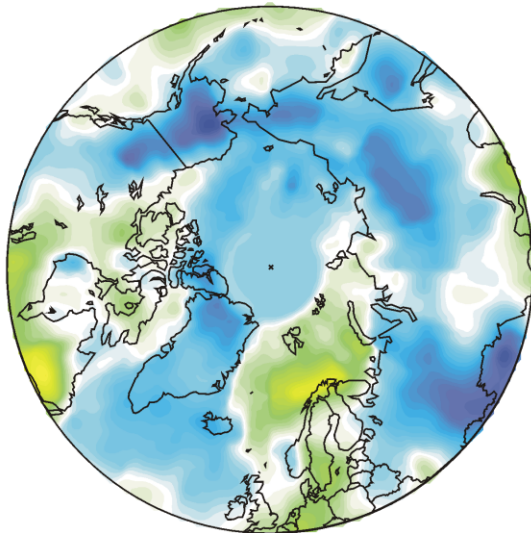
August 2024 surface air temperature compared to the average of August over the last 10 years. Green-yellow-red colours indicate areas with higher temperature than the 10-year average, while blue colours indicate lower than average temperatures. Data source: Remote Sensed Surface Temperature Anomaly, AIRS/Aqua L3 Monthly Standard Physical Retrieval 1-degree x 1-degree V006 (<https://airs.jpl.nasa.gov/>), obtained from the GISS data portal (https://data.giss.nasa.gov/gistemp/maps/index_v4.html).

August 2024 global surface air temperature compared to August 2023

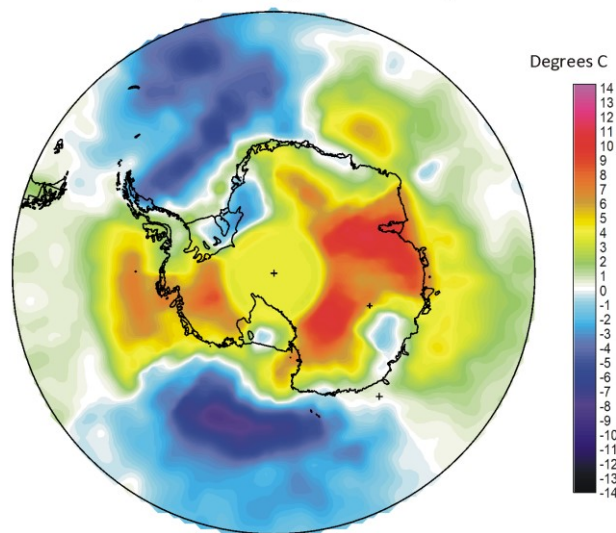


5

Surface air temperature August 2024 versus August 2023



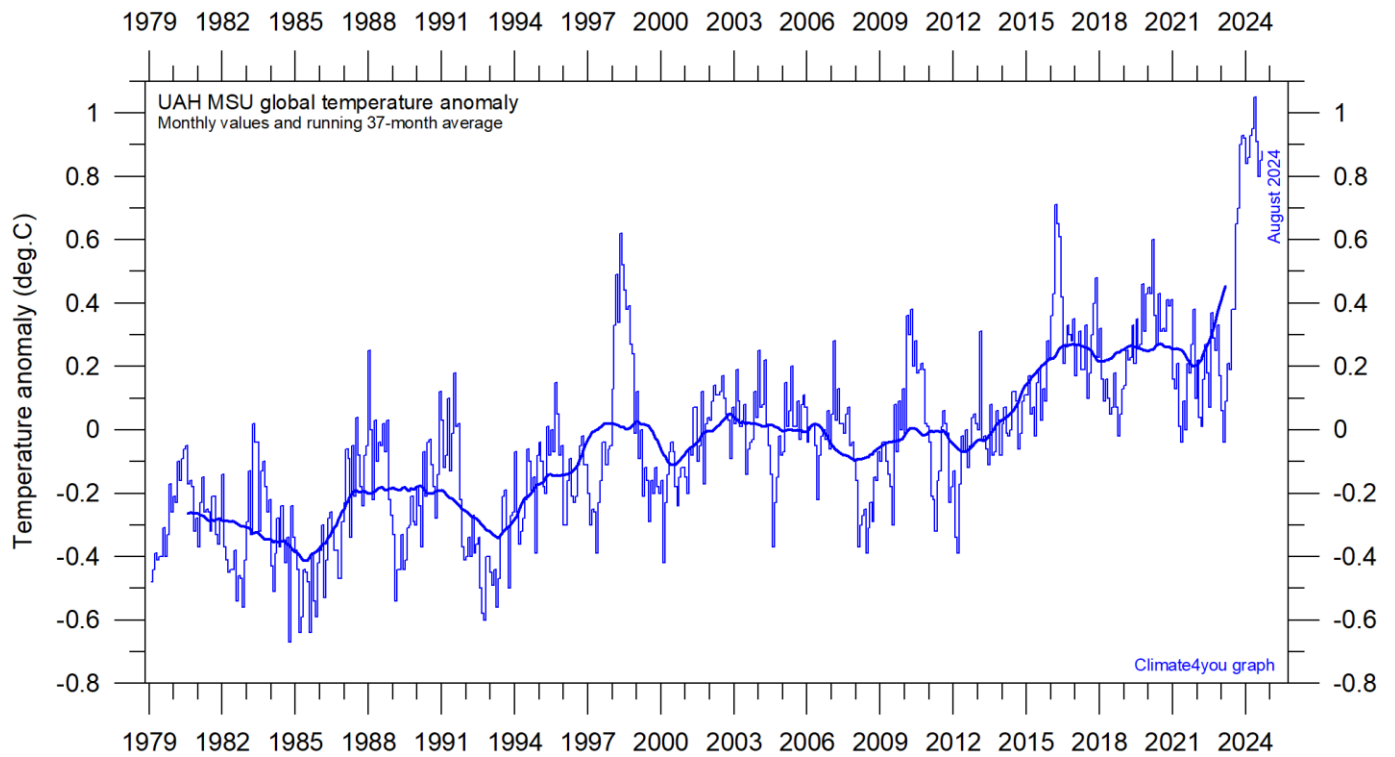
Surface air temperature August 2024 versus August 2023



August 2024 surface air temperature compared to August 2023. Green-yellow-red colours indicate regions where the present month was warmer than last year, while blue colours indicate regions where the present month was cooler than last year. Variations in monthly temperature from one year to the next has no tangible climatic importance but may nevertheless be interesting to study. Data source: Remote Sensed Surface Temperature Anomaly, AIRS/Aqua L3 Monthly Standard Physical Retrieval 1-degree x 1-degree V006 (<https://airs.jpl.nasa.gov/>), obtained from the GISS data portal (https://data.giss.nasa.gov/gistemp/maps/index_v4.html).

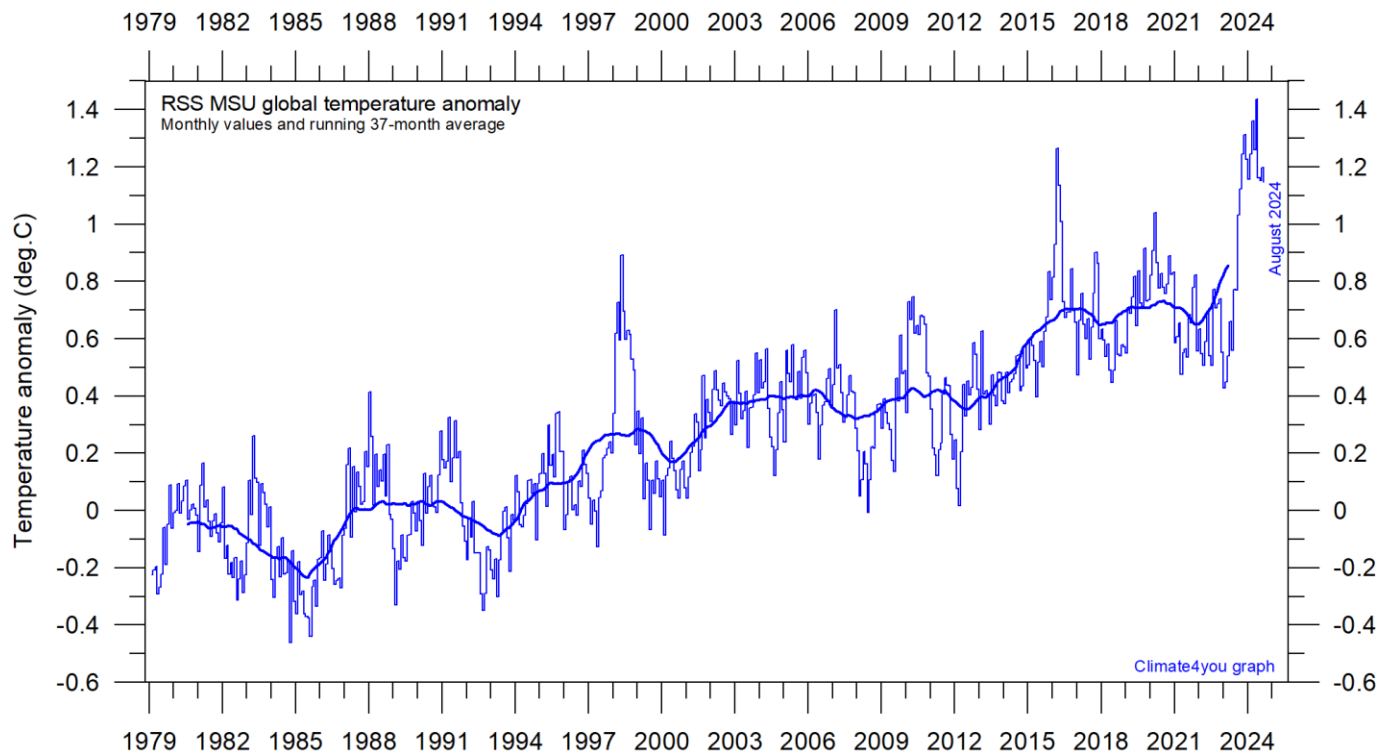
Temperature quality class 1: Lower troposphere temperature from satellites, updated to August 2024

(see page 9 for definition of classes)



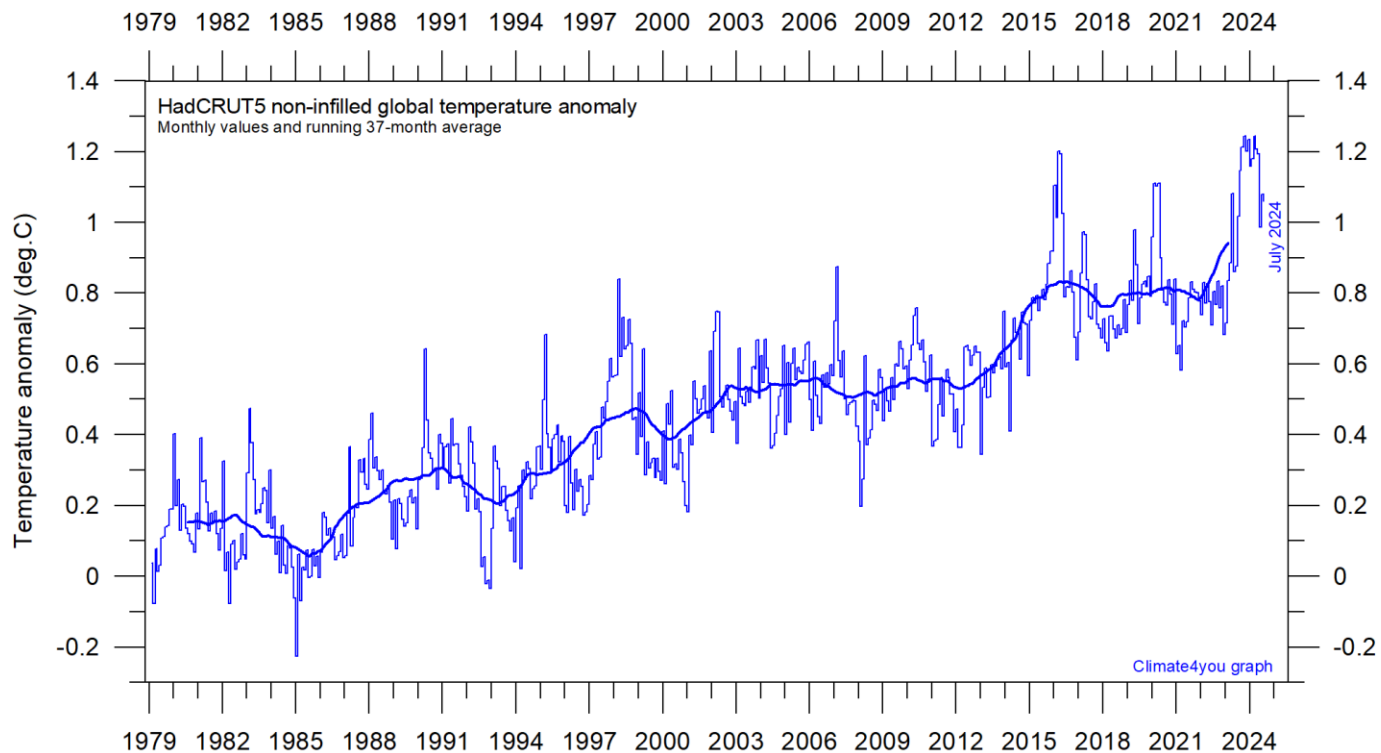
Global monthly average lower troposphere temperature (thin line) since 1979 according to [University of Alabama](#) at Huntsville, USA. The thick line is the simple running 37-month average. Reference period 1991-2020.

6



Global monthly average lower troposphere temperature (thin line) since 1979 according to according to [Remote Sensing Systems](#) (RSS), USA. The thick line is the simple running 37-month average.

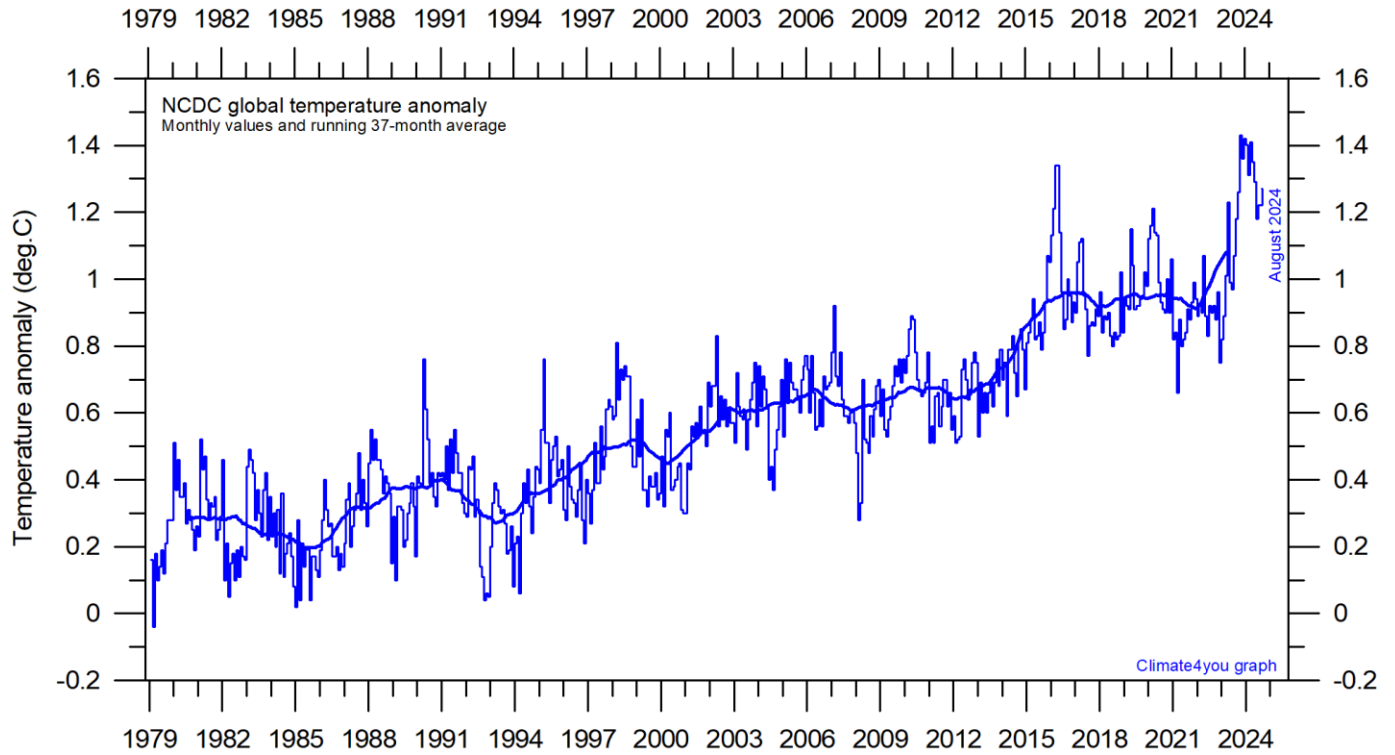
Temperature quality class 2: HadCRUT global surface air temperature, updated to July 2024



7

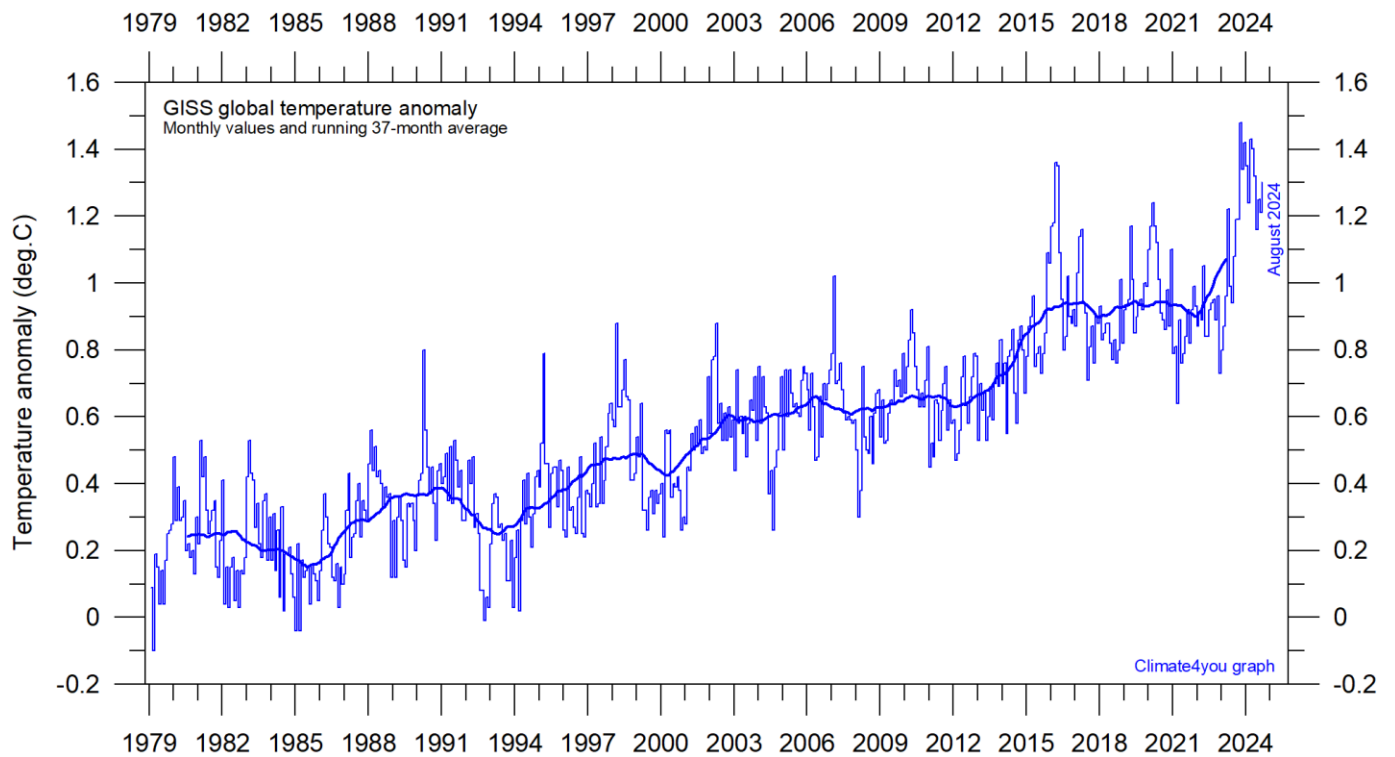
Global monthly average surface air temperature (thin line) since 1979 according to the Hadley Centre for Climate Prediction and Research and the University of East Anglia's [Climatic Research Unit \(CRU\)](#), UK. The thick line is the simple running 37-month average.

Temperature quality class 3: GISS and NCDC global surface air temperature, updated to August 2024



Global monthly average surface air temperature since 1979 according to according to the [National Climatic Data Center](#) (NCDC), USA. The thick line is the simple running 37-month average.

8



Global monthly average surface air temperature (thin line) since 1979 according to according to the [Goddard Institute for Space Studies](#) (GISS), at Columbia University, New York City, USA, using ERSST_v4 ocean surface temperatures. The thick line is the simple running 37-month average.

A note on data record stability and -quality:

The temperature diagrams shown above all have 1979 as starting year. This roughly marks the beginning of the recent episode of global warming, after termination of the previous episode of global cooling from about 1940. In addition, the year 1979 also represents the starting date for the satellite-based global temperature estimates (UAH and RSS). For the three surface air temperature records (HadCRUT, NCDC and GISS), they begin much earlier (in 1850 and 1880, respectively), as can be inspected on www.climate4you.com.

For all three surface air temperature records, but especially NCDC and GISS, administrative changes to anomaly values are quite often introduced, even affecting observations many years back in time. Some changes from the recent past may be due to the delayed addition of new station data or change of station location, while others probably have their origin in changes of the technique implemented to calculate average values from the raw data. It is clearly impossible to evaluate the validity of such administrative changes for the outside user of these records; it is only possible to note that such changes quite often are introduced (see example diagram next page).

In addition, the three surface records represent a blend of sea surface data collected by moving ships or by other means, plus data from land stations of partly unknown quality and unknown degree of representativeness for their region. Many of the land stations also has been moved geographically during their period of operation, instrumentation have been changed, and they are influenced by changes in their near surroundings (vegetation, buildings, etc.). The surface network is inherently heterogeneous (dense over continents but sparse over oceans) and probably contaminated by urbanization surrounding many measurement sites.

The satellite temperature records also have their problems, but these are generally of a more technical nature and probably therefore better correctable. In

addition, the temperature sampling by satellites is more regular and complete on a global basis than that represented by the surface records. It is also important that the sensors on satellites measure temperature directly by microwave radiance (thereby unobstructed by clouds), while most modern surface temperature measurements are indirect, using electronic resistance.

Everybody interested in climate science should gratefully acknowledge the big efforts put into maintaining the different temperature databases referred to in the present newsletter. At the same time, however, it is also important to realise that all temperature records cannot be of equal scientific quality. The simple fact that they to some degree differ shows that they cannot all be correct.

On this background, and for practical reasons, Climate4you therefore operates with three quality classes (1-3) for global temperature records, with 1 representing the highest quality level:

Quality class 1: The satellite records (UAH and RSS).

Quality class 2: The HadCRUT surface record.

Quality class 3: The NCDC and GISS surface records.

The main reason for discriminating between the three surface records is the following:

While both NCDC and GISS often experience quite large administrative changes (see example on p.10), and therefore essentially must be considered as unstable records, the changes introduced to HadCRUT are fewer and smaller. For obvious reasons, as the past does not change, any record undergoing continuing changes cannot describe the past correctly all the time. Frequent and large corrections in a database unavoidably signal a fundamental uncertainty about what is likely to represent the correct values.

You can find more on the issue of lack of temporal stability on www.climate4you.com (go to: *Global Temperature*, and then proceed to *Temporal Stability*).

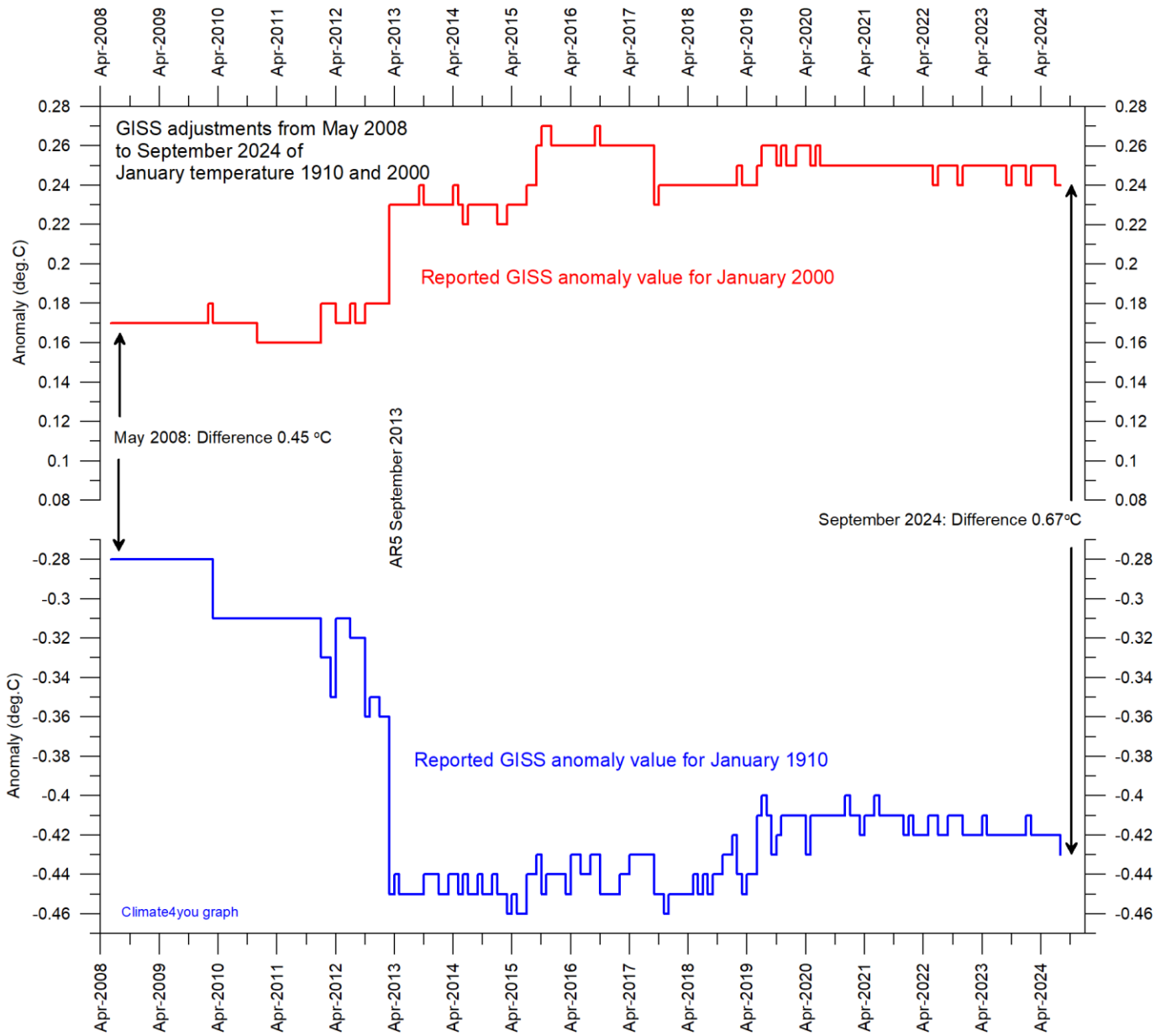
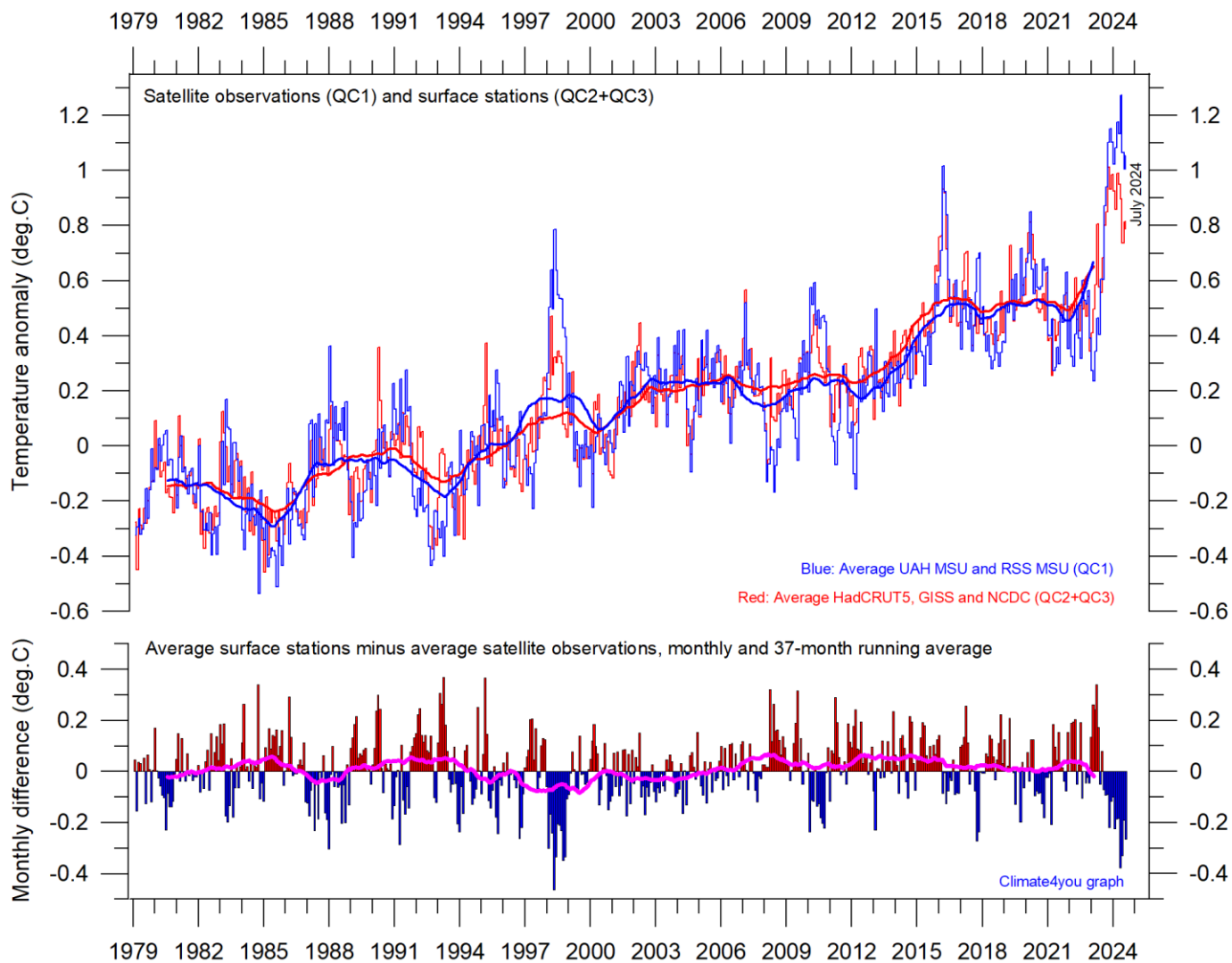


Diagram showing the monthly adjustments made since May 2008 by the [Goddard Institute for Space Studies](#) (GISS), USA, as recorded by published anomaly values for the two months January 1910 and January 2000. AR5 indicates timing of publication of IPCC report AR5 Climate Change 2013: The Physical Science Basis.

The administrative upsurge of the temperature increase from January 1915 to January 2000 has grown from 0.45 (reported May 2008) to 0.66°C (reported September 2024). This represents an about 49% administrative temperature increase over this

period, meaning that a significant part (about half) of the apparent global temperature increases from January 1910 to January 2000 (as reported by GISS) is caused by administrative changes of the original data since May 2008.

Comparing global surface air temperature and lower troposphere satellite temperatures; updated to July 2024



11

Plot showing the average of monthly global surface air temperature estimates (HadCRUT5, GISS and NCDC) and satellite-based temperature estimates (RSS MSU and UAH MSU). The thin lines indicate the monthly value, while the thick lines represent the simple running 37-month average, nearly corresponding to a running 3-yr average. The lower panel shows the monthly difference between average surface air temperature and satellite temperatures. As the base period differs for the different temperature estimates, they have all been normalised by comparing to the average value of 30 years from January 1979 to December 2008.

Global air temperature linear trends updated to July 2024

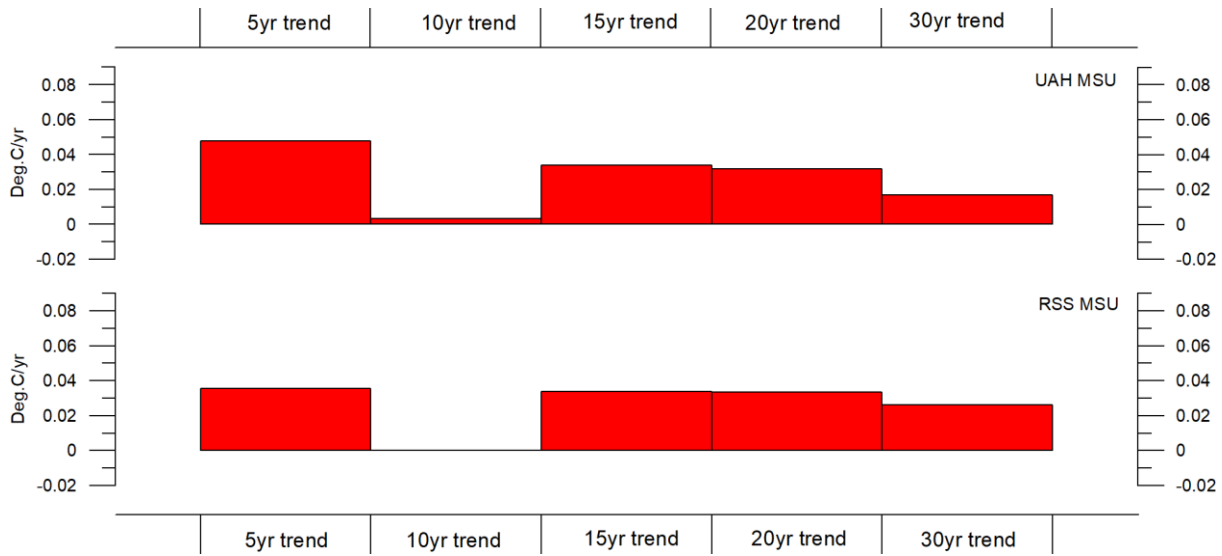


Diagram showing the latest 5, 10, 20 and 30-yr linear annual global temperature trend, calculated as the slope of the linear regression line through the data points, for two satellite-based temperature estimates (UAH MSU and RSS MSU).

12

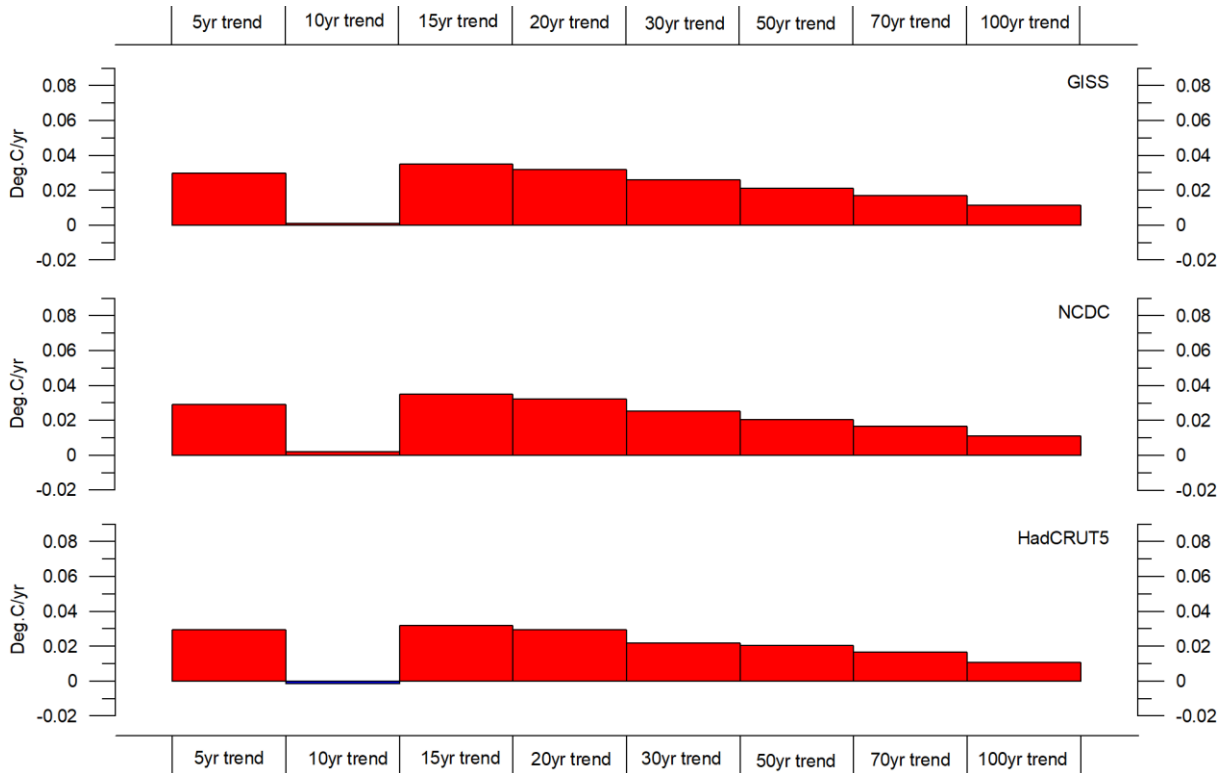
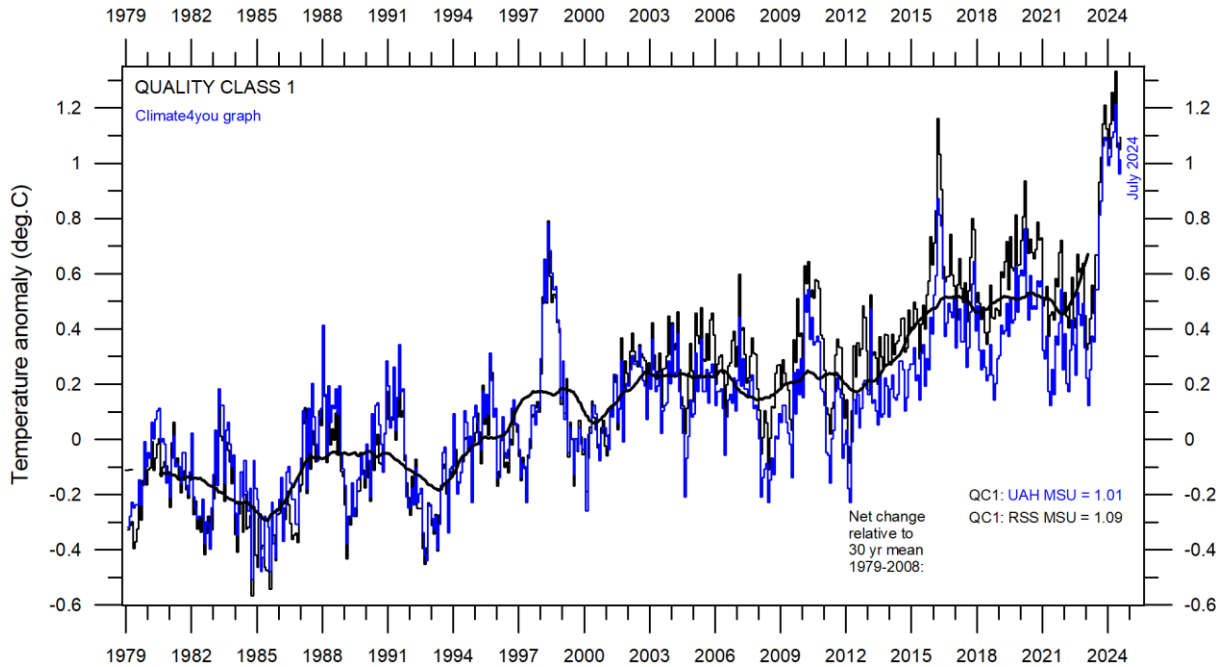


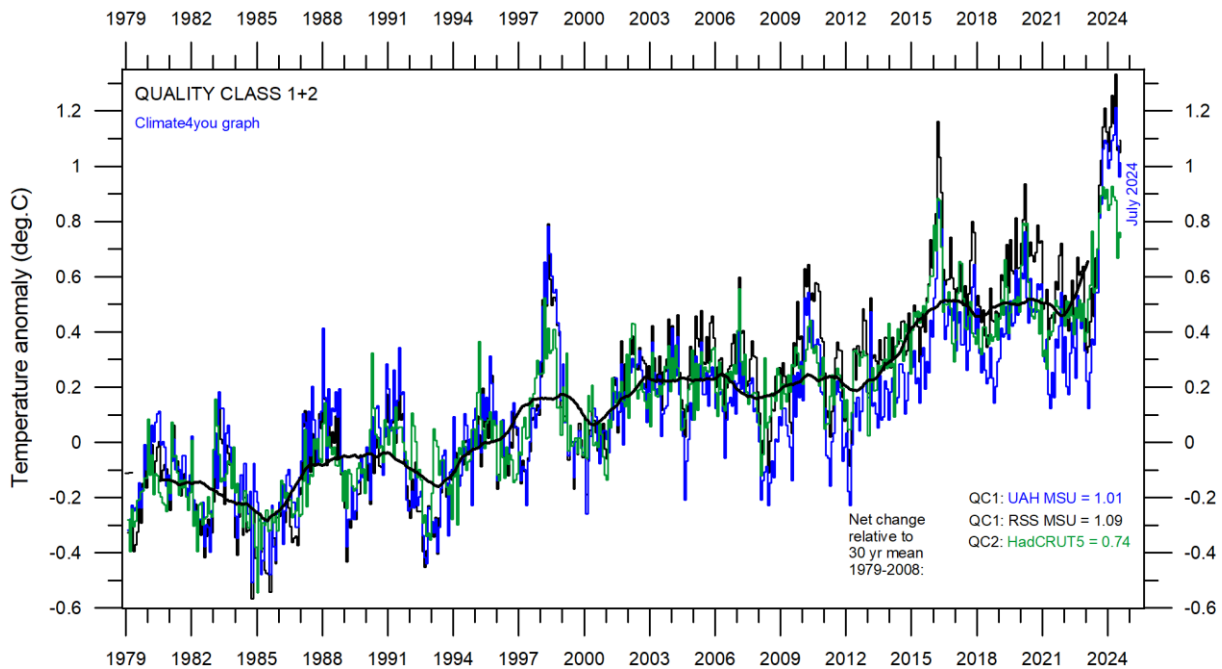
Diagram showing the latest 5, 10, 20, 30, 50, 70 and 100-year linear annual global temperature trend, calculated as the slope of the linear regression line through the data points, for three surface-based temperature estimates (GISS, NCDC and HadCRUT5).

All in one, Quality Class 1, 2 and 3; updated to July 2024

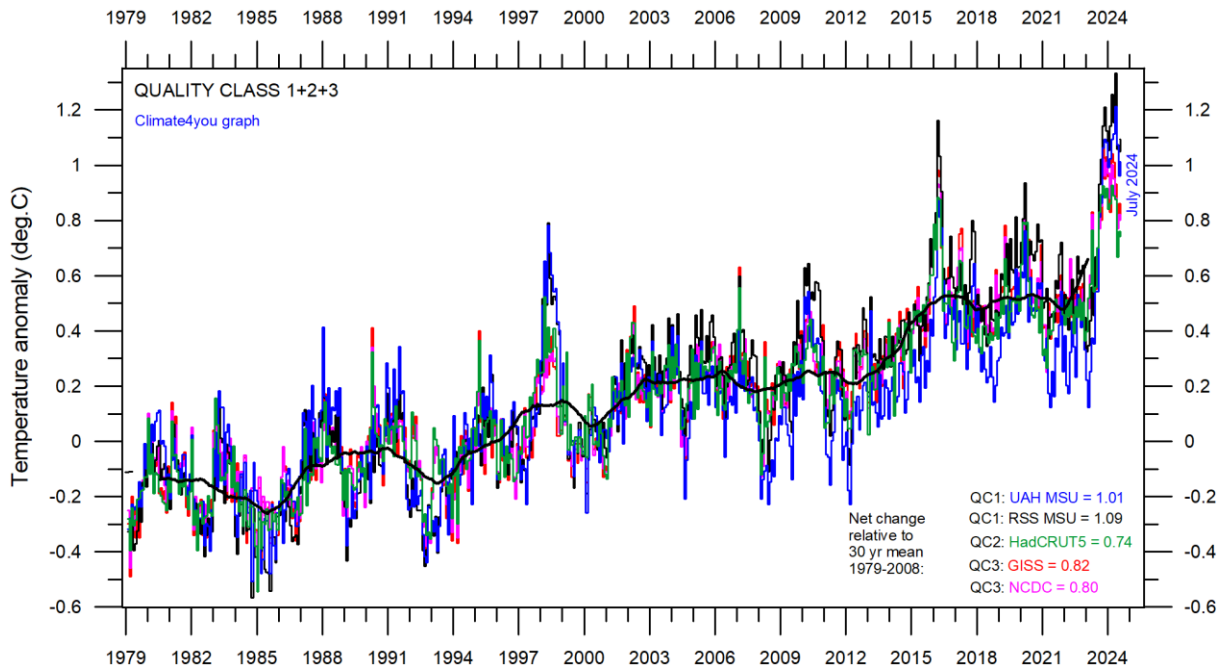


Superimposed plot of Quality Class 1 (UAH and RSS) global monthly temperature estimates. As the base period differs for the individual temperature estimates, they have all been normalised by comparing with the average value of the initial 120 months (30 years) from January 1979 to December 2008. The heavy black line represents the simple running 37 month (c. 3 year) mean of the average of both temperature records. The numbers shown in the lower right corner represent the temperature anomaly relative to the individual 1979-2008 averages.

13



Superimposed plot of Quality Class 1 and 2 (UAH, RSS and HadCRUT) global monthly temperature estimates. As the base period differs for the individual temperature estimates, they have all been normalised by comparing with the average value of the initial 120 months (30 years) from January 1979 to December 2008. The heavy black line represents the simple running 37 month (c. 3 year) mean of the average of all three temperature records. The numbers shown in the lower right corner represent the temperature anomaly relative to the individual 1979-2008 averages.



Superimposed plot of Quality Class 1, 2 and 3 global monthly temperature estimates (UAH, RSS, HadCRUT, GISS and NCDC). As the base period differs for the individual temperature estimates, they have all been normalised by comparing with the average value of the initial 120 months (30 years) from January 1979 to December 2008. The heavy black line represents the simple running 37 month (c. 3 year) mean of the average of all five temperature records. The numbers shown in the lower right corner represent the temperature anomaly relative to the individual 1979-2008 averages.

14 Please see reflections on page 9 relating to the above three quality classes.

Satellite- and surface-based temperature estimates are derived from different types of measurements and comparing them directly as in the above diagrams therefore may be somewhat ambiguous.

However, as both types of estimates often are discussed together in various news media, the above composite diagrams may nevertheless be of some interest.

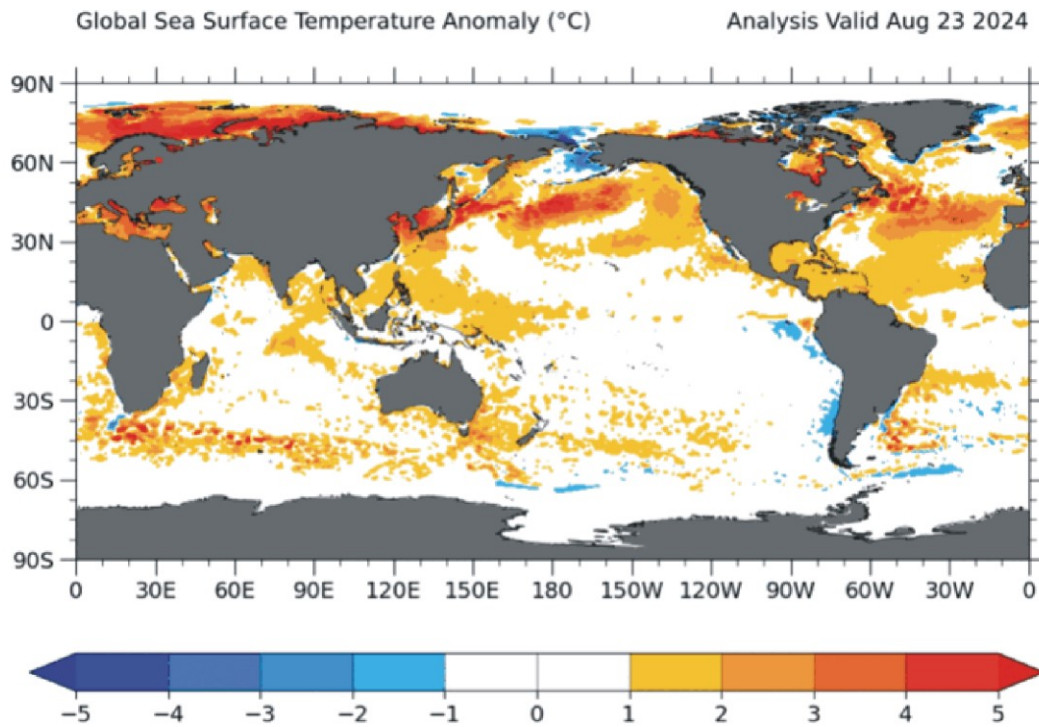
In fact, the different types of temperature estimates appear to agree as to the overall temperature variations on a 2-3-year scale, although on a shorter time scale there are often considerable differences between the individual records. However, since about 2003 the surface records used to be drifting towards higher temperatures than the combined satellite record, but this overall tendency was much removed by the major adjustment of the RSS satellite series in 2015 (see lower diagram on page 6).

The combined records (diagram above) suggest a modest global air temperature increase over the last 40 years, about 0.18°C per decade. It should be noted that the apparent temperature increases since about 2003 at least partly is the result of ongoing administrative adjustments (page 9-10). At the same time, none of the temperature records considered here indicates any overall temperature decrease during the last 20 years.

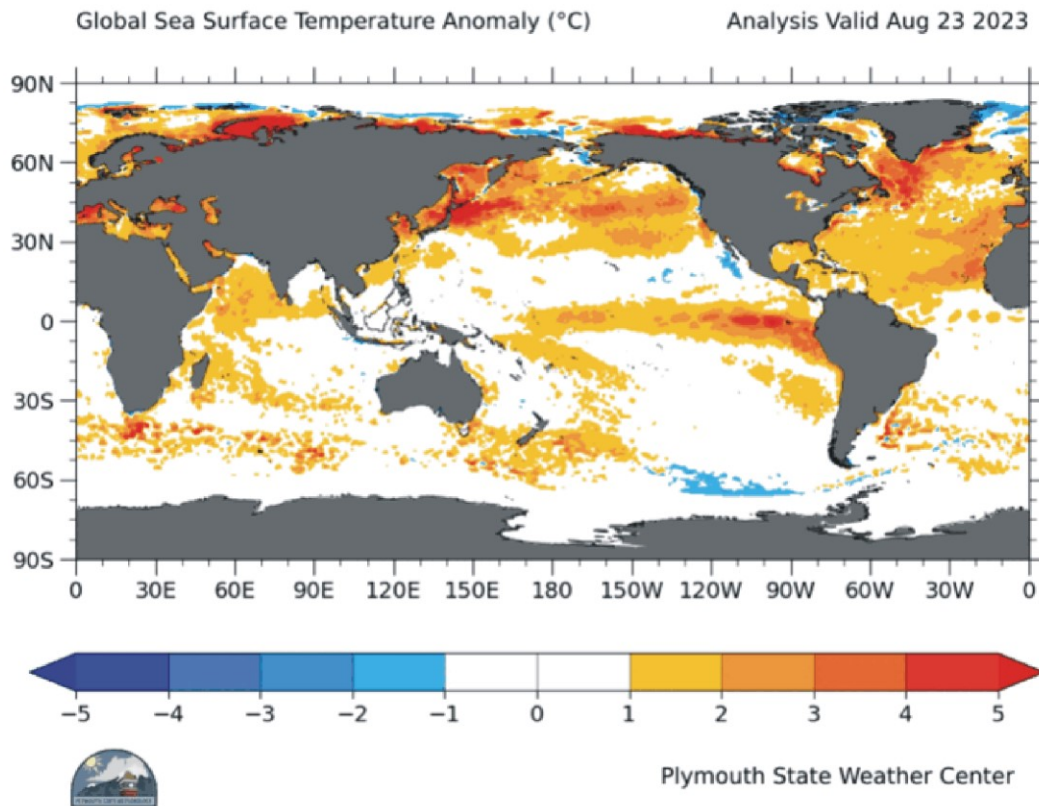
The present temperature development does not exclude the possibility that global temperatures may begin to increase significantly later. On the other hand, it also remains a possibility that Earth just now is passing an overall temperature peak, and that global temperatures may begin to decrease during the coming 5-10 years.

As always, time will show which of these possibilities is correct.

Global sea surface temperature, updated to August 2024



15



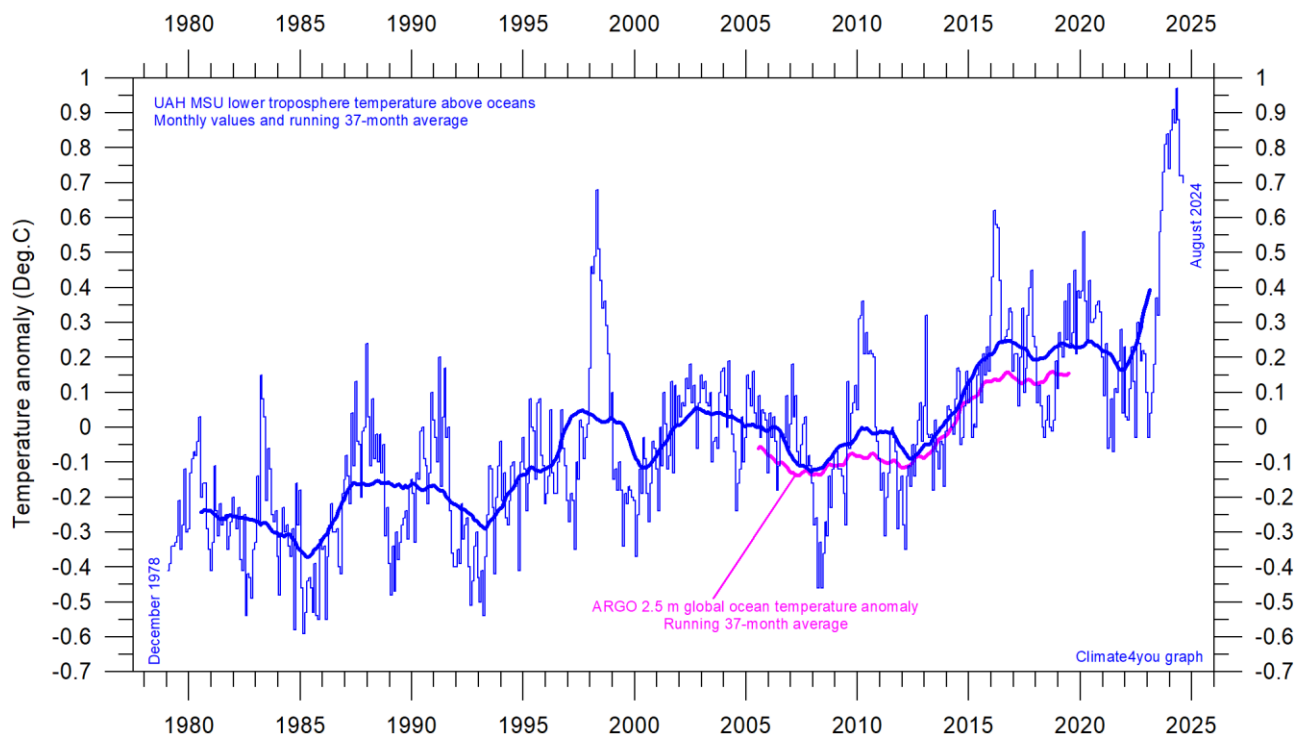
Sea surface temperature anomaly on 23 August 2024 (upper map) and 2023 (lower map). Map source: Plymouth State Weather Center. Reference period: 1977-1991.

Because of the large surface areas near Equator, the temperature of the surface water in these regions is especially important for the global atmospheric temperature (p. 6-8). In fact, 50% of planet Earth's surface area is located within 30°N and 30°S.

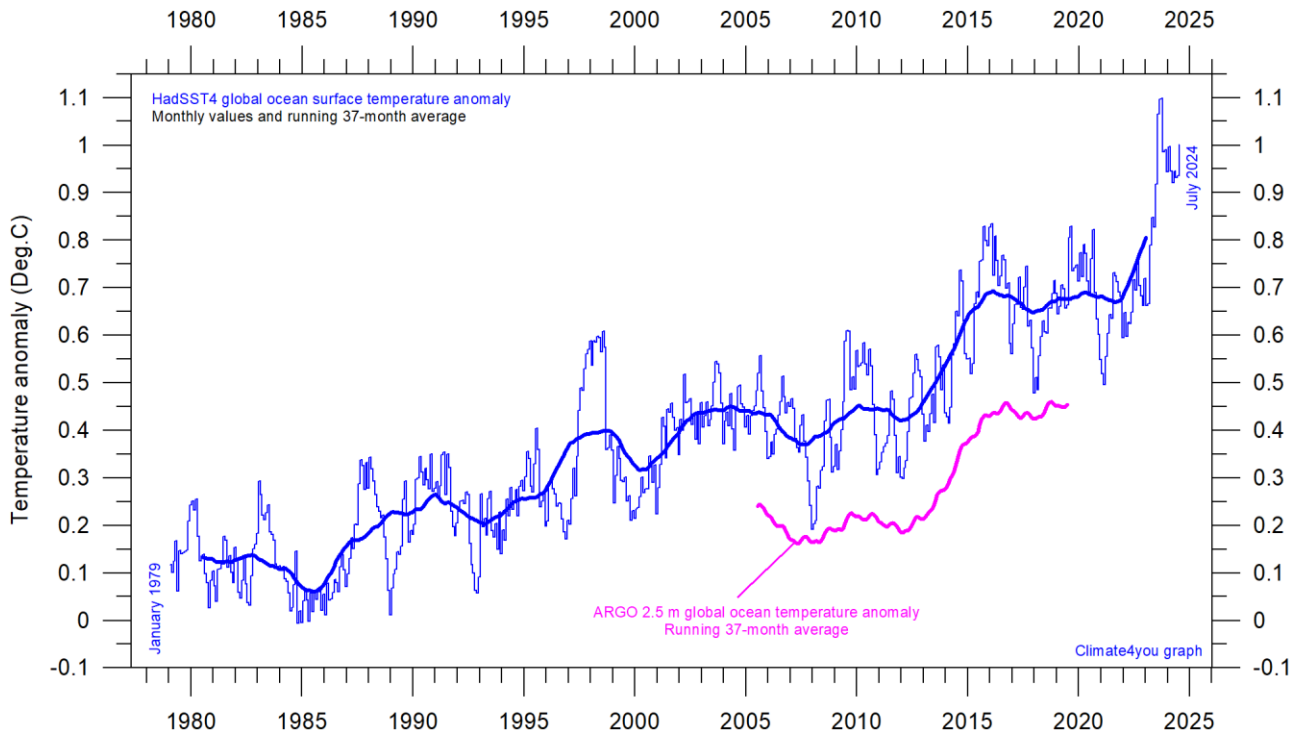
A mixture of relatively warm and cold water presently dominates much of the global ocean surface, but with notable variations from month to month. All such ocean surface temperature changes will be influencing global air temperatures in the months to come. A cold La Niña episode (Pacific Ocean) has recently ended and was followed by a warm (now ending) El Niño episode (maps p.15 and diagram p.25).

The significance of short-term cooling or warming reflected in air temperatures should never be overstated. Whenever Earth experiences cold La Niña or warm El Niño episodes major heat exchanges take place between the Pacific Ocean and the atmosphere above, sooner or later showing up in estimates of the global air temperature.

However, this does not necessarily reflect similar changes in the total heat content of the atmosphere-ocean system. In fact, global net changes can be small and such heat exchanges may mainly reflect redistribution of energy between ocean and atmosphere. What matters is the overall temperature development when seen over several years.

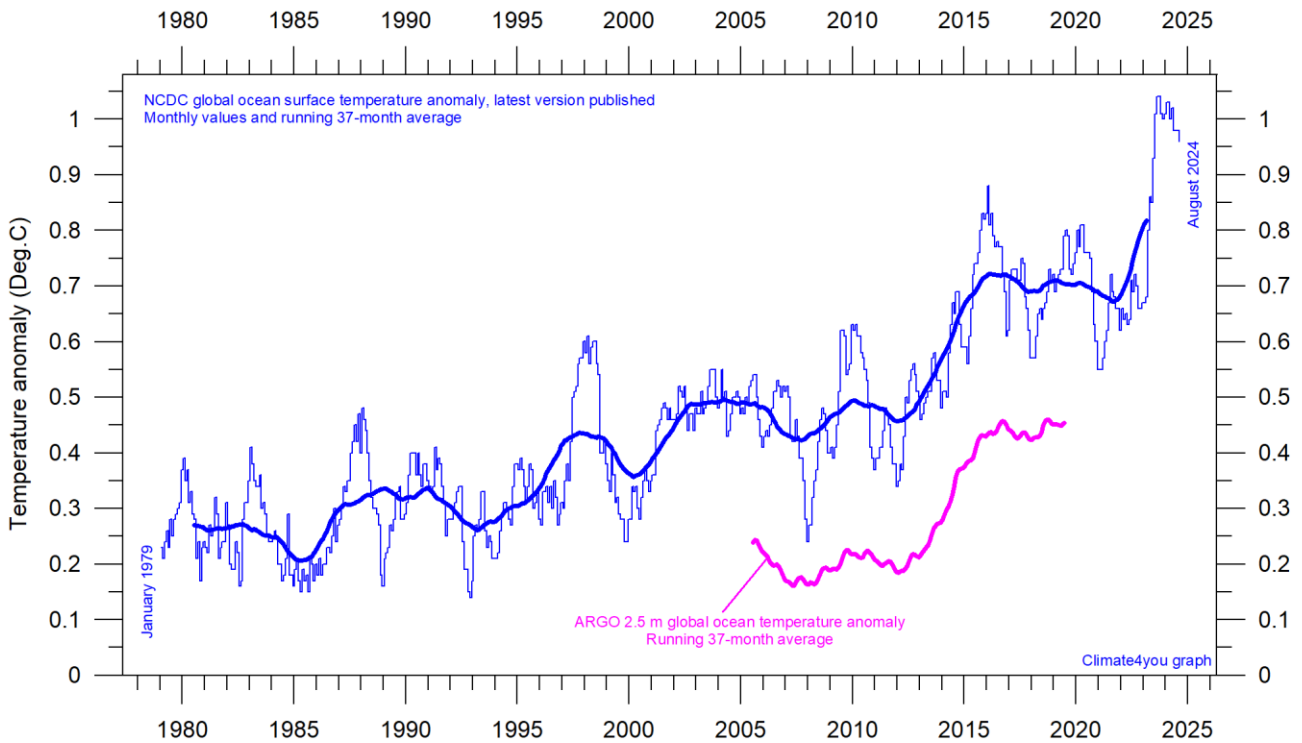


Global monthly average lower troposphere temperature over oceans (thin line) since 1979 according to [University of Alabama](#) at Huntsville, USA. The thick line is the simple running 37-month average. Insert: Argo global ocean temperature anomaly from floats, displaced vertically to make visual comparison easier. UAH reference period: 1991-2020.



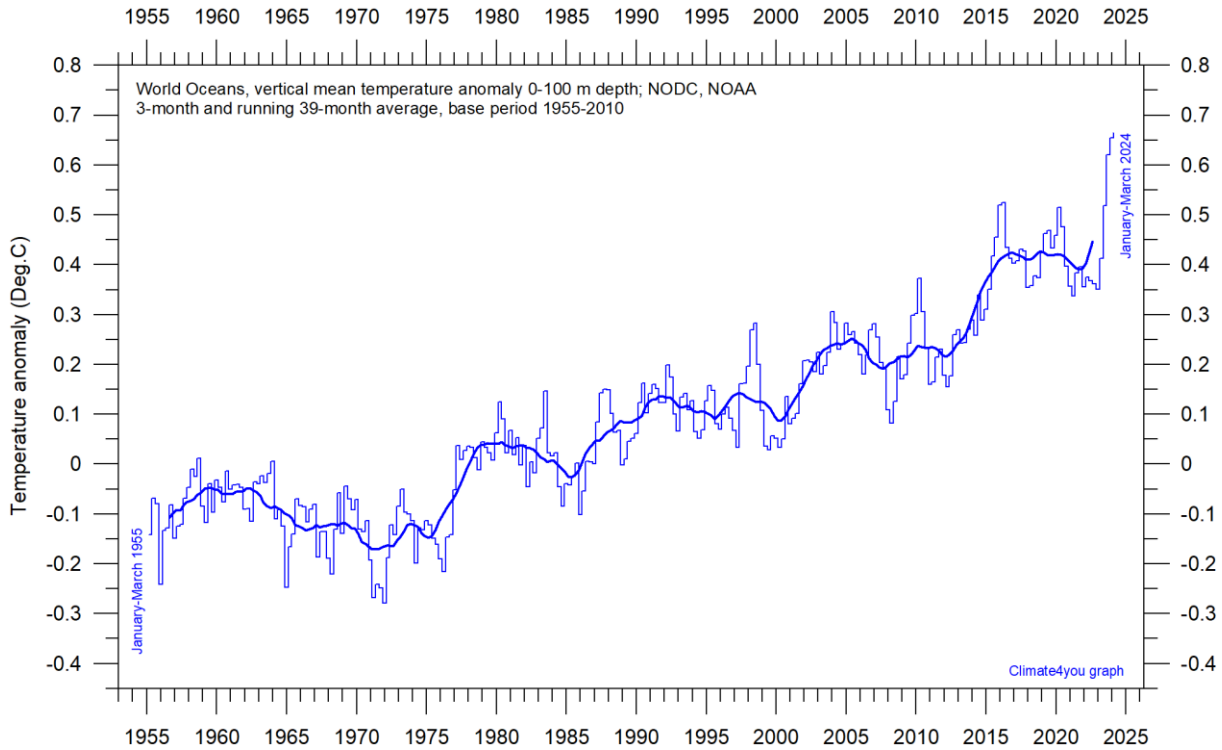
Global monthly average sea surface temperature since 1979 according to University of East Anglia's [Climatic Research Unit \(CRU\)](#), UK. Base period: 1961-1990. The thick line is the simple running 37-month average. Insert: Argo global ocean temperature anomaly from floats, displaced vertically to make visual comparison easier.

17



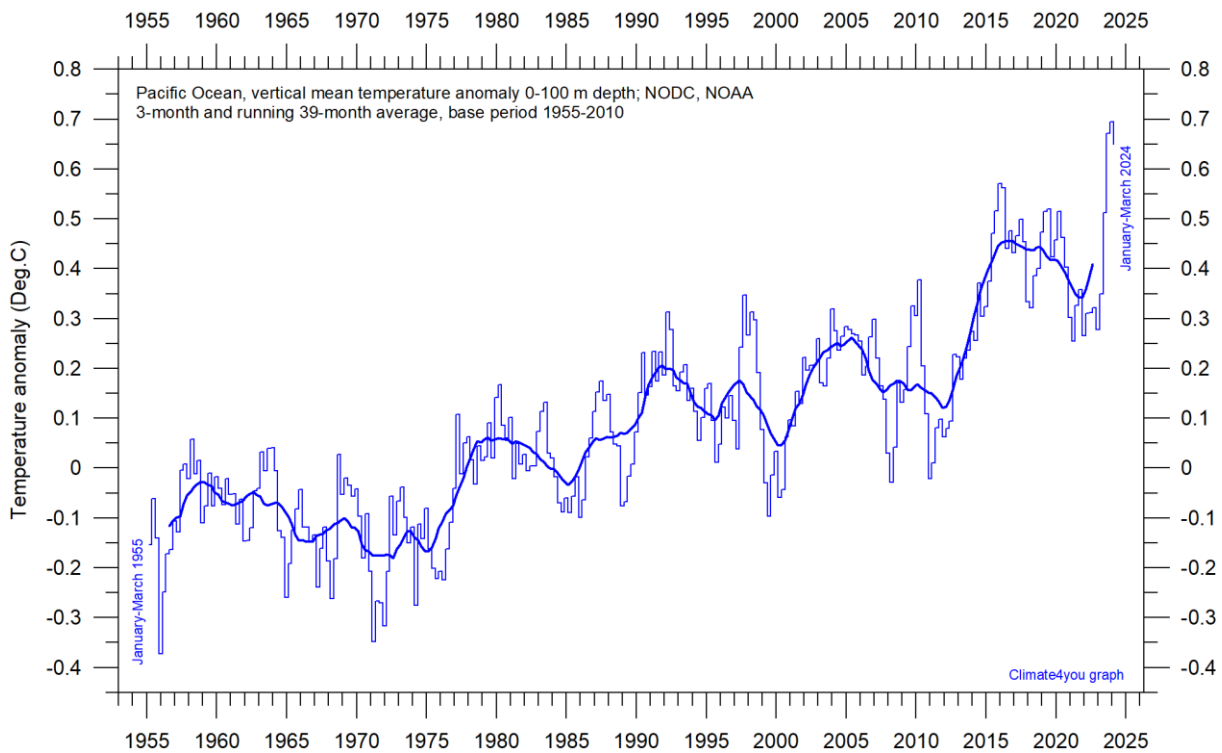
Global monthly average sea surface temperature since 1979 according to the [National Climatic Data Center \(NCDC\)](#), USA. Base period: 1901-2000. The thick line is the simple running 37-month average. Insert: Argo global ocean temperature anomaly from floats, displaced vertically to make visual comparison easier.

Ocean temperature in uppermost 100 m, updated to March 2024

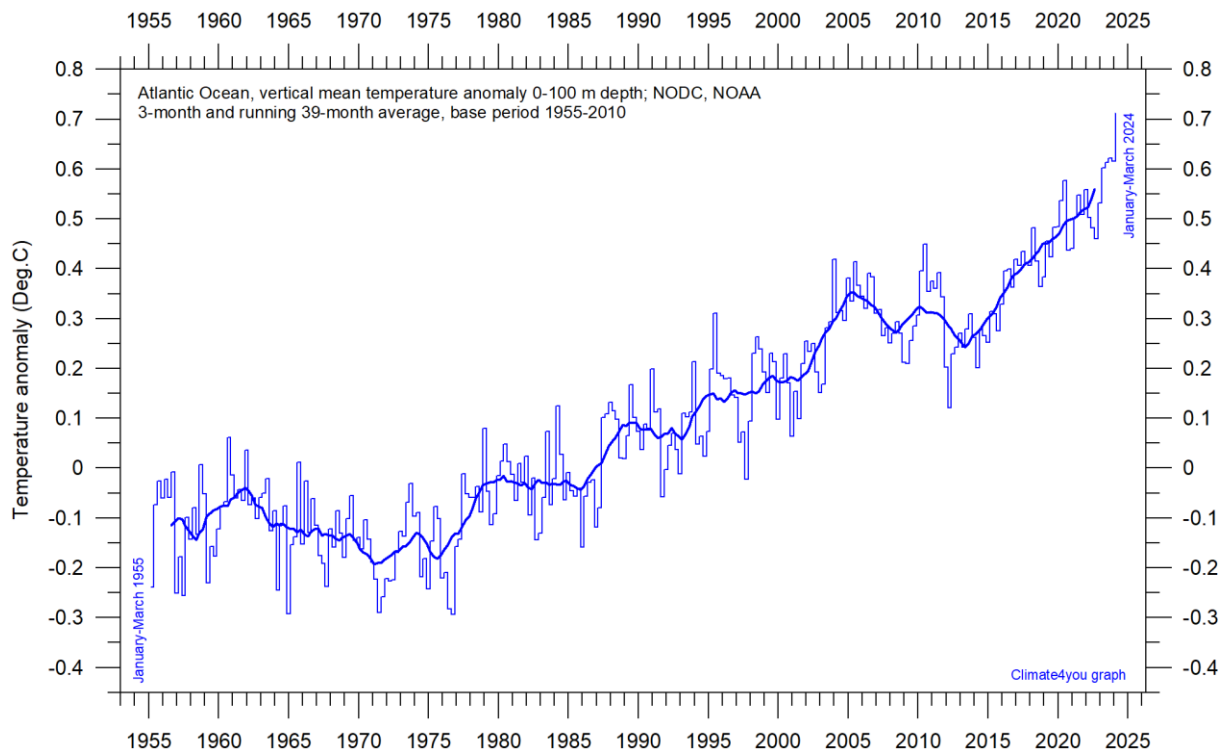


World Oceans vertical average temperature 0-100 m depth since 1955. The thin line indicates 3-month values, and the thick line represents the simple running 39-month (c. 3 year) average. Data source: [NOAA National Oceanographic Data Center \(NODC\)](#). Base period 1955-2010.

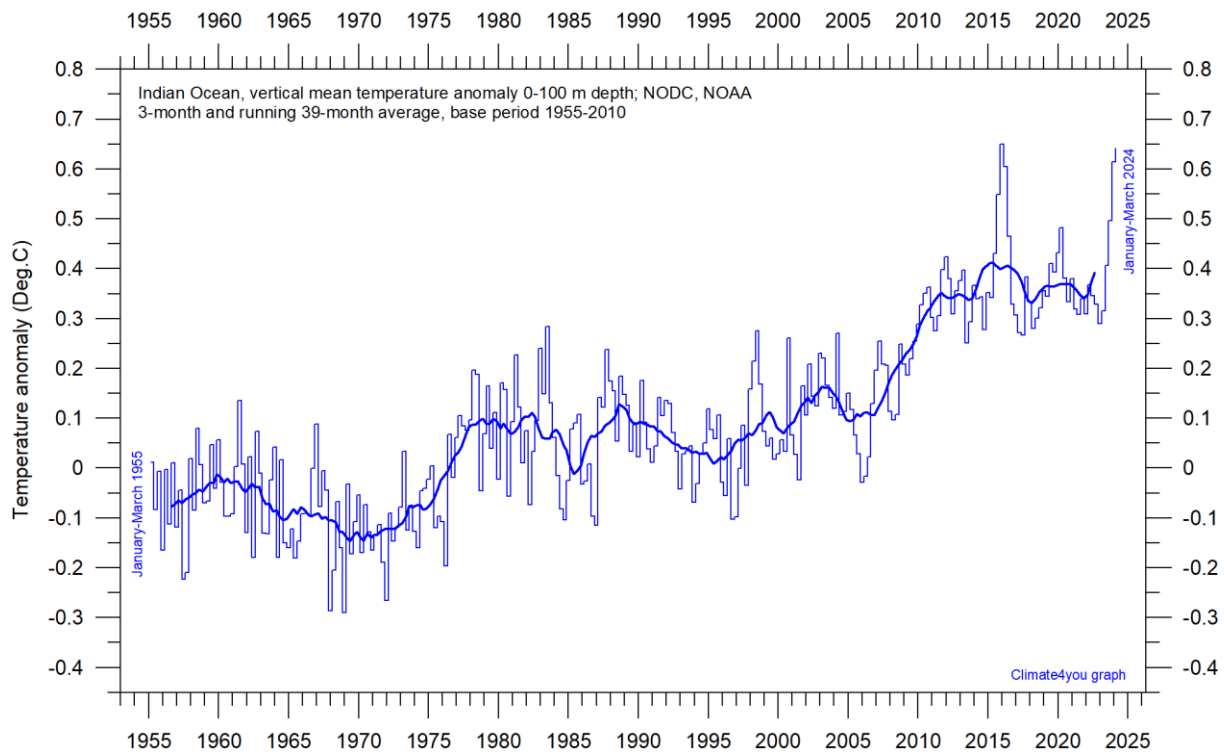
18



Pacific Ocean vertical average temperature 0-100 m depth since 1955. The thin line indicates 3-month values, and the thick line represents the simple running 39-month (c. 3 year) average. Data source: [NOAA National Oceanographic Data Center \(NODC\)](#). Base period 1955-2010.

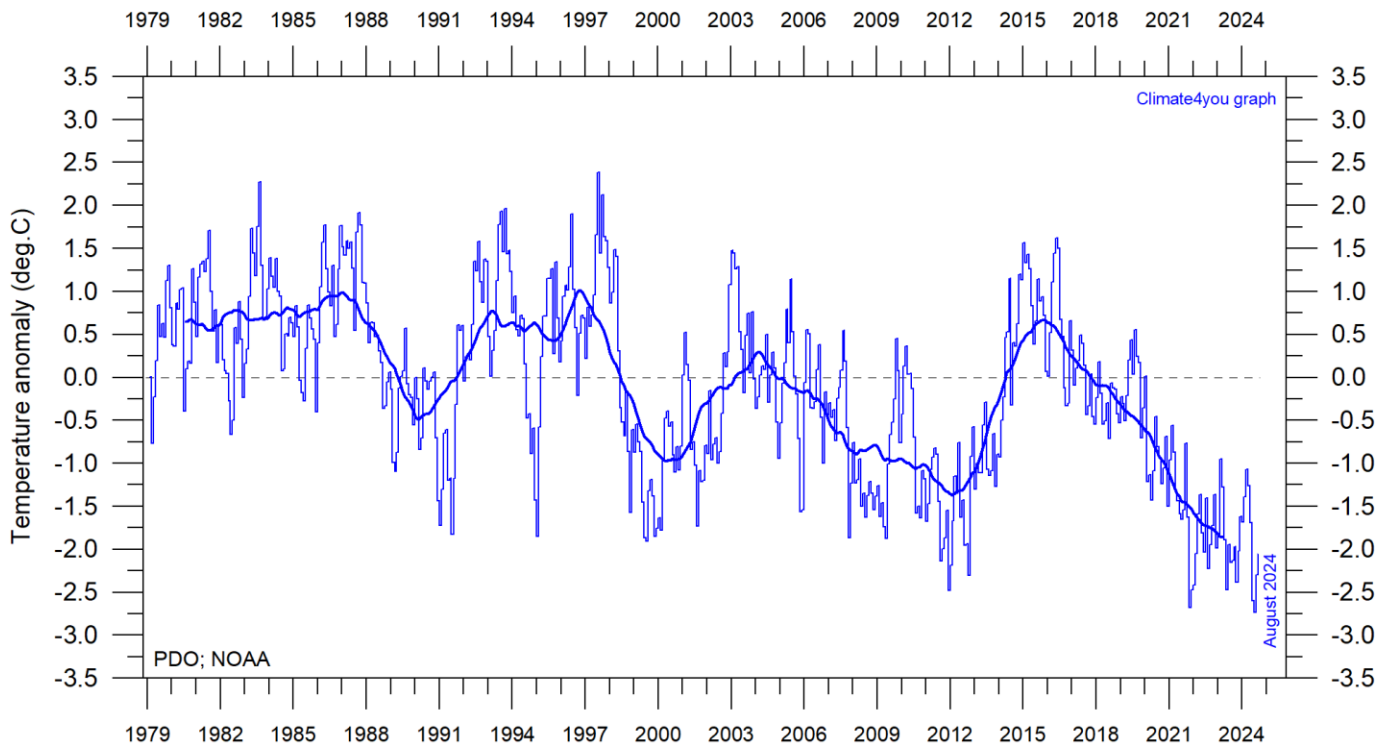


Atlantic Ocean vertical average temperature 0-100 m depth since 1955. The thin line indicates 3-month values, and the thick line represents the simple running 39-month (c. 3 year) average. Data source: [NOAA National Oceanographic Data Center](#) (NODC). Base period 1955-2010.



Indian Ocean vertical average temperature 0-100 m depth since 1955. The thin line indicates 3-month values, and the thick line represents the simple running 39-month (c. 3 year) average. Data source: [NOAA National Oceanographic Data Center](#) (NODC). Base period 1955-2010.

Pacific Decadal Oscillation (PDO), updated to August 2024



20

Monthly values of the Pacific Decadal Oscillation (PDO) since January 1979. The PDO is a long-lived El Niño-like pattern of Pacific climate variability, and the data series goes back to January 1854. Base period: 1982-2002. The thin line indicates monthly PDO values, and the thick line is the simple running 37-month average. Data source: [NOAA Physical Science Laboratory](#) (version PDO ERSST V5 plotted above).

The PDO is a long-lived El Niño-like pattern of Pacific climate variability, with data extending back to January 1854. Causes for PDO are not currently known, but even in the absence of a theoretical understanding, PDO climate information improves season-to-season and year-to-year climate forecasts for North America because of its strong tendency for multi-season and multi-year persistence. The PDO also appears to be roughly in phase with global temperature changes. Thus, from a societal impact's perspective, recognition of PDO is important because it shows that "normal" climate conditions can vary over time periods comparable to the length of a human's lifetime.

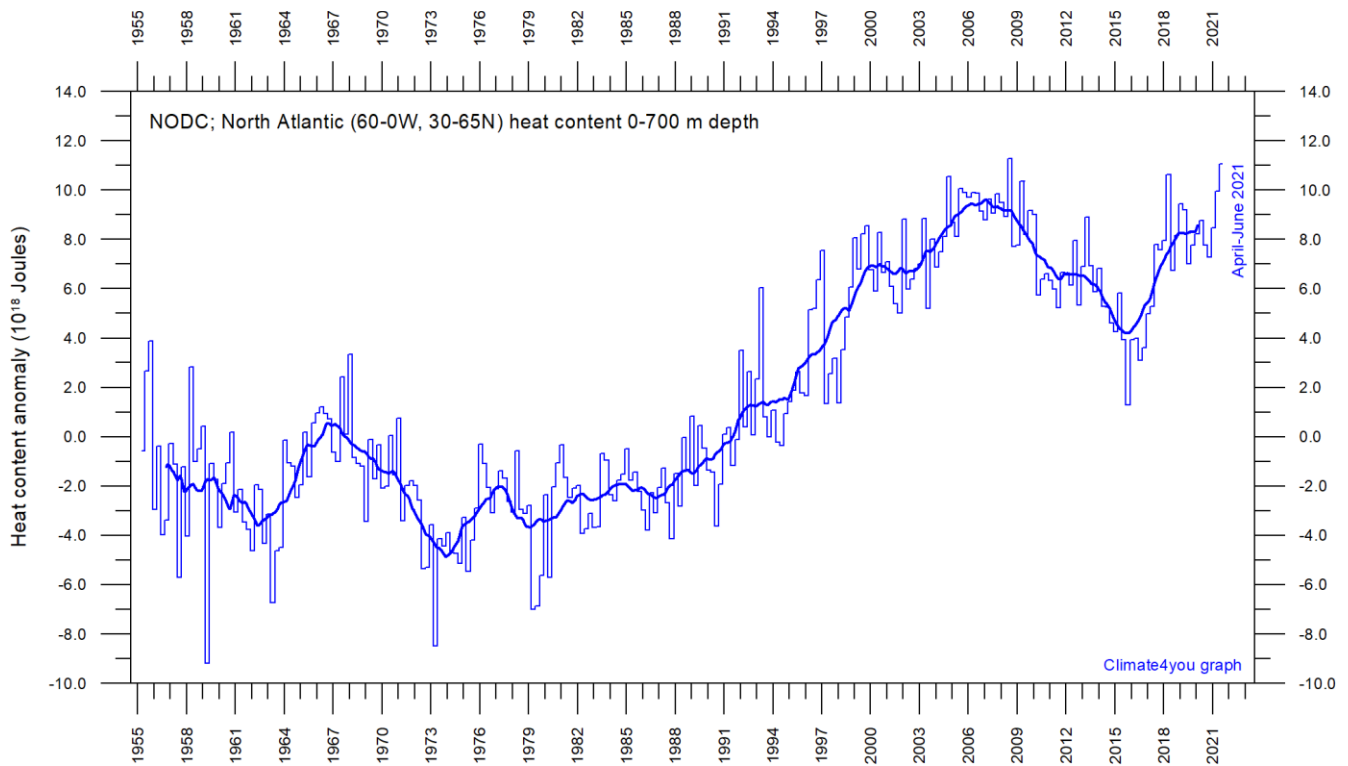
The PDO illustrates how global temperatures are tied to sea surface temperatures in the Pacific Ocean, the largest ocean on Earth. When sea surface temperatures are relatively low (negative phase PDO), as it was from 1945 to 1977, global air temperature often decreases. When Pacific Ocean surface temperatures are high (positive phase PDO), as from 1977 to 1998, global surface air temperature often increases.

A Fourier frequency analysis (not shown here) shows the PDO record to be influenced by a significant 5.6-year cycle, and feasibly also by a longer 18.6-year long period, corresponding to the length of the lunar nodal tide.

North Atlantic heat content uppermost 700 m, updated to June 2021

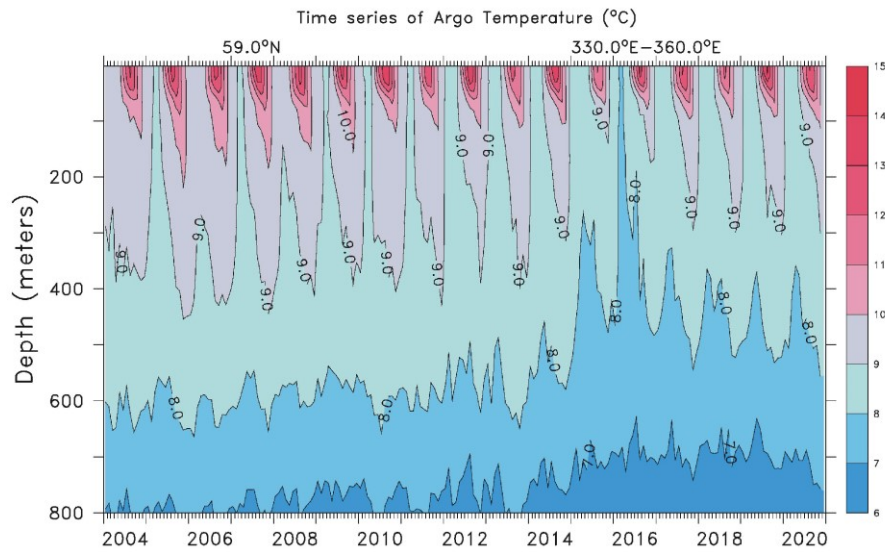


21



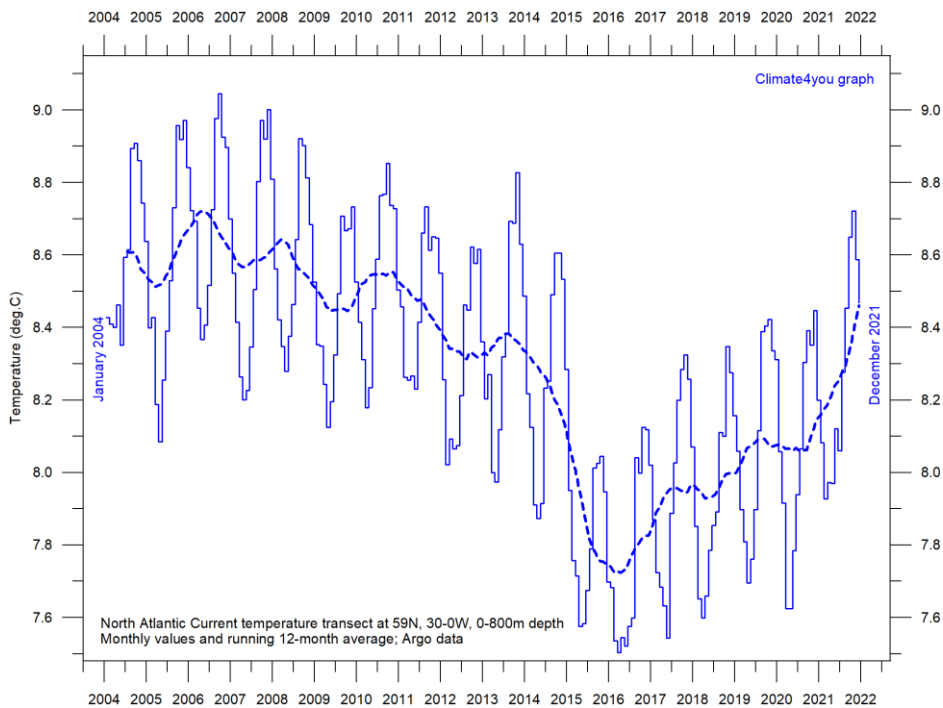
Global monthly heat content anomaly (10^{18} Joules) in the uppermost 700 m of the North Atlantic (60-0W, 30-65N; see map above) ocean since January 1955. The thin line indicates monthly values, and the thick line represents the simple running 37-month (c. 3 year) average. Data source: [National Oceanographic Data Center](https://www.nodc.noaa.gov/) (NODC).

North Atlantic temperatures 0-800 m depth along 59°N, 30-0W, updated to December 2021



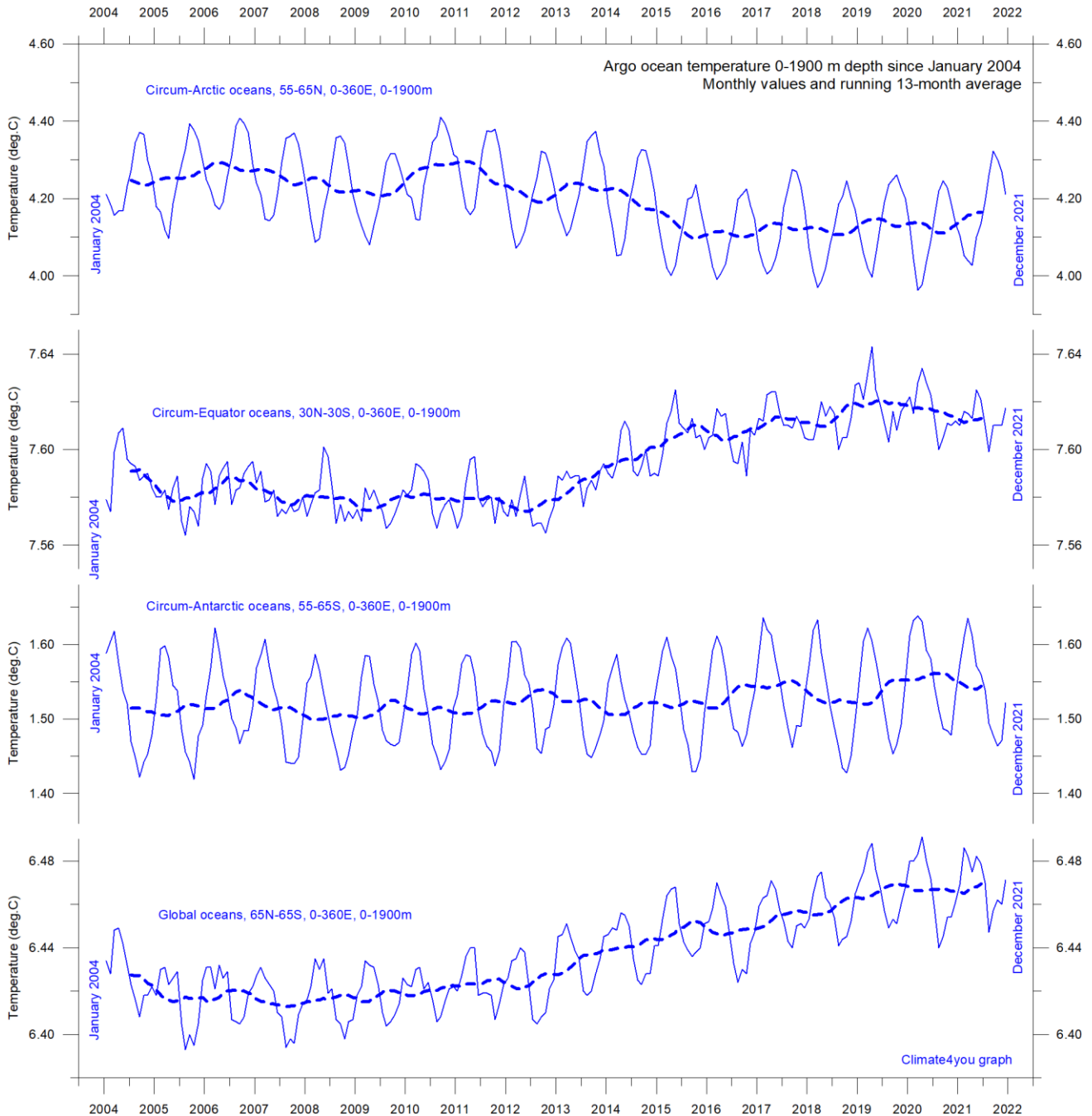
Time series depth-temperature diagram along 59 N across the North Atlantic Current from 30°W to 0°W, from surface to 800 m depth. Source: [Global Marine Argo Atlas](#). See also the diagram below.

22



Average temperature along 59 N, 30-0W, 0-800m depth, corresponding to the main part of the North Atlantic Current, using [Argo](#)-data. Source: [Global Marine Argo Atlas](#). Additional information can be found in: Roemmich, D. and J. Gilson, 2009. The 2004-2008 mean and annual cycle of temperature, salinity, and steric height in the global ocean from the Argo Program. [Progress in Oceanography](#), 82, 81-100.

Global ocean temperature 0-1900 m depth summary, updated to December 2021

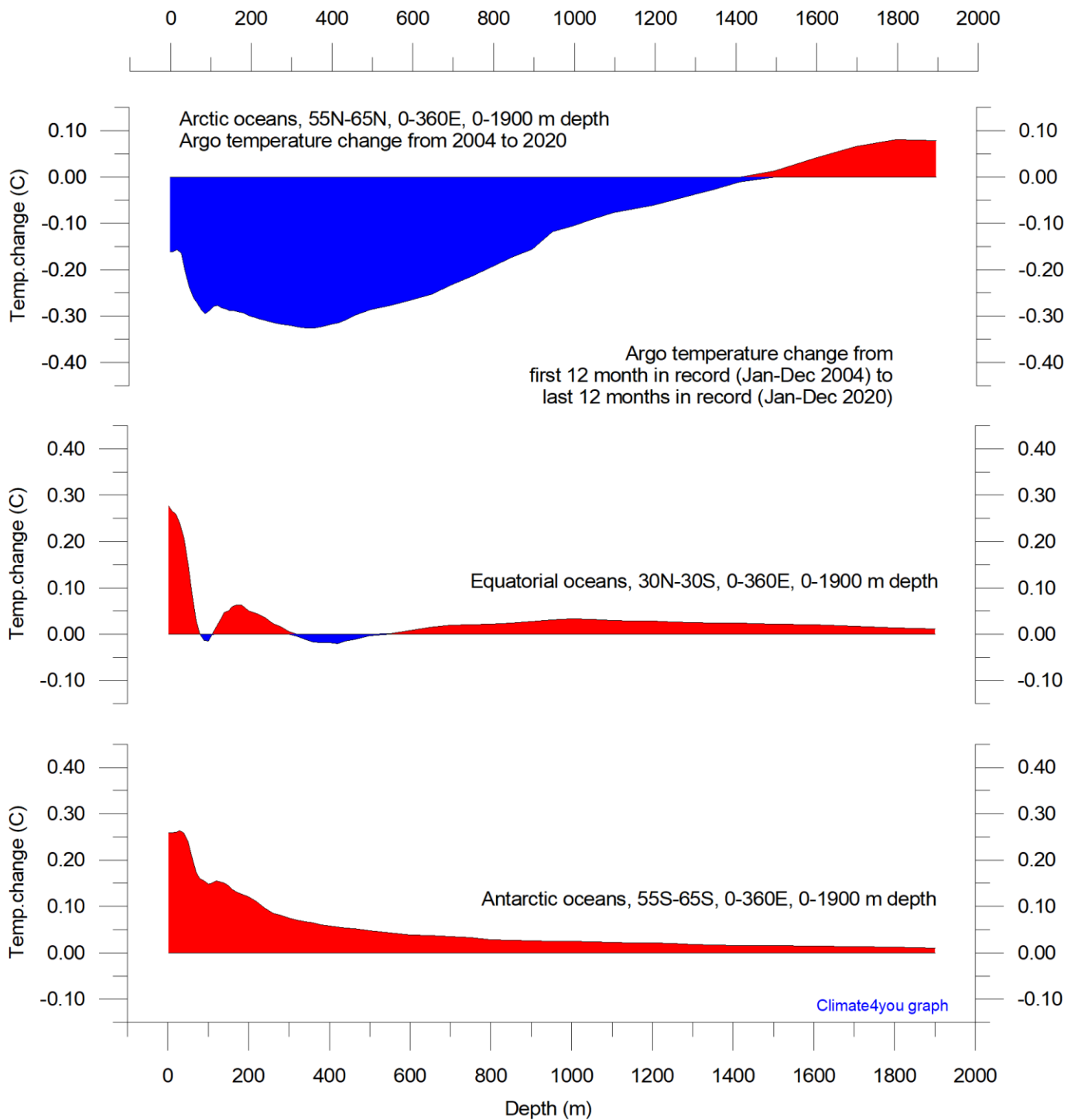


Summary of average temperature in uppermost 1900 m in different parts of the global oceans, using [Argo](#)-data. Source: [Global Marine Argo Atlas](#). Additional information can be found in: Roemmich, D. and J. Gilson, 2009. The 2004-2008 mean and annual cycle of temperature, salinity, and steric height in the global ocean from the Argo Program. [Progress in Oceanography](#), 82, 81-100.

The temperature of the global oceans down to 1900 m depth has been increasing since about 2011, but with a possible peak around 2020. The global increase since 2013 is mainly due to changes occurring near the Equator, between 30°N and 30°S. In contrast, for the circum-Arctic

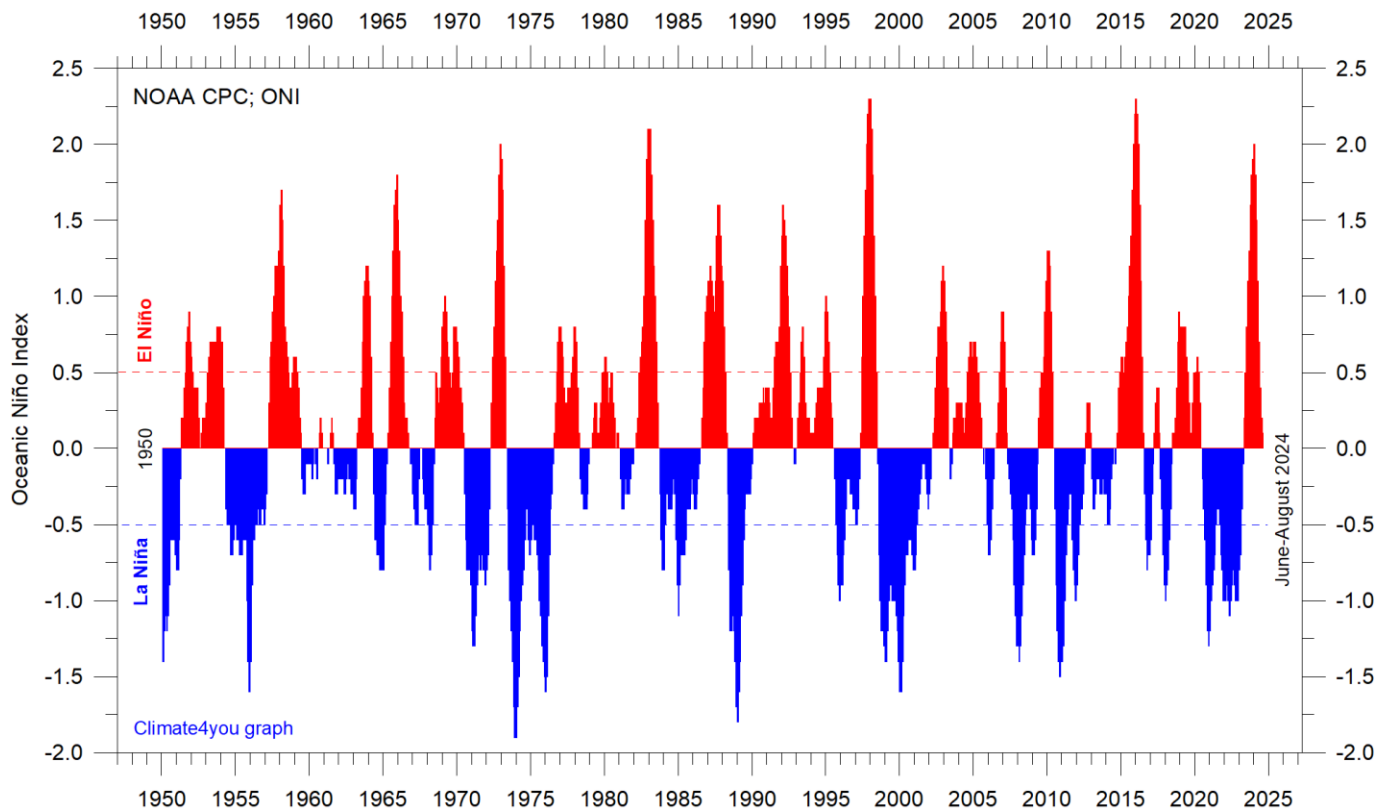
oceans north of 55°N, depth-integrated ocean temperatures have been decreasing since 2011, but with a possible low around 2019. Near the Antarctic, south of 55°S, temperatures have essentially been stable. At most latitudes, a clear annual rhythm is evident.

Global ocean net temperature change since 2004 at different depths, updated to December 2020



Net temperature change since 2004 from surface to 1900 m depth in different parts of the global oceans, using [Argo](#)-data. Source: [Global Marine Argo Atlas](#). Additional information can be found in: Roemmich, D. and J. Gilson, 2009. The 2004-2008 mean and annual cycle of temperature, salinity, and steric height in the global ocean from the Argo Program. [Progress in Oceanography](#), 82, 81-100. Please note that due to the spherical form of Earth, northern and southern latitudes represent only small ocean volumes, compared to latitudes near the Equator.

La Niña and El Niño episodes, Oceanic Niño Index (ONI), updated to August 2024



25

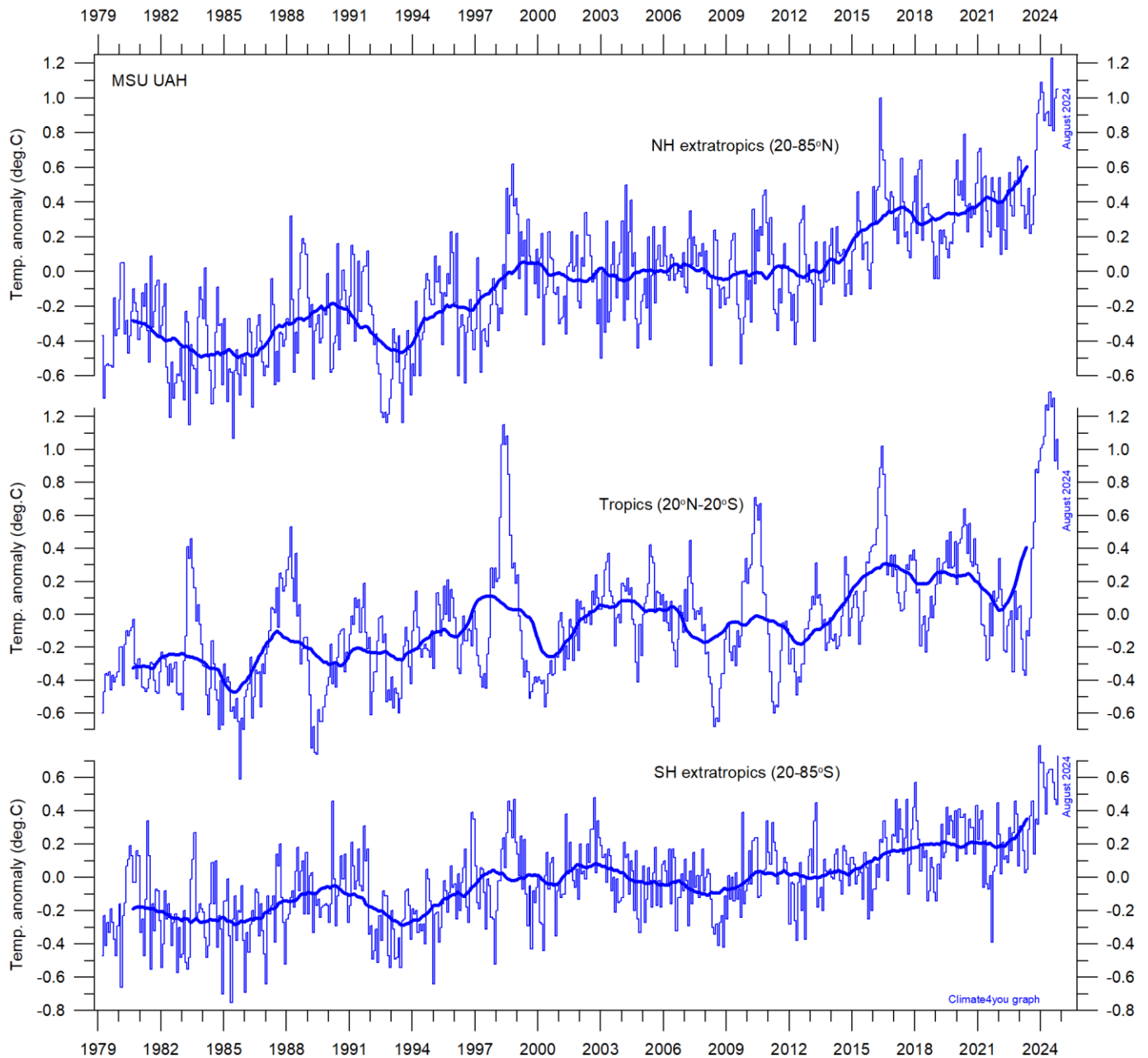
Warm ($>+0.5^{\circ}\text{C}$) and cold ($<-0.5^{\circ}\text{C}$) episodes for the [Oceanic Niño Index \(ONI\)](#), defined as 3 month running mean of ERSSTv4 SST anomalies in the Niño 3.4 region (5°N - 5°S , 120° - 170°W). For historical purposes cold and warm episodes are defined when the threshold is met for a minimum of 5 consecutive over-lapping seasons. Anomalies are centred on 30-yr base periods updated every 5 years.

In the Pacific Ocean, trade winds usually blow west along the equator, pushing warm water from South America towards Asia. To replace that warm water, cold water rises from the depths near South America. During El Niño episodes, trade winds weaken, and warm water is spreading back east, toward South America. In contrast, during La Niña episodes, trade winds are stronger than usual, pushing more warm water than usual toward Asia, and upwelling of cold water near South America therefore increases.

The 2015-16 El Niño episode is among the strongest since the beginning of the record in 1950. Considering the entire record, however, recent variations between El Niño and La Niña episodes do not appear abnormal in any way.

A Fourier frequency analysis (not shown here) shows the ONI record to be influenced by a significant 3.6-year cycle, and feasibly also by a longer 5.6-year cycle.

Zonal lower troposphere temperatures from satellites, updated to August 2024

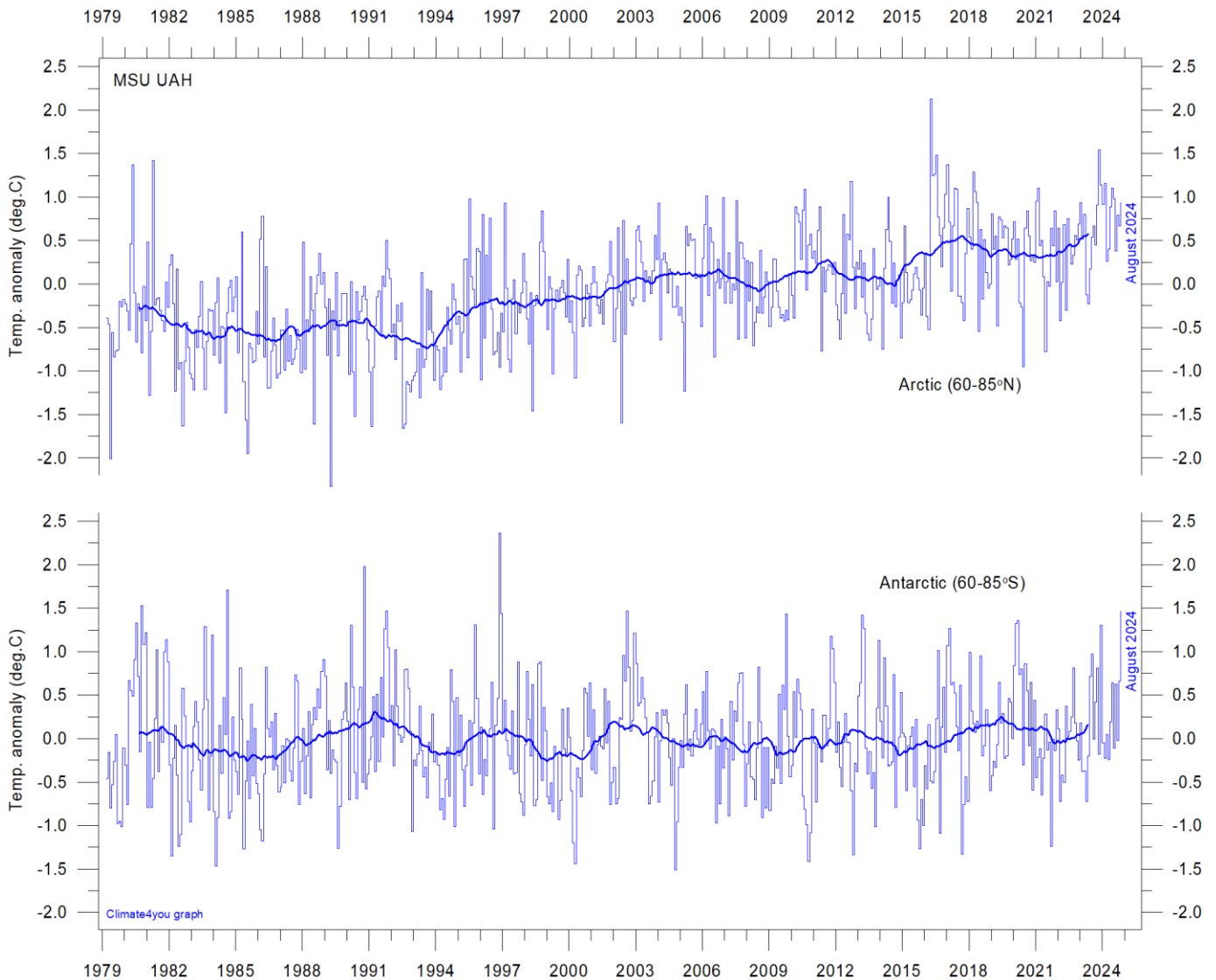


Global monthly average lower troposphere temperature since 1979 for the tropics and the northern and southern extratropics, according to University of Alabama at Huntsville, USA. Thin lines show the monthly temperature. Thick lines represent the simple running 37-month average, nearly corresponding to a running 3-year average. Reference period 1981-2010.

The overall warming since 1980 has dominantly been a northern hemisphere phenomenon, and mainly played out as a marked change between 1994 and 1999. However, this rather rapid temperature change is probably influenced by the Mt. Pinatubo eruption 1992-93 and the subsequent 1997 El Niño episode. The diagram also shows the

temperature effects of the strong Equatorial El Niño's in 1997 and 2015-16, as well as the moderate El Niño in 2019. Apparently, these effects were spreading to higher latitudes in both hemispheres with some delay. Recently, a new El Niño was playing out in the Pacific Ocean (p.25), as is clearly shown by tropics surface air temperatures.

Arctic and Antarctic lower troposphere temperature, updated to August 2024



Global monthly average lower troposphere temperature since 1979 for the North Pole and South Pole regions, based on satellite observations ([University of Alabama](https://climate4you.com) at Huntsville, USA). Thin lines show the monthly temperature. The thick line is the simple running 37-month average, nearly corresponding to a running 3-year average. Reference period 1991-2020.

In the Arctic region, warming mainly took place 1994-96, and less so subsequently. In 2016, however, temperatures peaked for several months, presumably because of oceanic heat given off to the atmosphere during the 2015-15 El Niño (see also diagram on page 25) and subsequently advected to higher latitudes.

This underscores how Arctic air temperatures may be affected not only by variations in local conditions but also by variations playing out in geographically remote regions.

A slight temperature decrease characterised the Arctic since the marked 2016 El Niño peak. However, the recent (2023-24) El Niño episode is recorded by Arctic temperatures in a less pronounced way.

In the Antarctic region, temperatures have basically remained stable since the onset of the satellite record in 1979. In 2016-17 a small temperature peak visible in the monthly record may be interpreted as the subdued effect of the recent El Niño episode.

Arctic and Antarctic surface air temperature, updated to December 2021

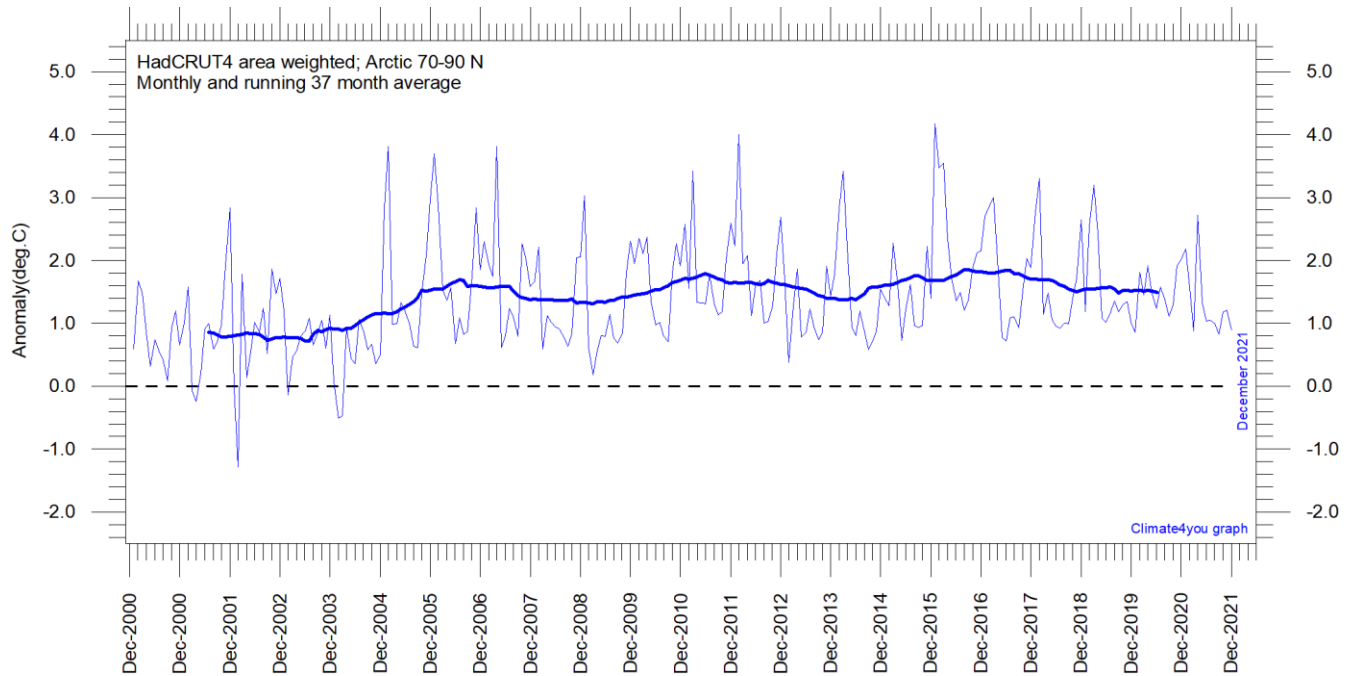


Diagram showing area weighted Arctic (70-90°N) monthly surface air temperature anomalies ([HadCRUT4](#)) since January 2000, in relation to the WMO [normal period](#) 1961-1990. The thin line shows the monthly temperature anomaly, while the thicker line shows the running 37-month (c. 3 year) average.

28

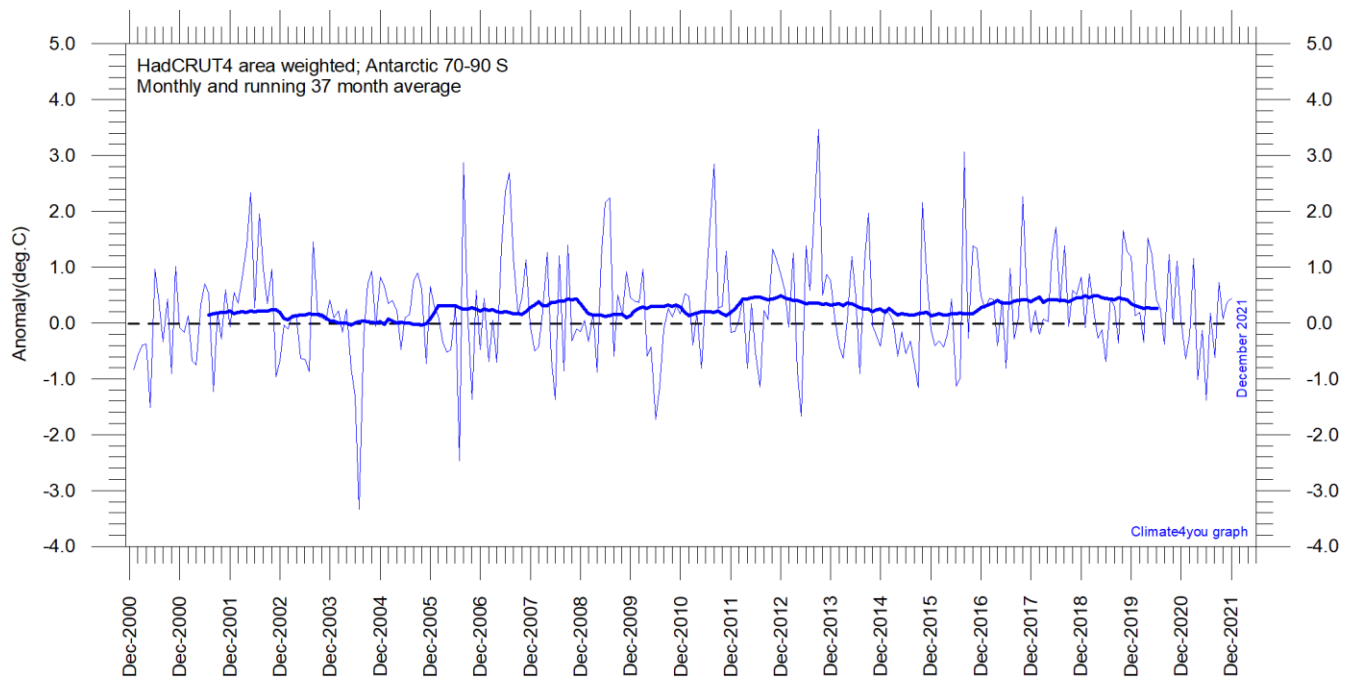


Diagram showing area weighted Antarctic (70-90°S) monthly surface air temperature anomalies ([HadCRUT4](#)) since January 2000, in relation to the WMO [normal period](#) 1961-1990. The thin line shows the monthly temperature anomaly, while the thicker line shows the running 37-month (c. 3 year) average.

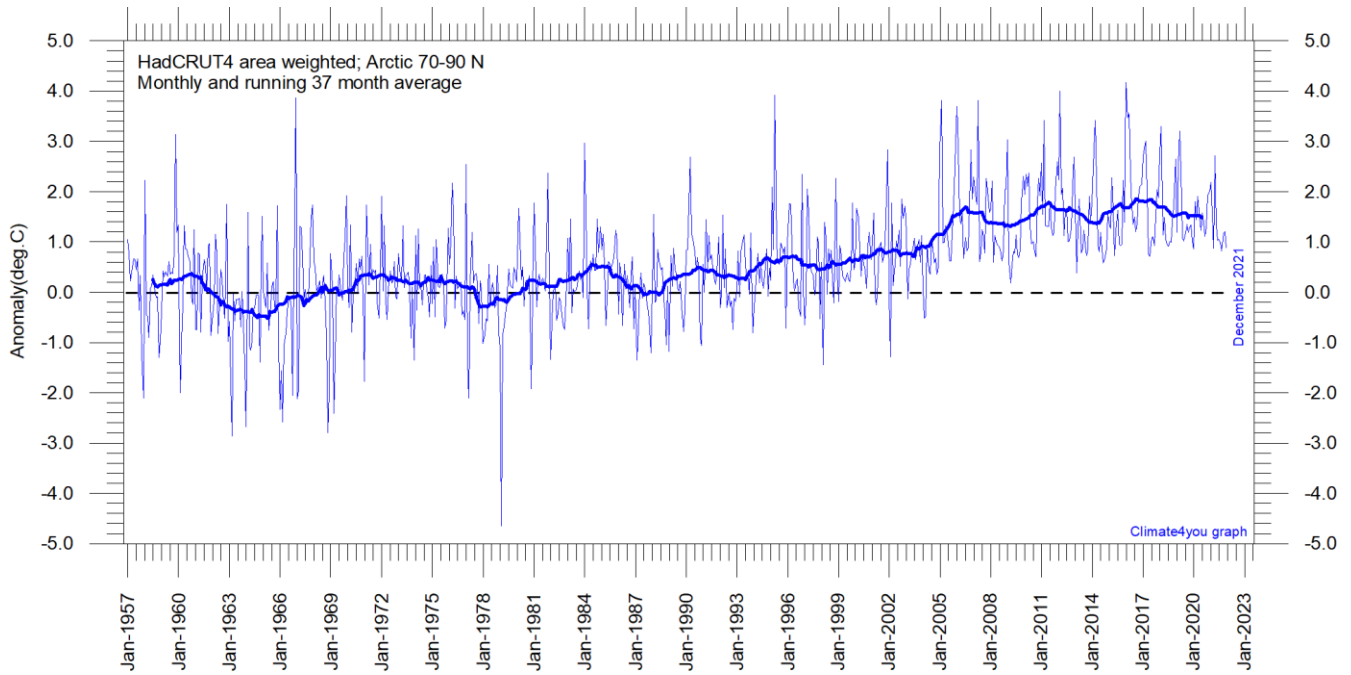


Diagram showing area weighted Arctic (70-90°N) monthly surface air temperature anomalies ([HadCRUT4](#)) since January 1957, in relation to the WMO [normal period](#) 1961-1990. The thin line shows the monthly temperature anomaly, while the thicker line shows the running 37-month (c. 3 year) average.

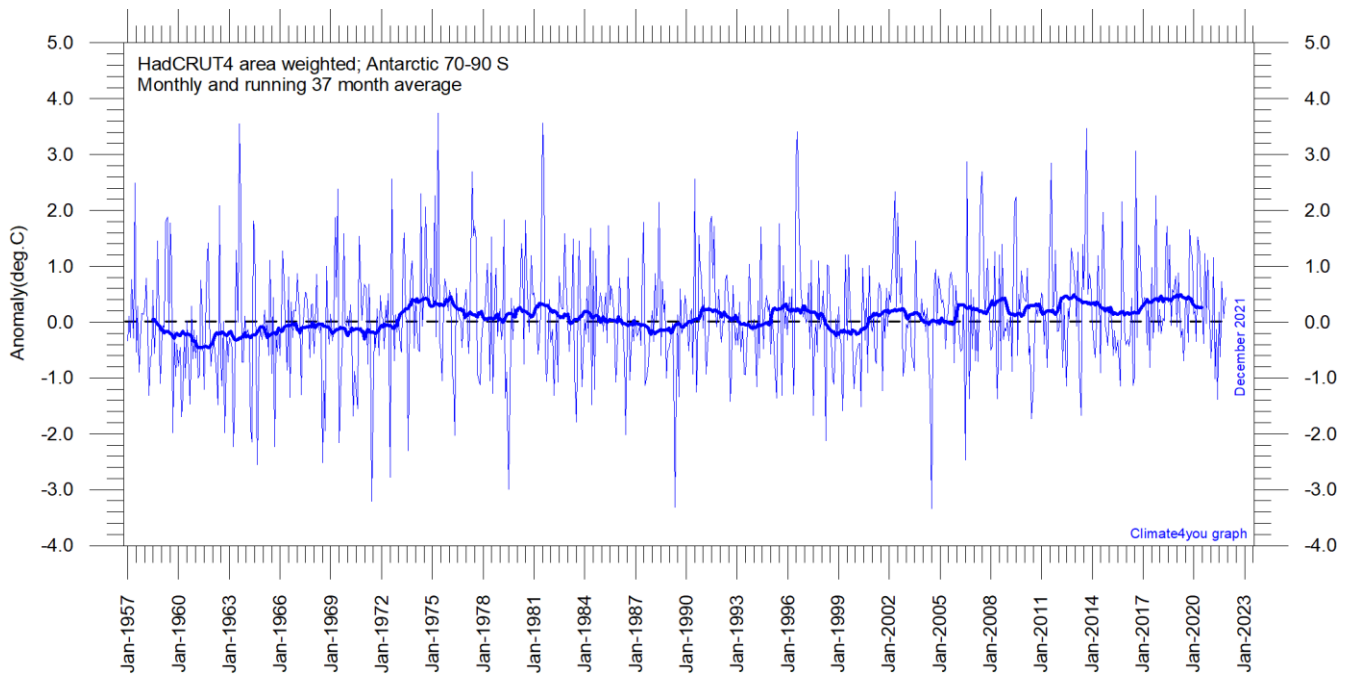


Diagram showing area weighted Antarctic (70-90°S) monthly surface air temperature anomalies ([HadCRUT4](#)) since January 1957, in relation to the WMO [normal period](#) 1961-1990. The thin line shows the monthly temperature anomaly, while the thicker line shows the running 37-month (c. 3 year) average.

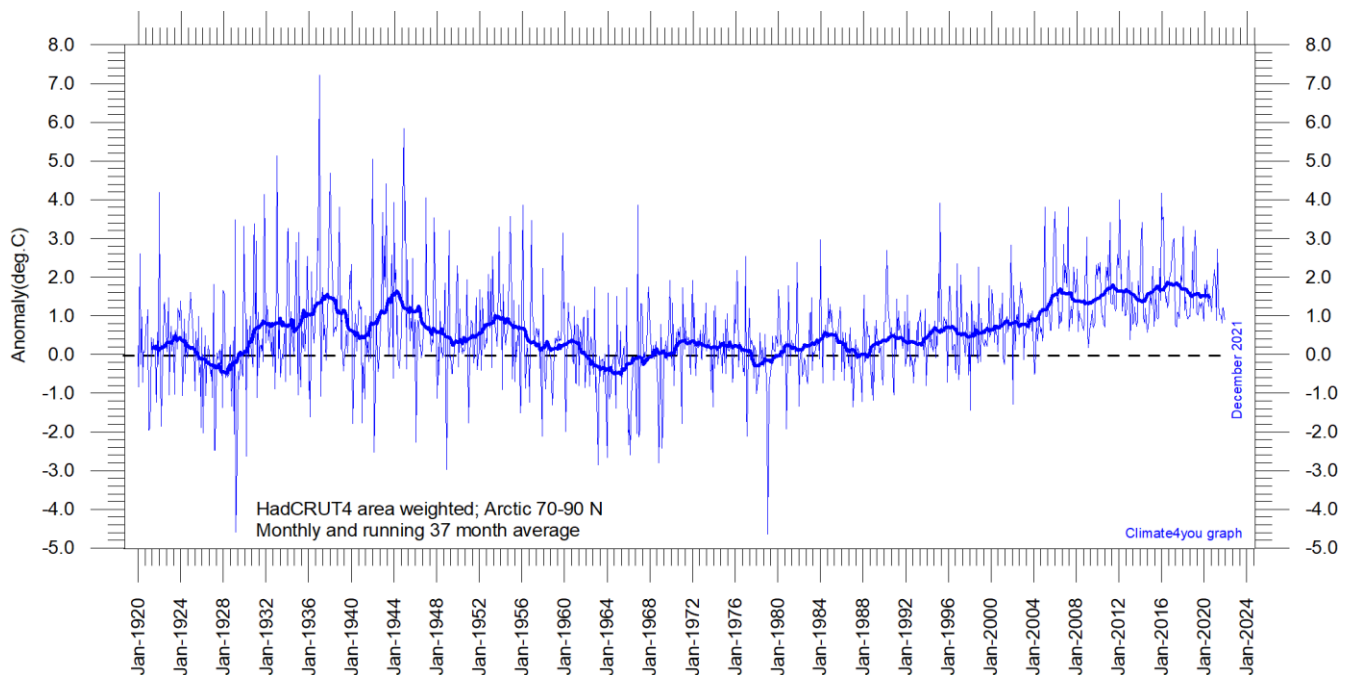


Diagram showing area-weighted Arctic (70-90°N) monthly surface air temperature anomalies ([HadCRUT4](#)) since January 1920, in relation to the WMO [normal period](#) 1961-1990. The thin line shows the monthly temperature anomaly, while the thicker line shows the running 37-month (c. 3 year) average.

Because of the relatively small number of Arctic stations before 1930, month-to-month variations in the early part of the Arctic temperature record 1920-2018 are higher than later (diagram above).

The period from about 1930 saw the establishment of many new Arctic meteorological stations, first in Russia and Siberia, and following the 2nd World War, also in North America, explaining the above difference.

The period since 2005 is warm, about as warm as the period 1930-1940.

As the HadCRUT4 data series has improved high latitude coverage data coverage (compared to the HadCRUT3 series), the individual 5°x5° grid cells have been weighted according to their surface area. This area correction is especially important for polar

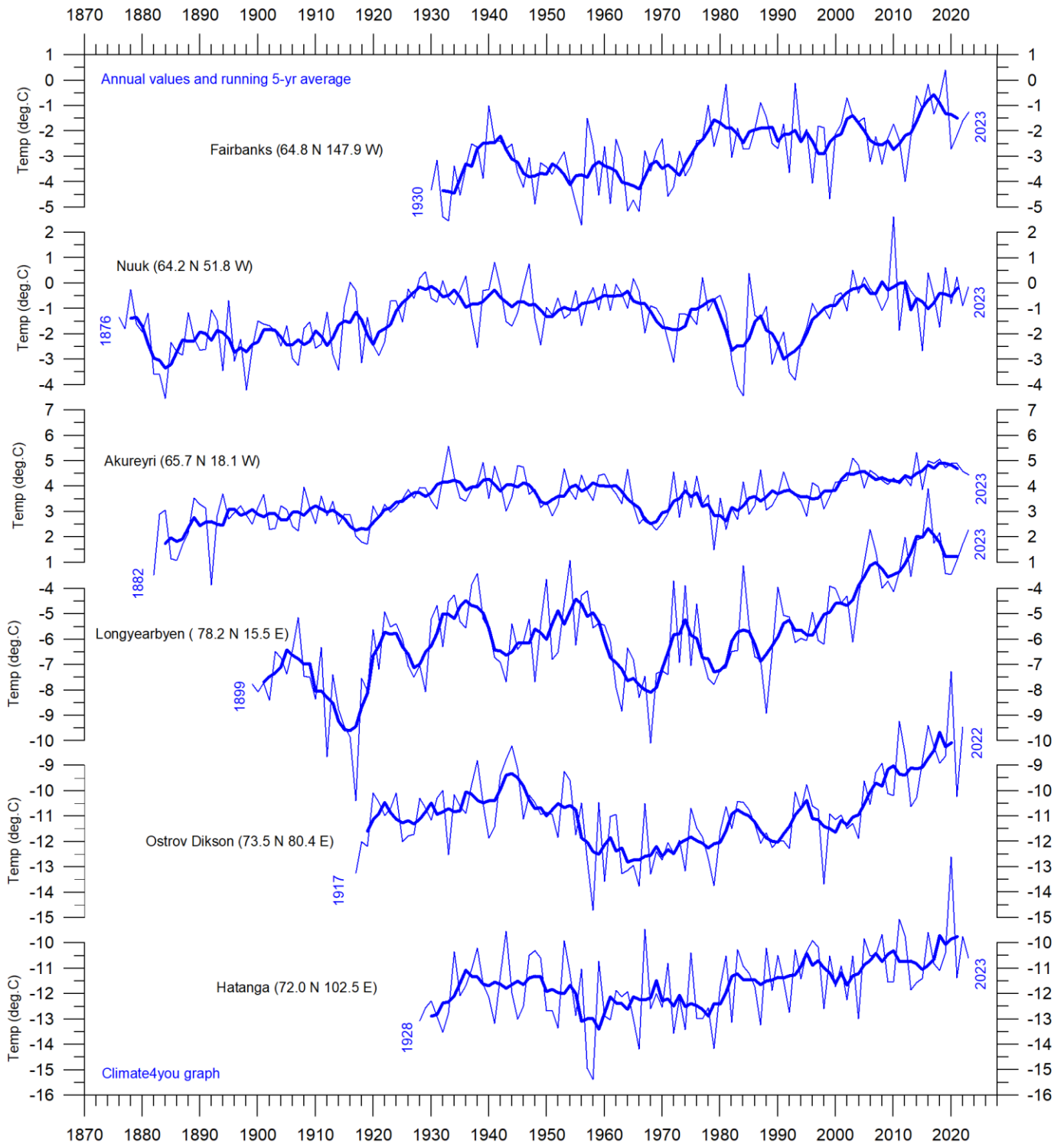
regions, where longitudes converge rapidly. This approach differs from the approach used by Gillett et al. 2008, which calculated a simple average, with no correction for the substantial latitudinal surface area effect in polar regions.

The area weighted Arctic HadCRUT4 surface air temperature anomalies (p.28-30) correspond rather well to the lower troposphere temperature anomalies recorded by satellites (p.27).

Literature:

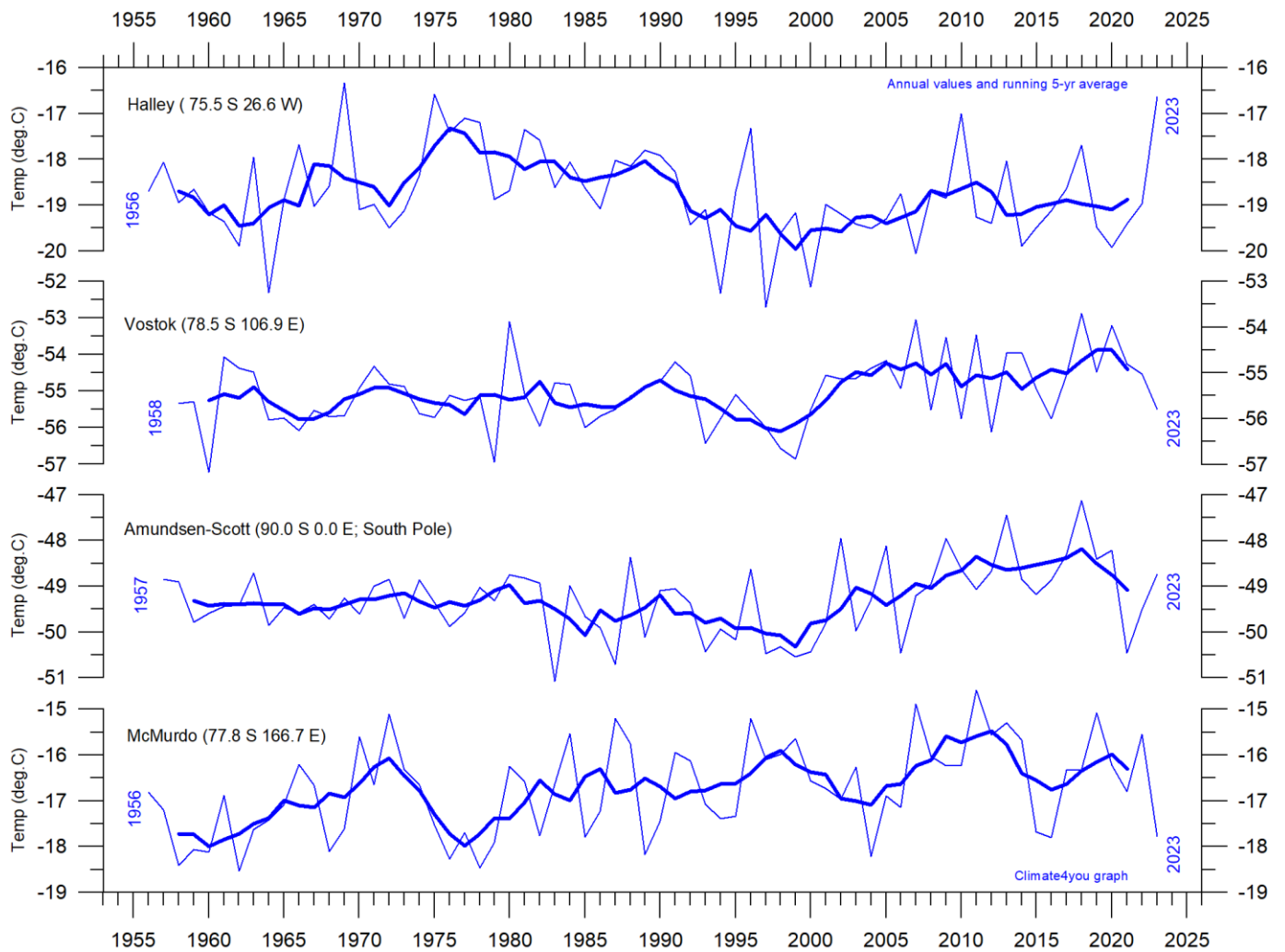
Gillett, N.P., Stone, D.A., Stott, P.A., Nozawa, T., Karpechko, A.Y.U., Hegerl, G.C., Wehner, M.F. and Jones, P.D. 2008. Attribution of polar warming to human influence. *Nature Geoscience* 1, 750-754.

Long Arctic annual surface air temperature series, updated to year 2023



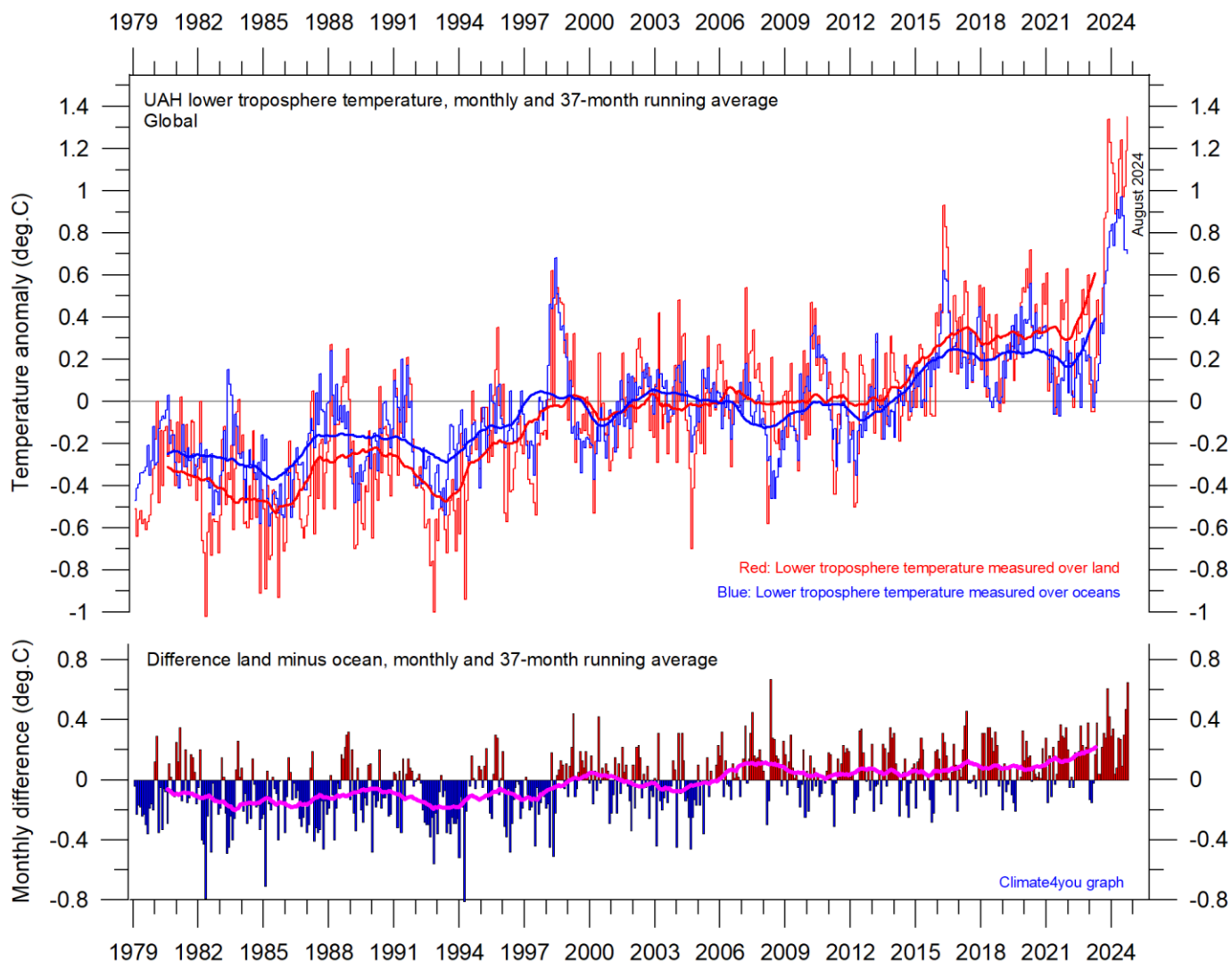
Arctic annual surface air temperature series, selected because of their length of observation time. The thin blue line represents the mean annual air temperature, and the thick blue line is the running 5-year average. Annual values were calculated from monthly average temperatures. More info on [Climate4you](#).

Long Antarctic annual surface air temperature series, updated to year 2023



Antarctic annual surface air temperature series, selected because of their length of observation time. The thin blue line represents the mean annual air temperature, and the thick blue line is the running 5-year average. Annual values were calculated from monthly average temperatures. More info on [Climate4you](#).

Temperature over land versus over oceans, updated to August 2024



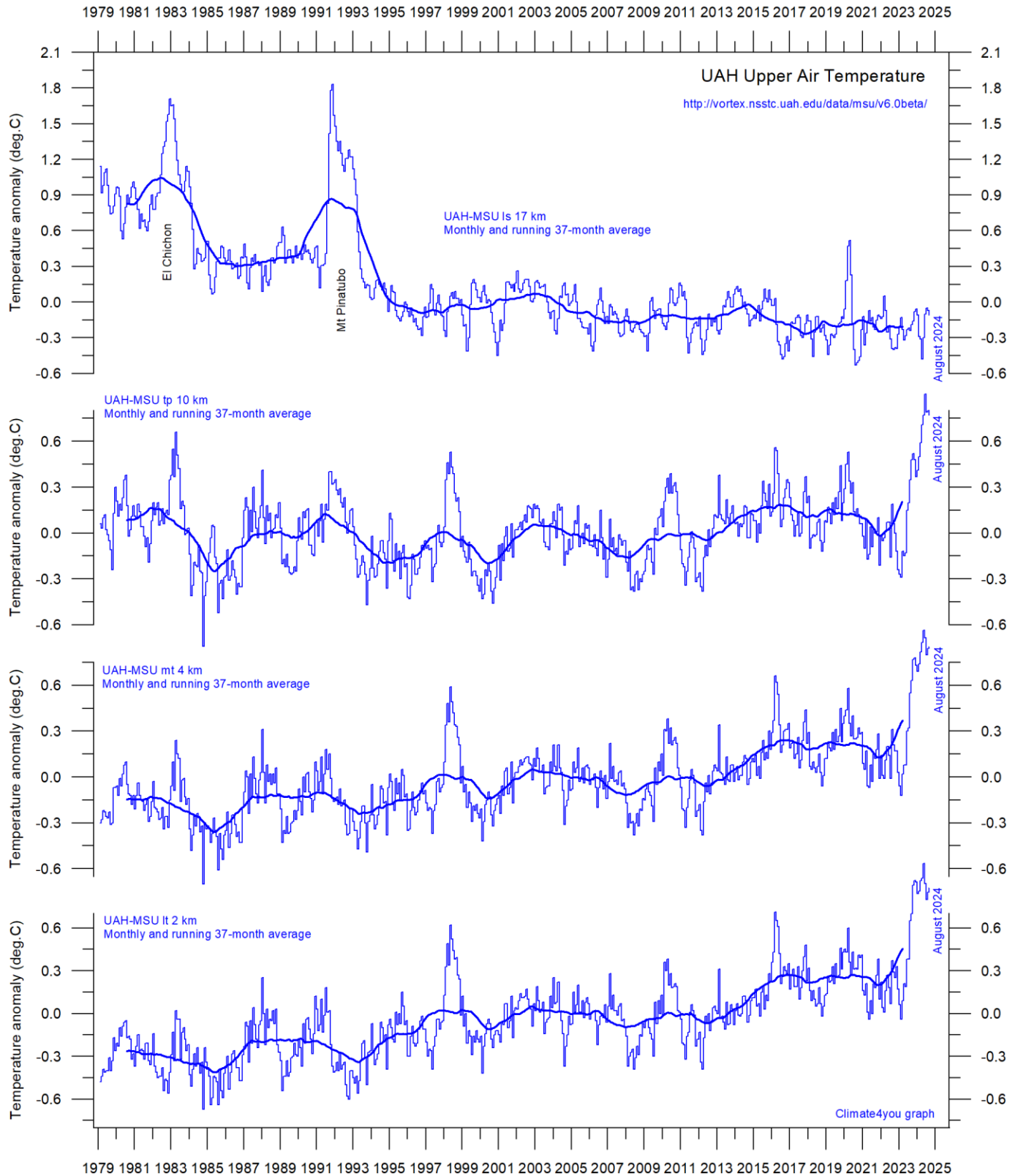
Global monthly average lower troposphere temperature since 1979 measured over land and oceans, respectively, according to [University of Alabama](https://climate4you.com) at Huntsville, USA. Thick lines are the simple running 37-month average, nearly corresponding to a running 3-year average. Reference period 1991-2020.

Since 1979, the lower troposphere over land has warmed much more than over oceans, suggesting that the overall warming is derived mainly from incoming solar radiation. In addition, there may be supplementary reasons for this divergence, such as,

e.g., variations in cloud cover and changes in land use. Compare also with cloud cover diagram on page 60.

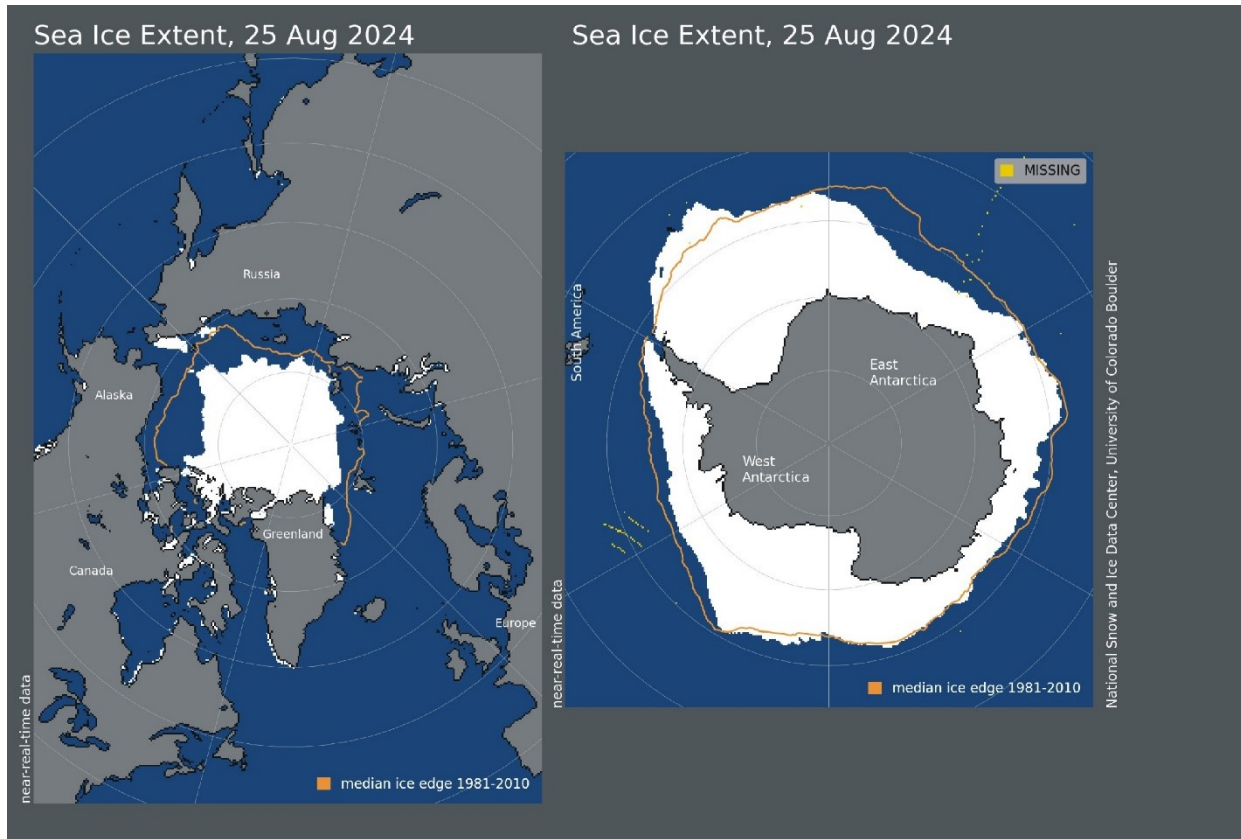
The temperature effect of the recent (2023-24) El Niño episode was recorded more pronounced over land regions, compared to ocean regions.

Troposphere and stratosphere temperatures from satellites, updated to August 2024



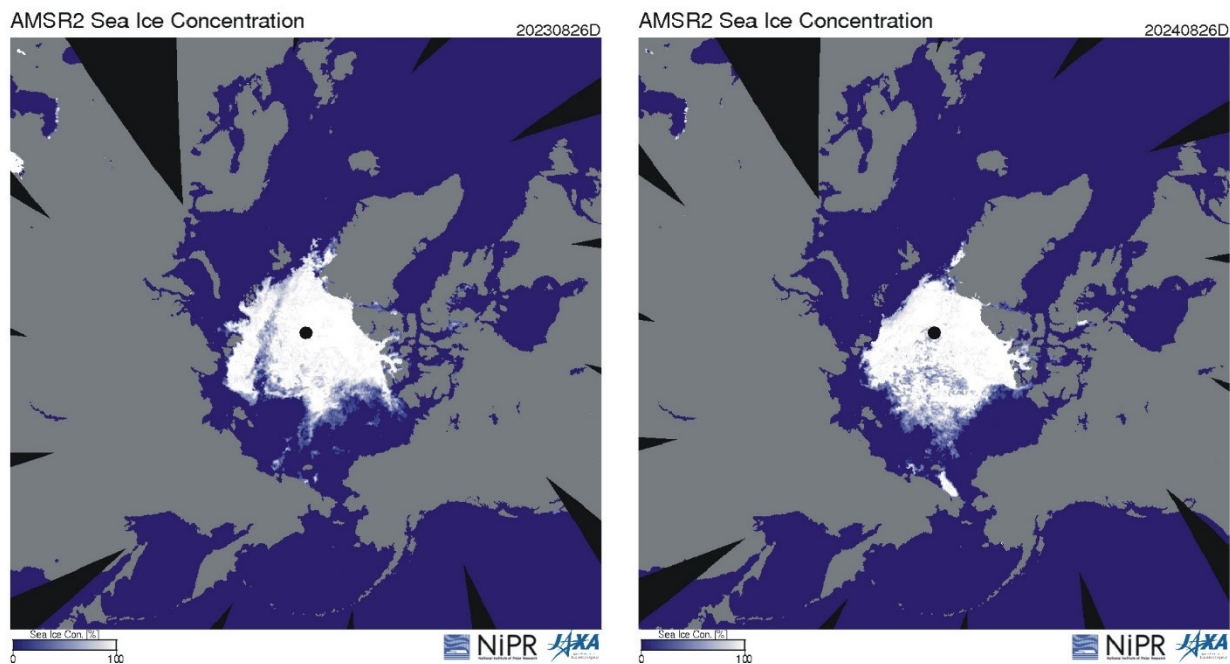
Global monthly average temperature in different according to University of Alabama at Huntsville, USA. The thin lines represent the monthly average, and the thick line the simple running 37-month average, nearly corresponding to a running 3-year average. Reference period 1991-2020.

Arctic and Antarctic sea ice, updated to August 2024

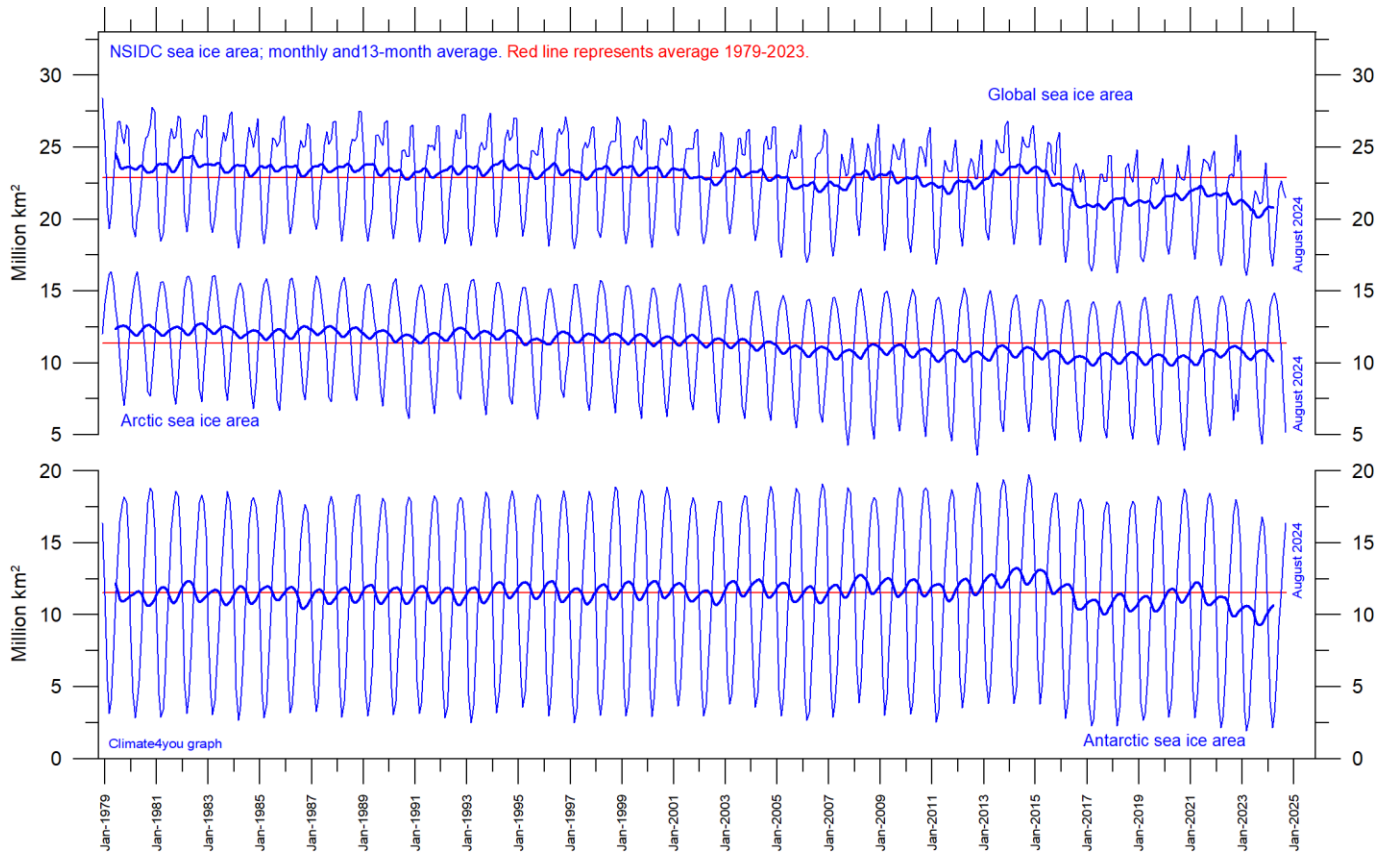


35

Sea ice extent 25 August 2024. The median limit of sea ice (orange line) is defined as 15% sea ice cover, according to the average of satellite observations 1981-2010 (both years included). Sea ice may therefore well be encountered outside and open water areas inside the limit shown in the diagrams above. Map source: National Snow and Ice Data Center (NSIDC).



Diagrams showing Arctic sea ice extent and concentration 26 August 2023 (left) and 2024 (right), according to the Japan Aerospace Exploration Agency (JAXA).



Graphs showing monthly Antarctic, Arctic, and global sea ice extent since November 1978, according to the [National Snow and Ice data Center \(NSIDC\)](#).

36

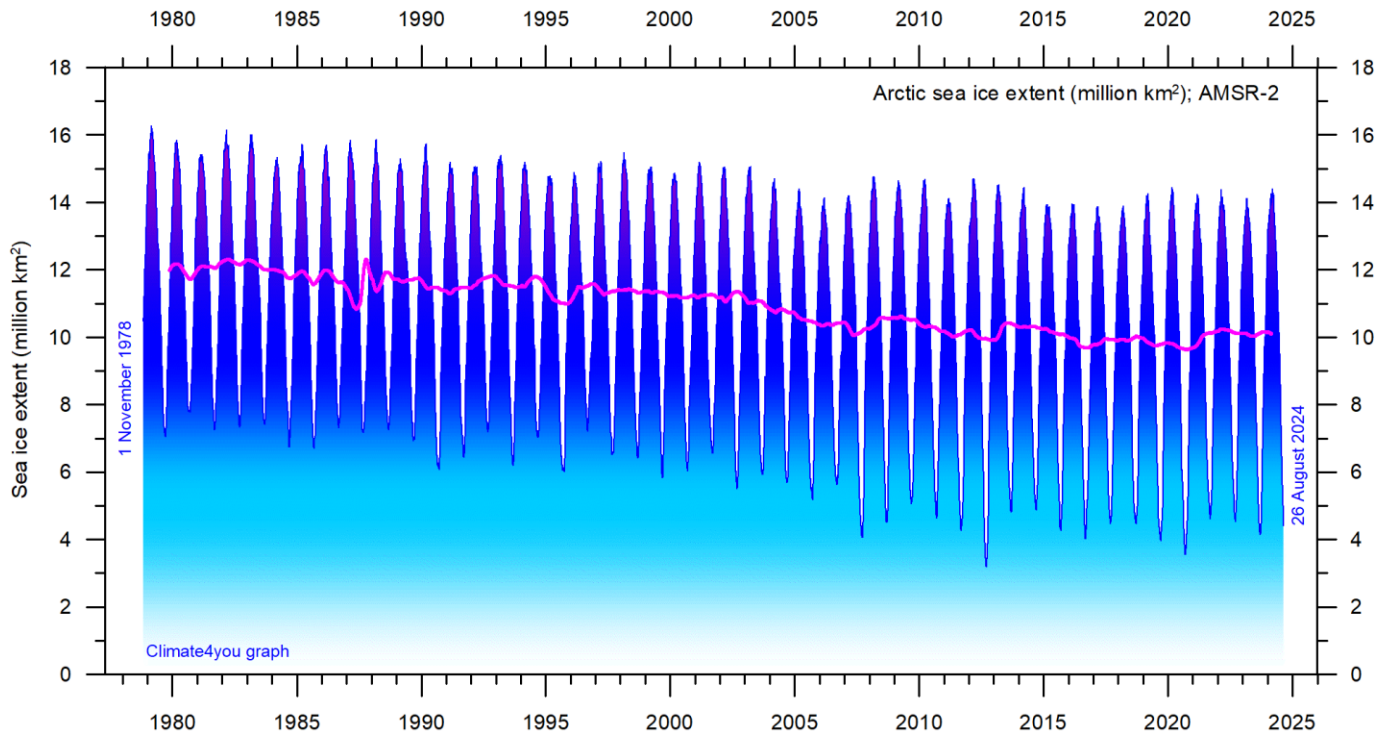
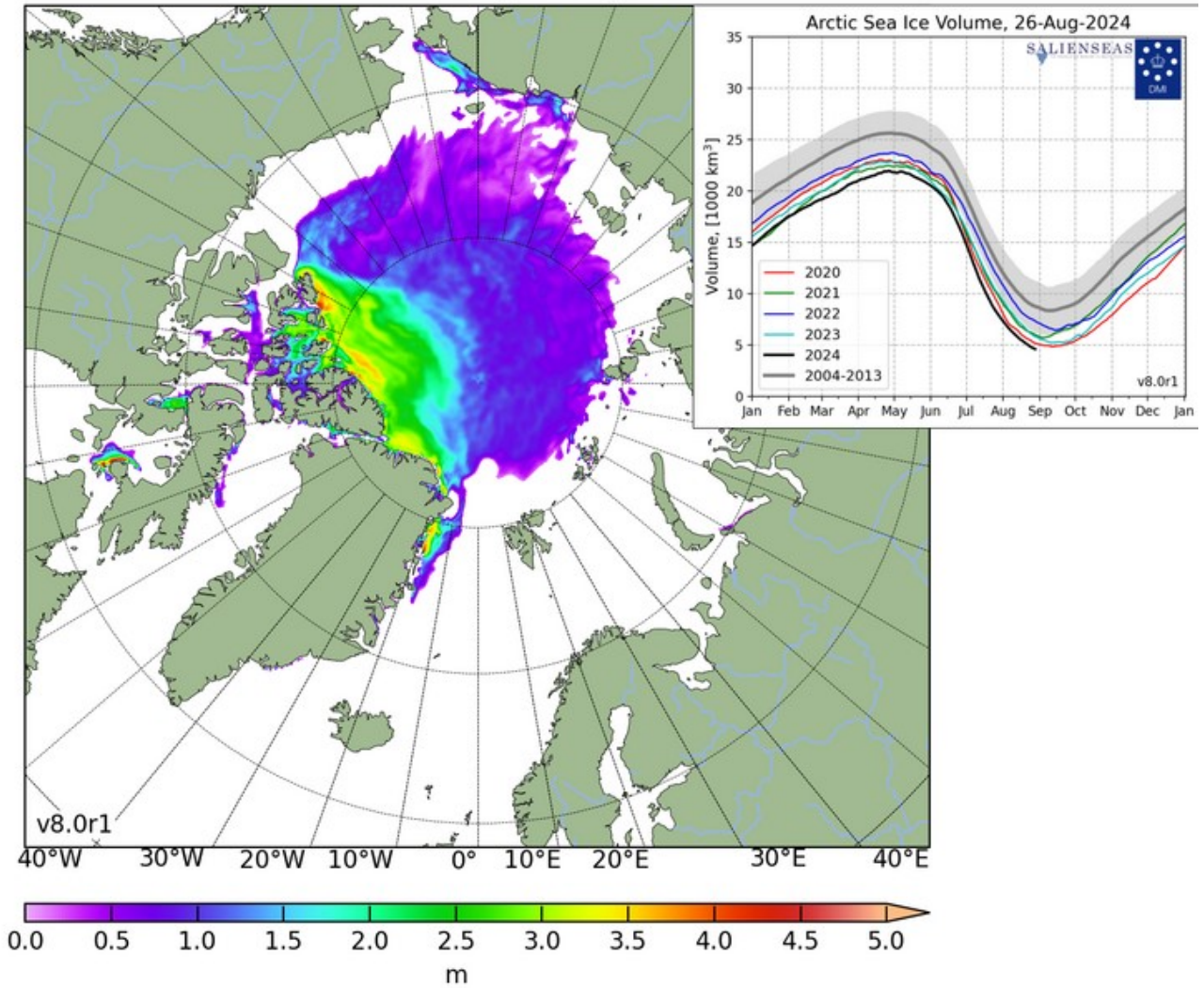
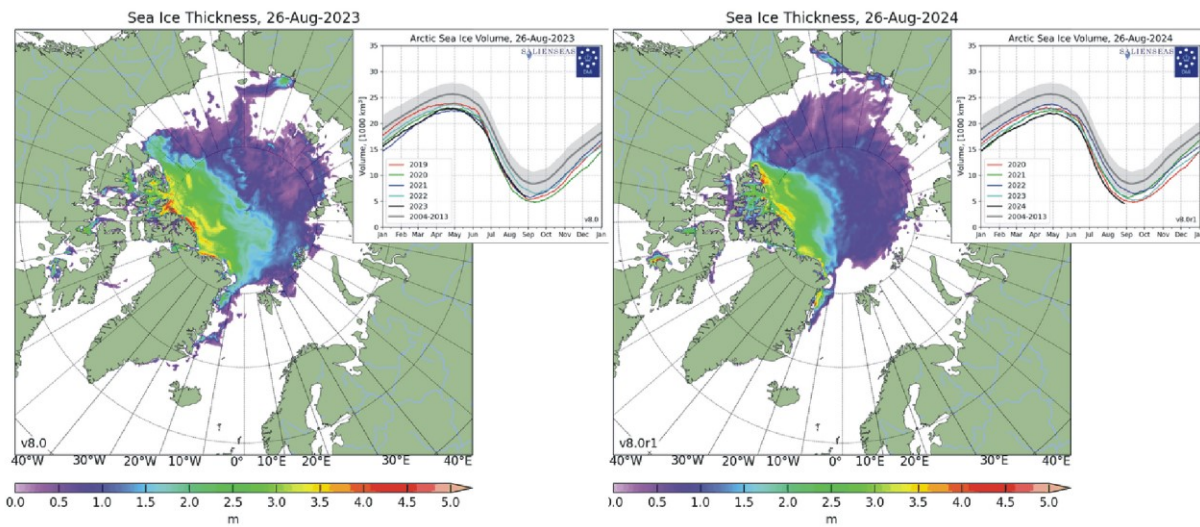


Diagram showing daily Arctic sea ice extent since November 1978, to 26 August 2024, data courtesy of [Japan Aerospace Exploration Agency \(JAXA\)](#).

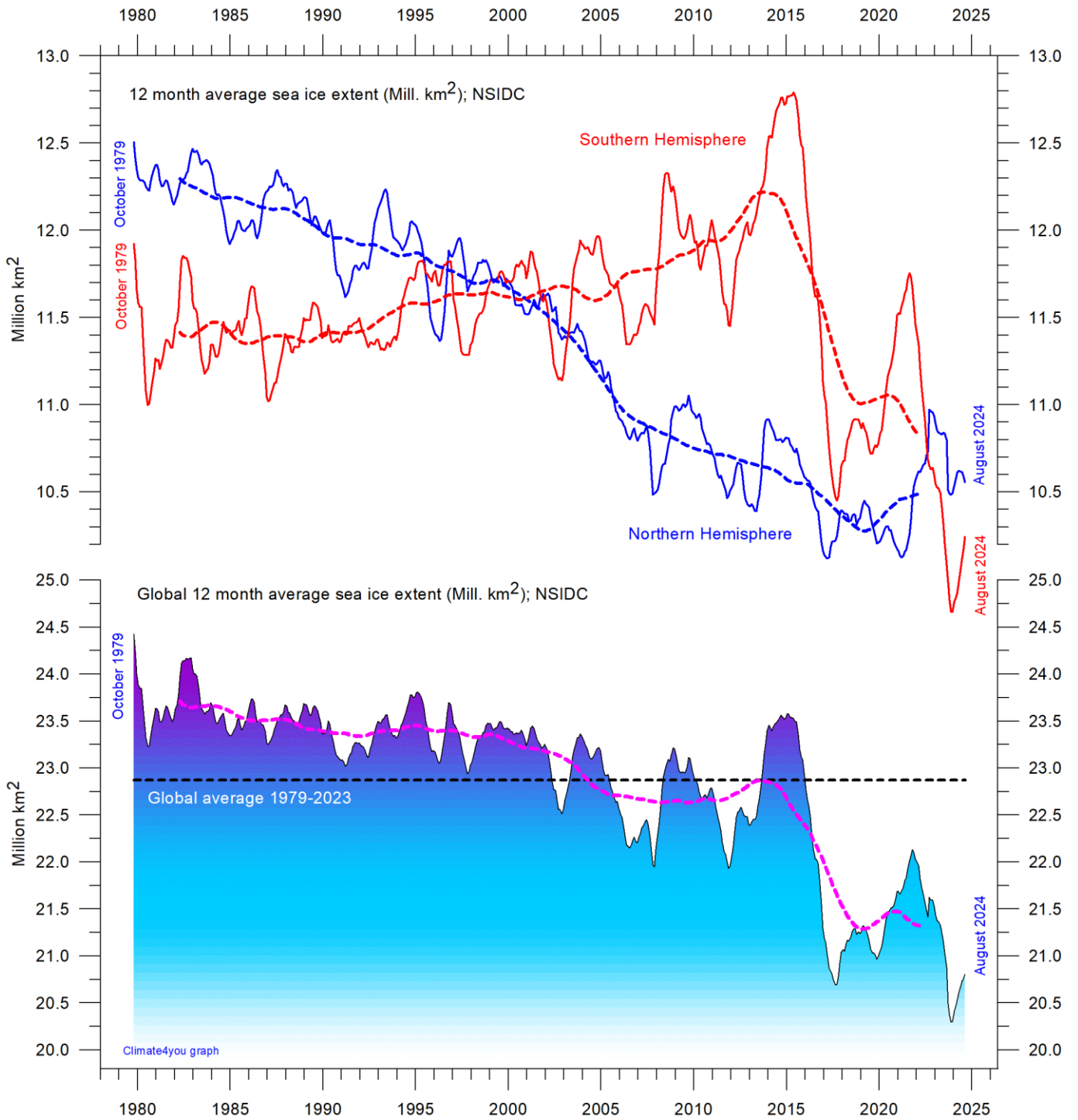
Sea Ice Thickness, 26-Aug-2024



37



Diagrams showing Arctic sea ice extent and thickness 26 August 2023 (left) and 2024 (right and above) and the seasonal cycles of the calculated total arctic sea ice volume, according to [The Danish Meteorological Institute \(DMI\)](https://www.dmi.dk/). The mean sea ice volume and standard deviation for the period 2004-2013 are shown by grey shading. Please note that DMI on 7 December 2021 changed their sea ice calculation model. DMI's description of the model version change can be read here: <http://polarportal.dk/en/sea-ice-and-icebergs/sea-ice-thickness-and-volume/>



12 month running average sea ice extension, global and in both hemispheres since 1979, the satellite-era. The October 1979 value represents the monthly 12-month average of November 1978 - October 1979, the November 1979 value represents the average of December 1978 - November 1979, etc. The stippled lines represent a 61-month (ca. 5 years) average. Data source: National Snow and Ice Data Center (NSIDC).

Sea level in general

Global (or eustatic) sea-level change is measured relative to an idealised reference level, the geoid, which is a mathematical model of planet Earth's surface (Carter et al. 2014). Global sea-level is a function of the volume of the ocean basins and the volume of water they contain. Changes in global sea-level are caused by – but not limited to - four main mechanisms:

1. Changes in local and regional air pressure and wind, and tidal changes introduced by the Moon.
2. Changes in ocean basin volume by tectonic (geological) forces.
3. Changes in ocean water density caused by variations in currents, water temperature and salinity.
4. Changes in the volume of water caused by changes in the mass balance of terrestrial glaciers.

In addition to these there are other mechanisms influencing sea-level, such as storage of ground water, storage in lakes and rivers, evaporation, etc.

Mechanism 1 is controlling sea-level at many sites on a time scale from months to several years. As an example, many coastal stations show a pronounced annual variation reflecting seasonal changes in air pressures and wind speed. Longer-term climatic changes playing out over decades or centuries will also affect measurements of sea-level changes. Hansen et al. (2011, 2015) provide excellent analyses of sea-level changes caused by recurrent changes of the orbit of the Moon and other phenomena.

Mechanism 2 – with the important exception of earthquakes and tsunamis - typically operates over long (geological) time scales and is not significant on human time scales. It may relate to variations in the seafloor spreading rate, causing volume changes in mid-ocean mountain ridges, and to the slowly changing configuration of land and oceans. Another effect may be the slow rise of basins due to isostatic offloading by deglaciation after an ice age. The floor of the Baltic Sea and the Hudson Bay are

presently rising, causing a slow net transfer of water from these basins into the adjoining oceans. Slow changes of excessively big glaciers (ice sheets) and movements in the mantle will affect the gravity field and thereby the vertical position of the ocean surface. Any increase of the total water mass as well as sediment deposition into oceans increase the load on their bottom, generating sinking by viscoelastic flow in the mantle below. The mantle flow is directed towards the surrounding land areas, which will rise, thereby partly compensating for the initial sea level increase induced by the increased water mass in the ocean.

Mechanism 3 (temperature-driven expansion) only affects the uppermost part of the oceans on human time scales. Usually, temperature-driven changes in density are more important than salinity-driven changes. Seawater is characterised by a relatively small coefficient of expansion, but the effect should however not be overlooked, especially when interpreting satellite altimetry data. Temperature-driven expansion of a column of seawater will not affect the total mass of water within the column considered and will therefore not affect the potential at the top of the water column. Temperature-driven ocean water expansion will therefore not in itself lead to any lateral displacement of water, but only locally lift the ocean surface. Near the coast, where people are living, the depth of water approaches zero, so no measurable temperature-driven expansion will take place here (Mörner 2015). Mechanism 3 is for that reason not important for coastal regions.

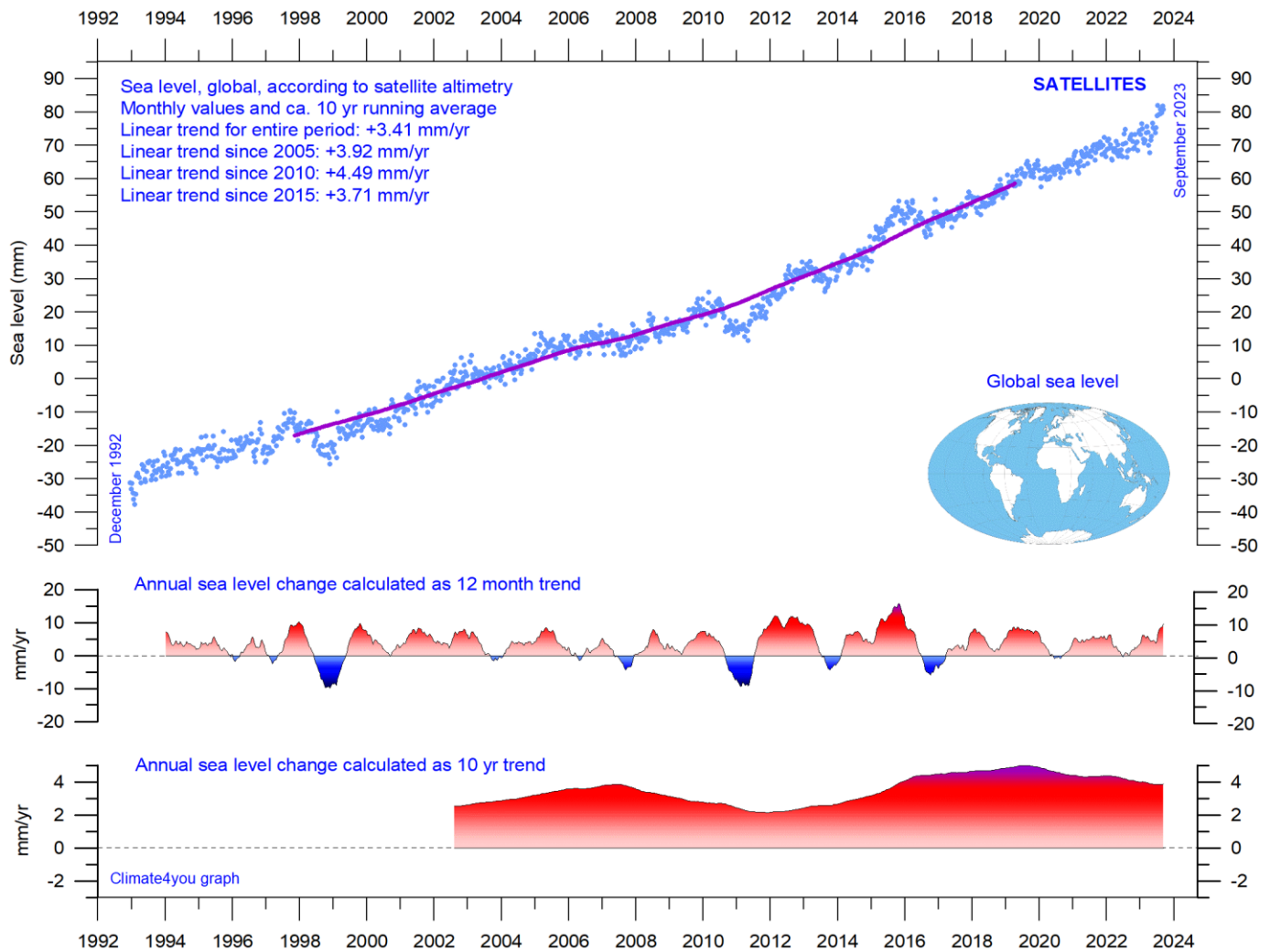
Mechanism 4 (changes in glacier mass balance) is an important driver for global sea-level changes along coasts, for human time scales. Volume changes of floating glaciers – ice shelves – has no influence on the global sea-level, just like volume changes of floating sea ice has no influence. Only the mass-balance of grounded or land-based glaciers is important for the global sea-level along coasts.

Summing up: Presumably, mechanism 1 and 4 are the most important for understanding sea-level changes along coasts.

References:

- Carter R.M., de Lange W., Hansen, J.M., Humlum O., Idso C., Kear, D., Legates, D., Mörner, N.A., Ollier C., Singer F. & Soon W. 2014. Commentary and Analysis on the Whitehead& Associates 2014 NSW Sea-Level Report. Policy Brief, NIPCC, 24. September 2014, 44 pp. <http://climatechangereconsidered.org/wp-content/uploads/2014/09/NIPCC-Report-on-NSW-Coastal-SL-9z-corrected.pdf>
- Hansen, J.-M., Aagaard, T. and Binderup, M. 2011. Absolute sea levels and isostatic changes of the eastern North Sea to central Baltic region during the last 900 years. *Boreas*, 10.1111/j.1502-3885.2011.00229.x. ISSN 0300–9483.
- Hansen, J.-M., Aagaard, T. and Huijpers, A. 2015. Sea-Level Forcing by Synchronization of 56- and 74-Year Oscillations with the Moon's Nodal Tide on the Northwest European Shelf (Eastern North Sea to Central Baltic Sea). *Journ. Coastal Research*, 16 pp.
- Mörner, Nils-Axel 2015. Sea Level Changes as recorded in nature itself. *Journal of Engineering Research and Applications*, Vol.5, 1, 124-129.

Global sea level from satellite altimetry, updated to September 2023



Global sea level since December 1992 according to the Colorado Center for Astrodynamics Research at University of Colorado at Boulder. The blue dots are the individual observations, and the purple line represents the running 121-month (ca. 10 year) average. The two lower panels show the annual sea level change, calculated for 1 and 10-year time windows, respectively. These values are plotted at the end of the interval considered. Compare with tide-gauge diagram on page 41.

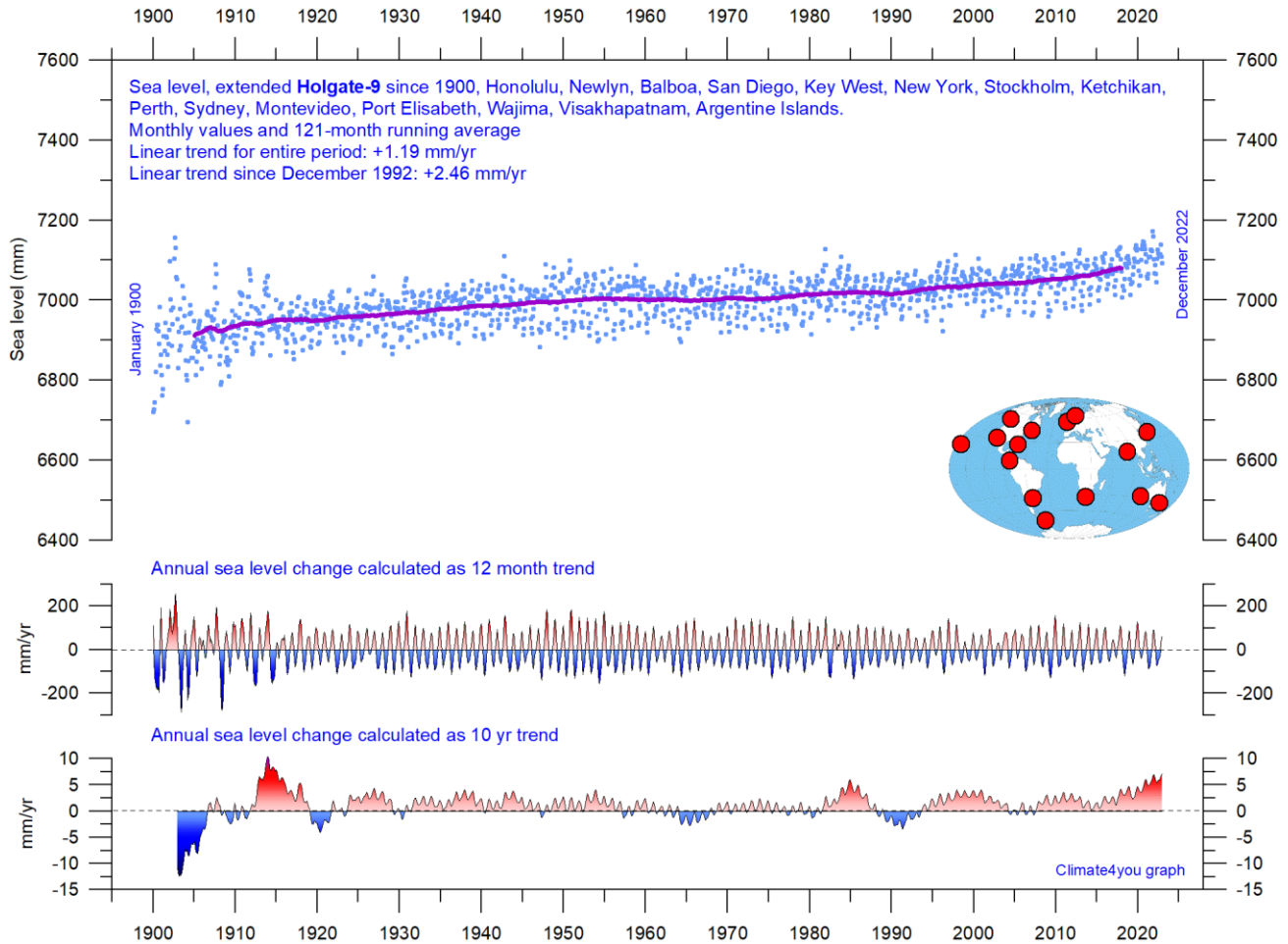
Ground truth is a term used in various fields to refer to information provided by direct observation as opposed to information provided by inference, such as, e.g., by satellite observations.

In remote sensing using satellite observations, ground truth data refers to information collected on location. Ground truth allows the satellite data to be related to real features observed on the planet surface. The collection of ground truth data enables calibration of remote-sensing data, and

aids in the interpretation and analysis of what is being sensed or recorded by satellites. Ground truth sites allow the remote sensor operator to correct and improve the interpretation of satellite data.

For satellite observations on sea level ground true data are provided by the classical tide gauges (example diagram on next page), that directly measures the local sea level many places distributed along the coastlines on the surface of the planet.

Global sea level from tide-gauges, extended Holgate-9, updated to December 2022



Extended Holgate-9 monthly tide-gauge data from PSMSL Data Explorer. Holgate (2007) suggested 9 stations to capture the global variability found in a larger number of stations over the last half century studied previously. However, some of the stations suggested by Holgate has not reported values for several years, leading to the southern hemisphere now being seriously underrepresented in his original data set. Therefore, in the above diagram several other long tide-gauge series have been included, to provide a more balanced representation of both hemispheres (15 stations in total). The blue dots are the individual average monthly observations, and the purple line represents the running 121-month (ca. 10 year) average. The two lower panels show the average annual sea level change, calculated for moving 1 and 10-year windows, respectively. These values are plotted at the end of the time window considered, month by month.

Data from tide-gauges all over the world suggest an average global sea-level rise of 1-2 mm/year, while the modern satellite-derived record (since 1992, page 40) suggest a rise of about 3.4 mm/year, or more. The difference between the two data sets is remarkable. It is however known that satellite observations are facing

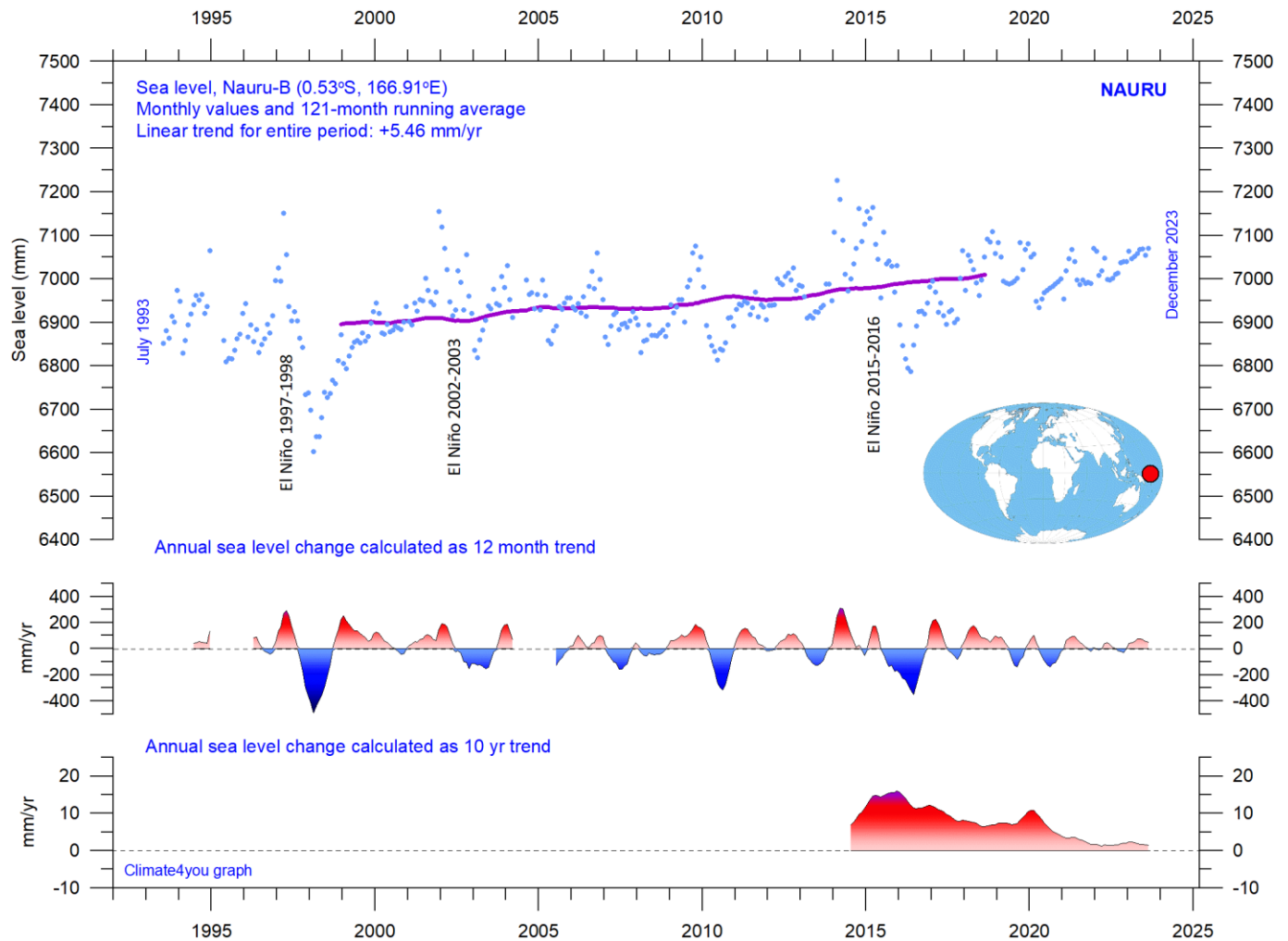
References:

Holgate, S.J. 2007. On the decadal rates of sea level change during the twentieth century. *Geophys. Res. Letters*, 34, L01602, doi:10.1029/2006GL028492

Vignudelli et al. 2019. Satellite Altimetry Measurements of Sea Level in the Coastal Zone. *Surveys in Geophysics*, Vol. 40, p. 1319–1349. <https://link.springer.com/article/10.1007/s10712-019-09569-1>

several complications in areas near the coast. Vignudelli et al. (2019) provide an updated overview of the current limitations of classical satellite altimetry in coastal regions. Since 2015 a sea level increase rate may be suggested by the above composite record.

This month's selected sea level station (tide-gauge): Nauru, western Pacific Ocean



Saint Helena monthly tide gauge data from [PSMSL Data Explorer](#). The blue dots are the individual monthly observations, and the purple line represents the running 121-month (ca. 10 yr) average. The two lower panels show the annual sea level change, calculated for 1 and 10 yr time windows, respectively. These values are plotted at the end of the interval considered.

Nauru

Nauru, officially the Republic of Nauru and previously known as Pleasant Island, is an island country and microstate in Oceania, western Central Pacific Ocean. The island is surrounded by a coral reef, which is exposed at low tide. With a surface area of only a 21 km², Nauru is the third-smallest country in the world after the Vatican City, and Monaco, making it the smallest republic. Additionally, its population of

10,670 is the world's second smallest, after the Vatican City.

Inhabited by people coming by boats from Micronesia and Polynesia c. 1000 BC, Nauru was annexed and claimed as a colony by the German Empire in the late 19th century. Following World War I, Nauru became a League of Nations mandate administered by Australia, New Zealand and the United Kingdom. During World War II, Nauru

became occupied by Japan, and was later bypassed by the Allied advance across the Pacific. After the war, the country entered into United Nations trusteeship. Nauru gained its independence in 1968, and became a member of the Pacific Community (SPC) in 1969. Nauru is a phosphate-rock island with rich deposits near the surface, which allowed easy strip mining operations. Its remaining phosphate resources are today not economically viable for further extraction.

If the observed relative sea level rise since July 1993 at Nauru continues, relative sea level (in relation to land) will have increased about 41 cm by year 2100. The effects of El Niño and subsequent La Niña episodes (diagram p.25) are clearly visible in the Nauru sea level record.

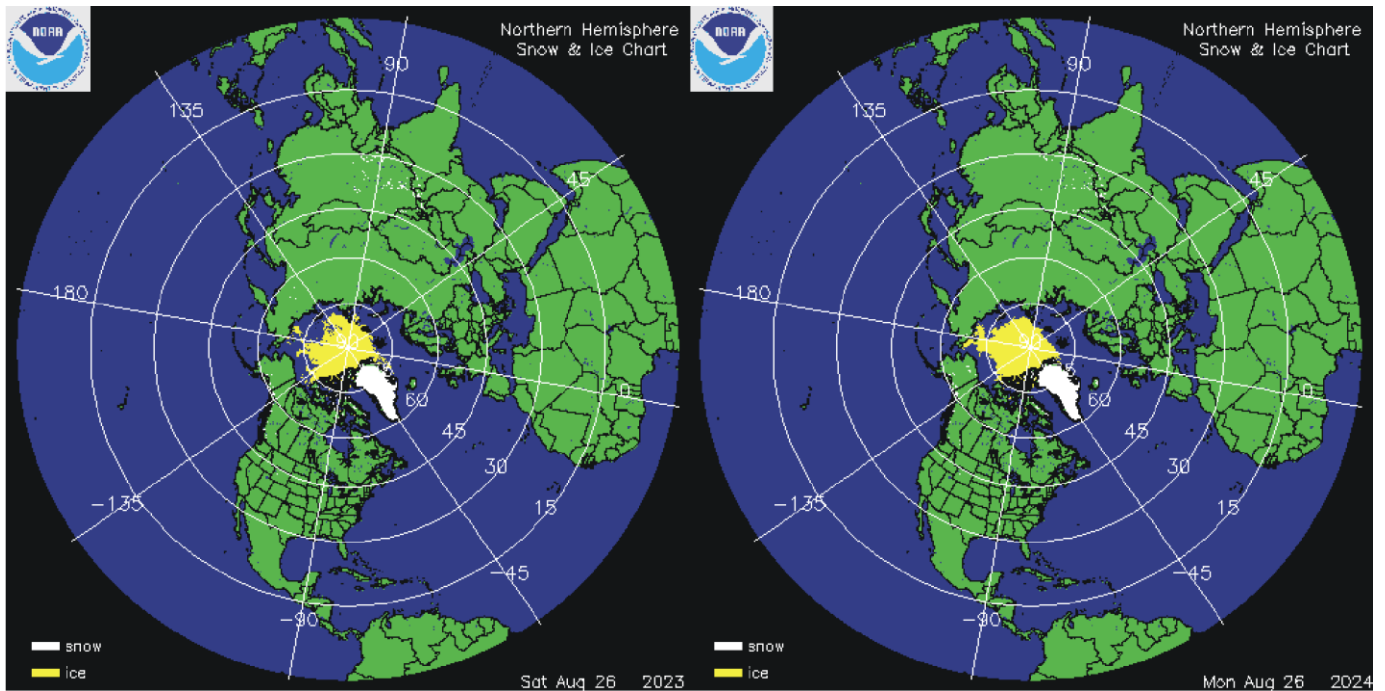
The Pacific Ocean

The Pacific Ocean (North and South) is the largest and deepest of Earth's oceans. It extends from the Arctic Ocean in the north to the Southern Ocean (north of Antarctica) in the south and is bounded by the continents of Asia and Australia in the west and the Americas in the east. It covers about 32% of planet Earth's total surface area, making it larger than all of Earth's land areas combined. Due to the effects of plate tectonics, the Pacific Ocean is currently shrinking horizontally by 2-3 cm per year on three sides, roughly averaging a surface loss of 0.5 km² a year. By contrast, the Atlantic Ocean is increasing in size.

The Pacific Ocean's name was coined by the Portuguese explorer Ferdinand Magellan during the Spanish circumnavigation of the world in year 1521, as he encountered favourable winds navigating this ocean. He therefore named it Mar Pacifico, which in both Portuguese and Spanish means "peaceful sea". However, the Pacific is not always peaceful. Often tropical storms batter the islands of the Pacific. Volcanoes are widespread around the Pacific Rim and often affected by earthquakes. Tsunamis, caused by underwater earthquakes, have devastated many islands and in some cases destroyed entire towns.

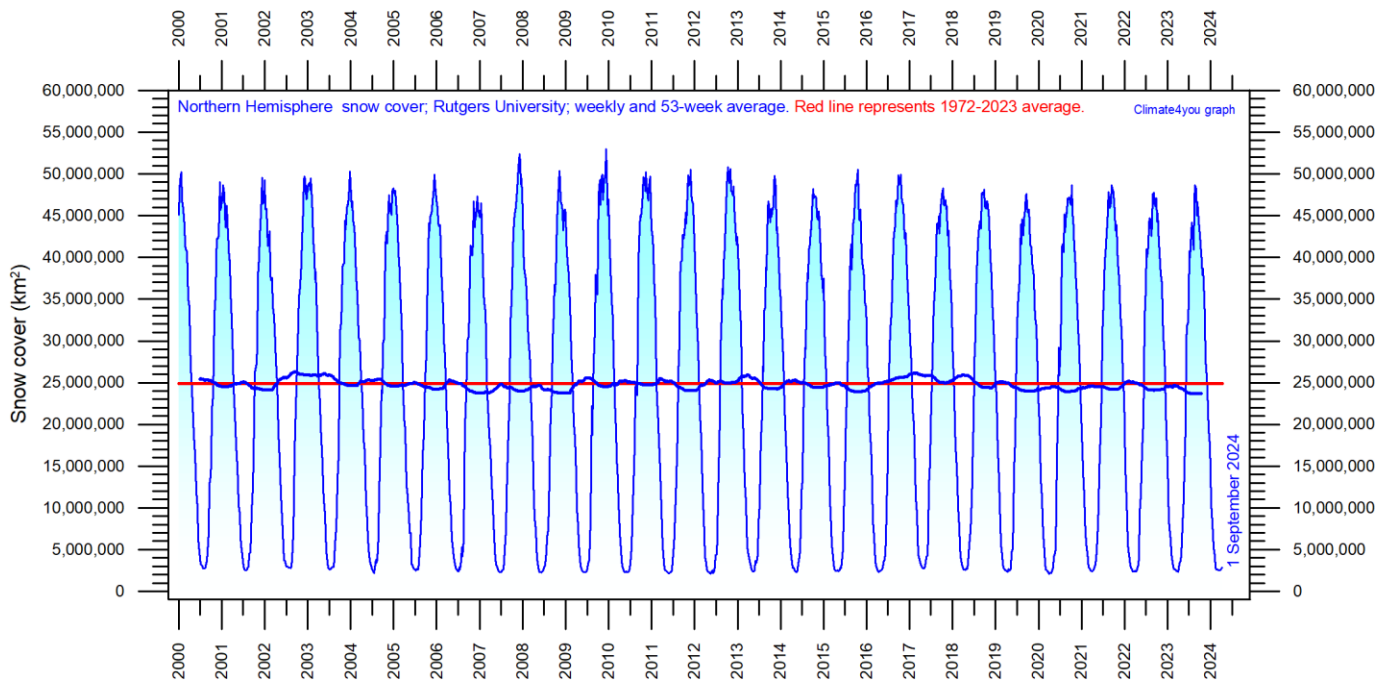
The South Pacific Ocean is the part of the bigger Pacific Ocean south of the Equator. The South Pacific Ocean contains the deepest point in the Southern Hemisphere, the Horizon Deep in the Tonga Trench, at 10,823 meters below the sea surface. Many islands in the South Pacific Ocean are of volcanic origin, and due to their high bedrock density, they will inevitably sink slowly because of crustal deformation. Several of these volcanic islands were eroded down to the former 120-130 m lower and long-lasting sea level during the Quaternary glaciations. The position and outline of several of these eroded and drowned volcanoes are today indicated at the ocean surface by fringing coral reefs, where colonies of reef building corals have been able to accommodate the about 120 m sea level rise since the maximum of the last glacial period, keeping pace with rising sea level by vertical growth and accretion. In the South Pacific Ocean, coral reefs are widespread north of 30°S.

Northern Hemisphere weekly and seasonal snow cover, updated to August 2024

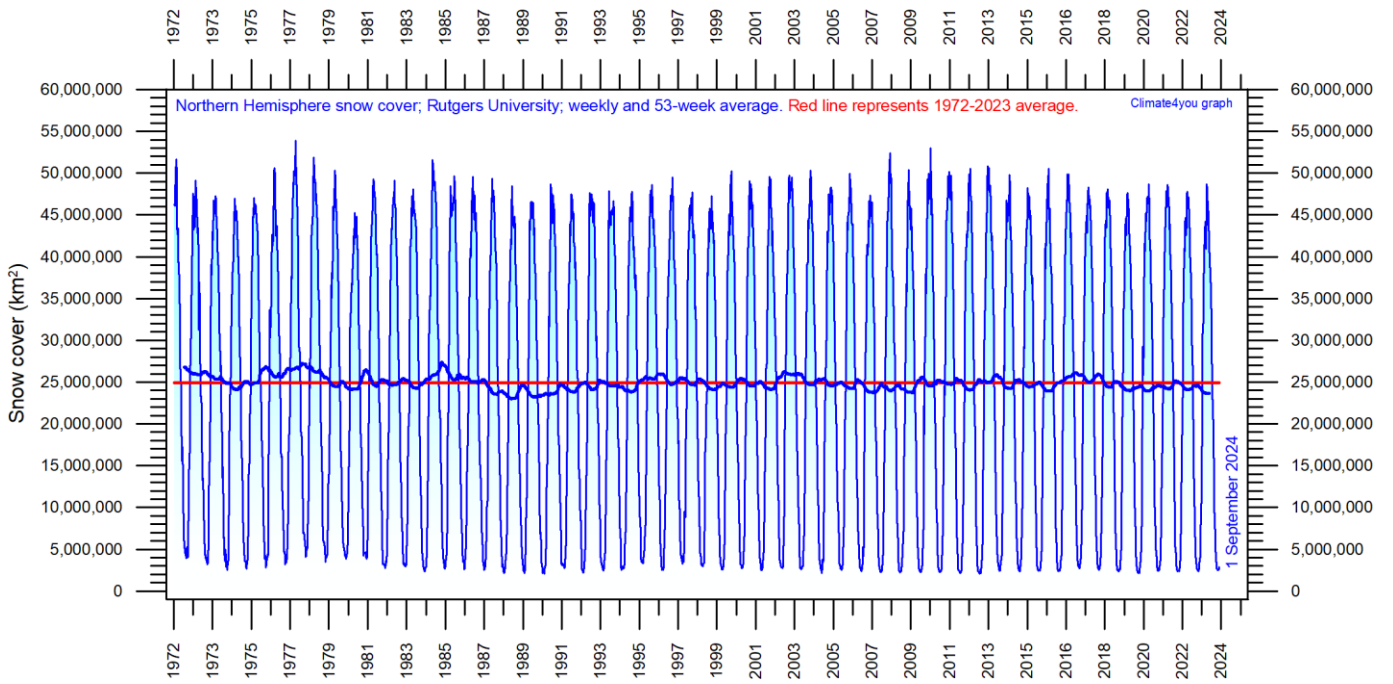


Northern hemisphere snow cover (white) and sea ice (yellow) 26 August 2023 (left) and 2024 (right). Map source: [National Ice Center \(NIC\)](#).

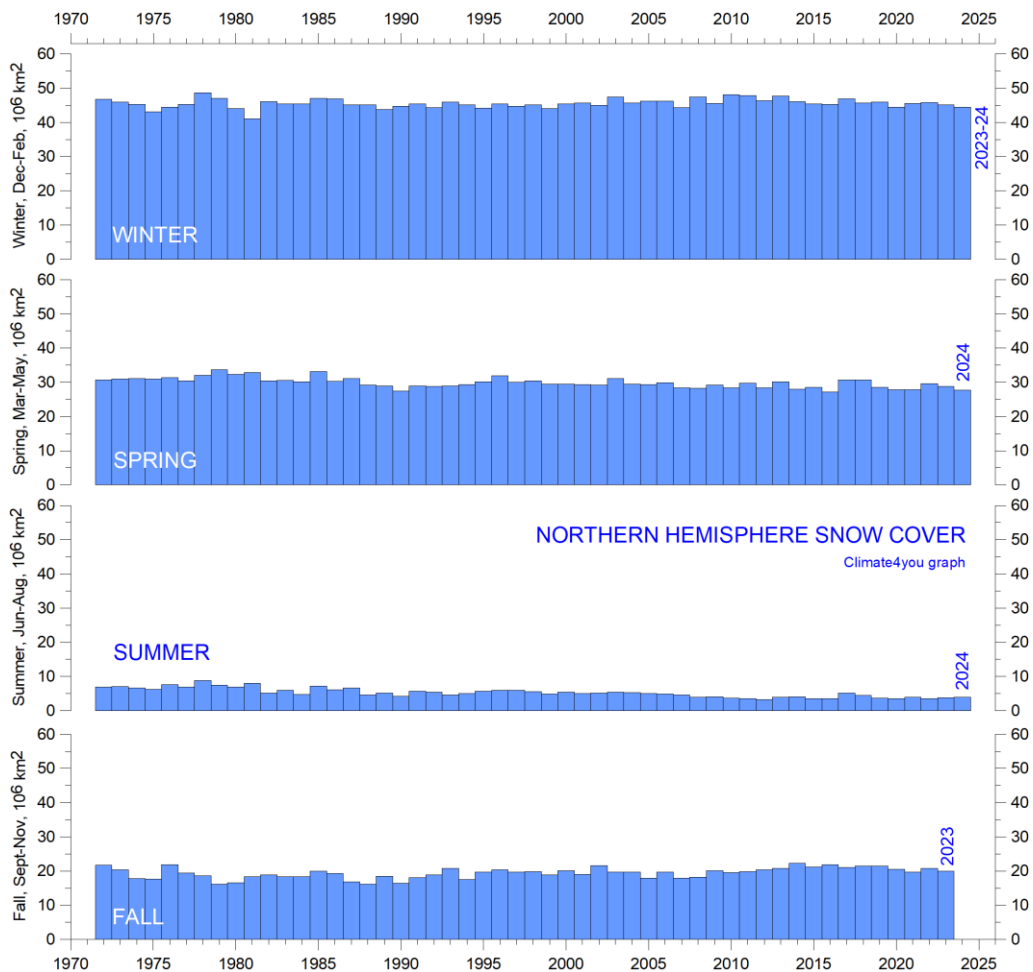
44



Northern hemisphere weekly snow cover since January 2000 according to Rutgers University Global Snow Laboratory. The thin blue line is the weekly data, and the thick blue line is the running 53-week average (approximately 1 year). The horizontal red line is the 1972-2023 average.



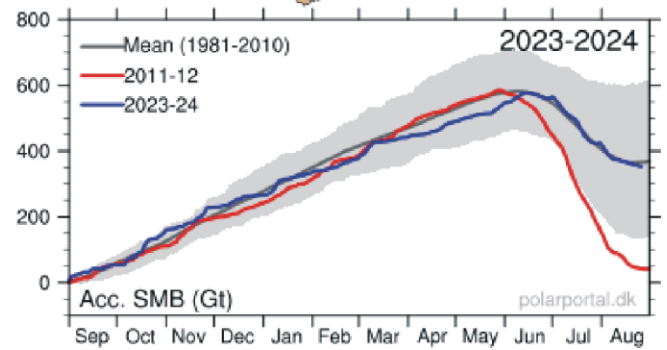
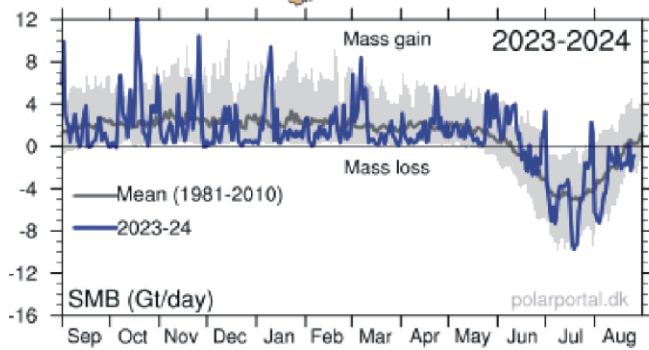
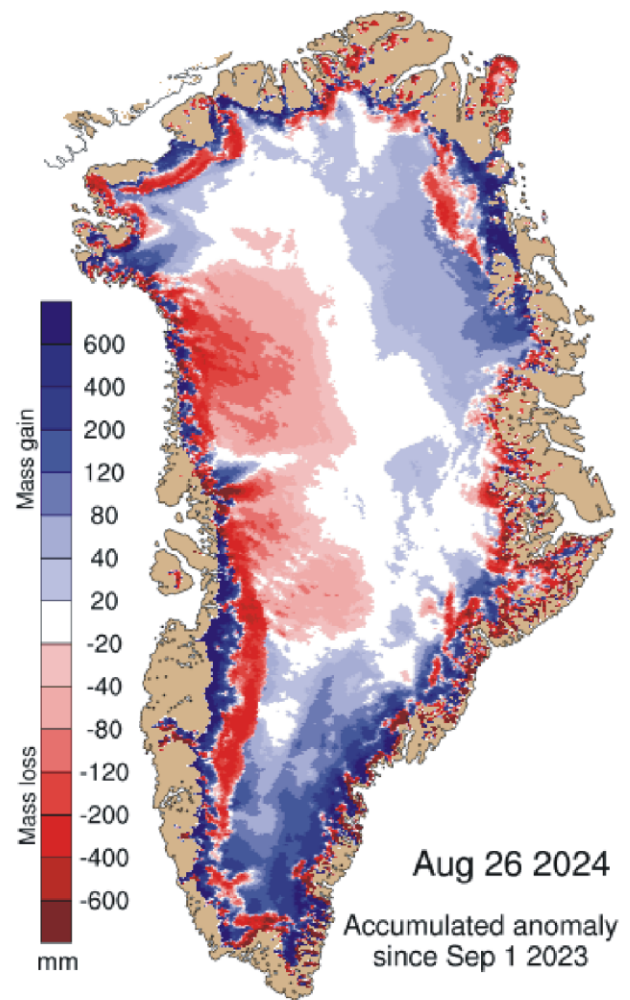
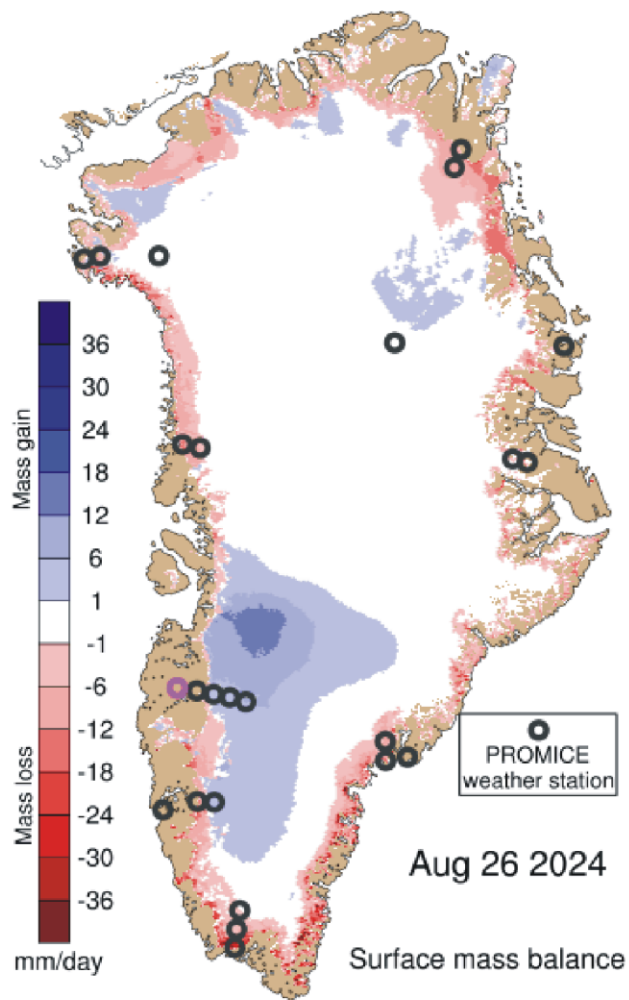
Northern hemisphere weekly snow cover since January 1972 according to Rutgers University Global Snow Laboratory. The thin blue line is the weekly data, and the thick blue line is the running 53-week average (approximately 1 year). The horizontal red line is the 1972-2023 average.



Northern hemisphere seasonal snow cover since January 1972 according to Rutgers University Global Snow Laboratory.

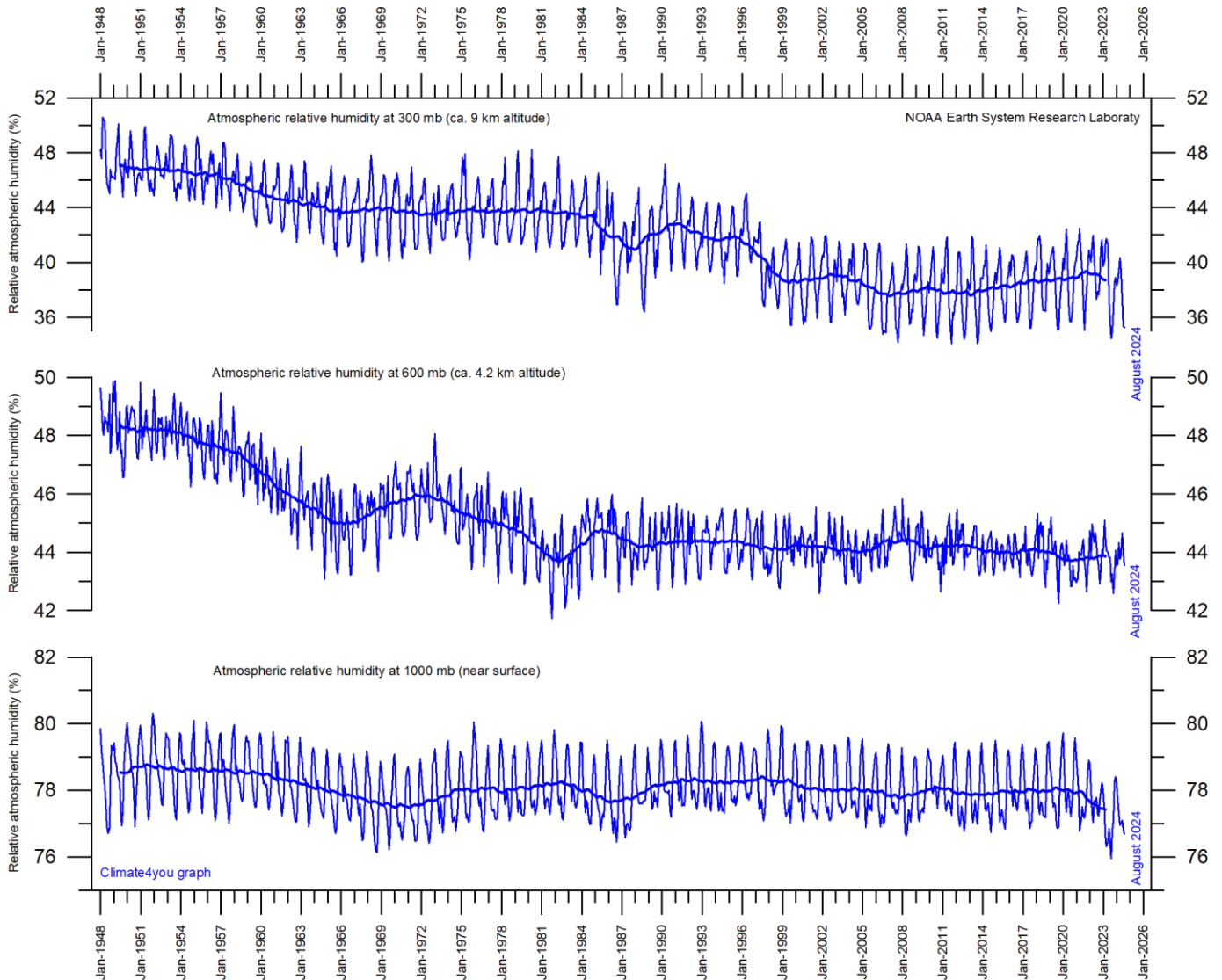
Greenland Ice Sheet net surface mass balance, updated to August 2024

46

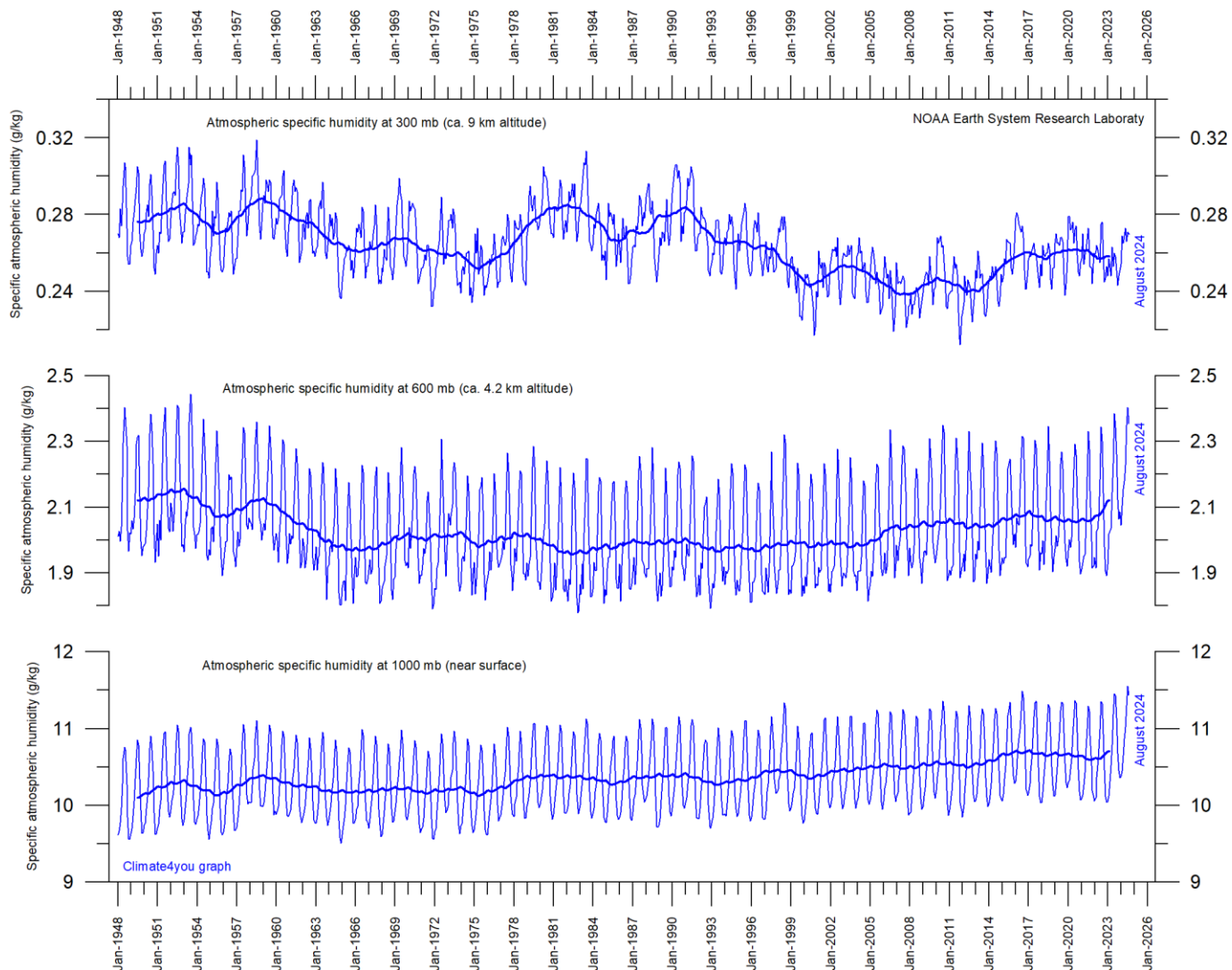


Left: Surface mass balance 29 July 2024. Right: Net surface mass balance anomaly since September 1, 2023. Courtesy of Danish Meteorological Institute (DMI).

Atmospheric relative and specific humidity, updated to August 2024



[Relative atmospheric humidity](#) (g/kg) at three different altitudes in the lower part of the atmosphere ([the Troposphere](#)) since January 1948 ([Kalnay et al. 1996](#)). The thin blue lines show monthly values, while the thick blue lines show the running 37-month average (about 3 years). Data source: [Earth System Research Laboratory \(NOAA\)](#).



[Specific atmospheric humidity](#) (g/kg) at three different altitudes in the lower part of the atmosphere ([the Troposphere](#)) since January 1948 ([Kalnay et al. 1996](#)). The thin blue lines show monthly values, while the thick blue lines show the running 37-month average (about 3 years). Data source: [Earth System Research Laboratory \(NOAA\)](#).

Water vapor is the most important greenhouse gas in the Troposphere. The highest concentration is found within a latitudinal range from 50°N to 60°S. The two polar regions of the Troposphere are comparatively dry.

Climate models assume that the atmosphere during a CO₂ induced warming should display rising specific humidity but maintain a constant relative humidity.

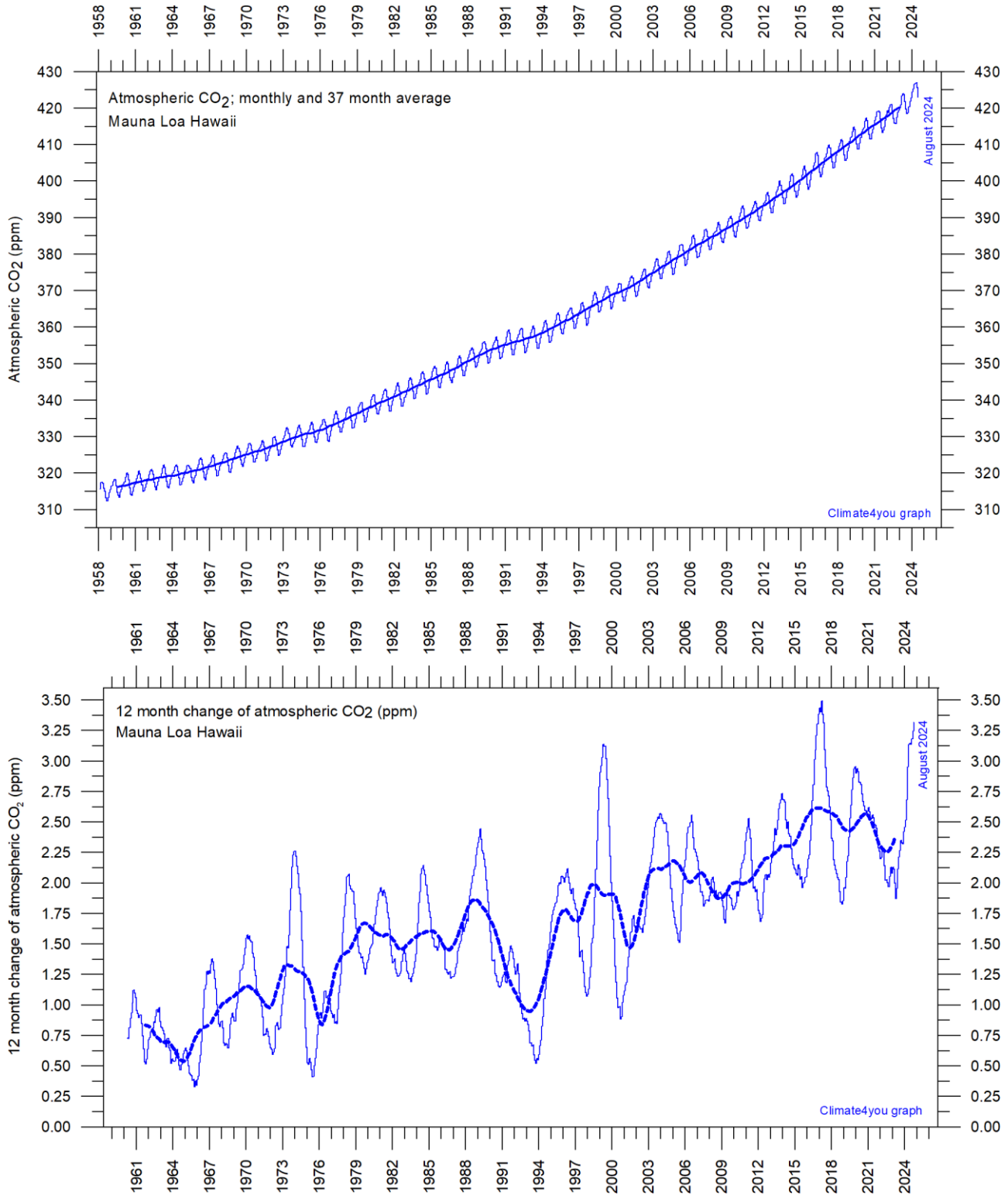
The diagram above shows the specific atmospheric humidity to be stable or slightly increasing up to about 4-5 km altitude. At higher levels in the Troposphere (about 9 km), the specific humidity has been decreasing for the

duration of the record (since 1948), although with shorter variations superimposed on the falling trend.

The persistent decrease in specific humidity at about 9 km altitude is particularly noteworthy, as this altitude roughly corresponds to the level where the theoretical temperature effect of increased atmospheric CO₂ is expected initially to play out. In contrast, climate models assume specific humidity to increase at this height.

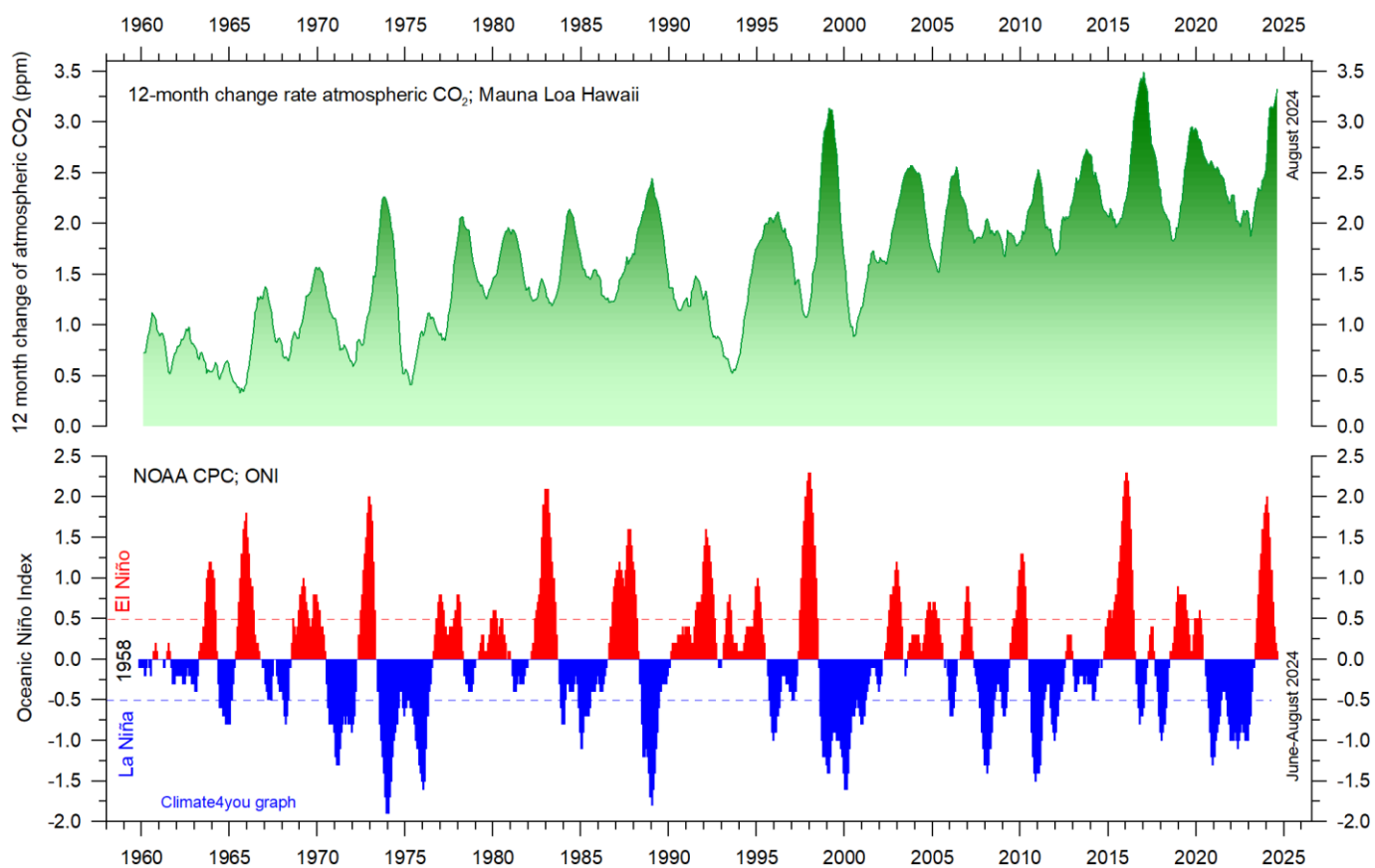
A Fourier frequency analysis (not shown here) suggests these changes are influenced, not only by the significant annual variation, but feasibly also by a longer variation of about 35-years' duration.

Atmospheric CO₂, updated to August 2024



Monthly amount of atmospheric CO₂ (upper diagram) and annual growth rate (lower diagram); average last 12 months minus average preceding 12 months, thin line) of atmospheric CO₂ since 1959, according to data provided by the [Mauna Loa Observatory](#), Hawaii, USA. The thick, stippled line is the simple running 37-observation average, nearly corresponding to a running 3-year average. A Fourier frequency analysis (not shown here) shows the 12-month change of Tropospheric CO₂ to be influenced especially by periodic variations of 2.5- and 3.8-years' duration.

The relation between annual change of atmospheric CO₂ and La Niña and El Niño episodes, updated to August 2024



Visual association between annual growth rate of atmospheric CO₂ (upper panel) and Oceanic Niño Index (lower panel). See also diagrams on page 47 and 25, respectively.

Changes in the global atmospheric CO₂ is seen to vary roughly in concert with changes in the Oceanic Niño Index. The typical sequence of events is that changes in the global atmospheric CO₂ to a certain degree follows changes in the Oceanic Niño Index, but clearly not in all details. Many processes, natural as well as anthropogenic, controls the amount of atmospheric CO₂, but oceanographic processes are clearly particularly important (see also diagram on next page).

Atmospheric CO₂ and the recent coronavirus pandemic

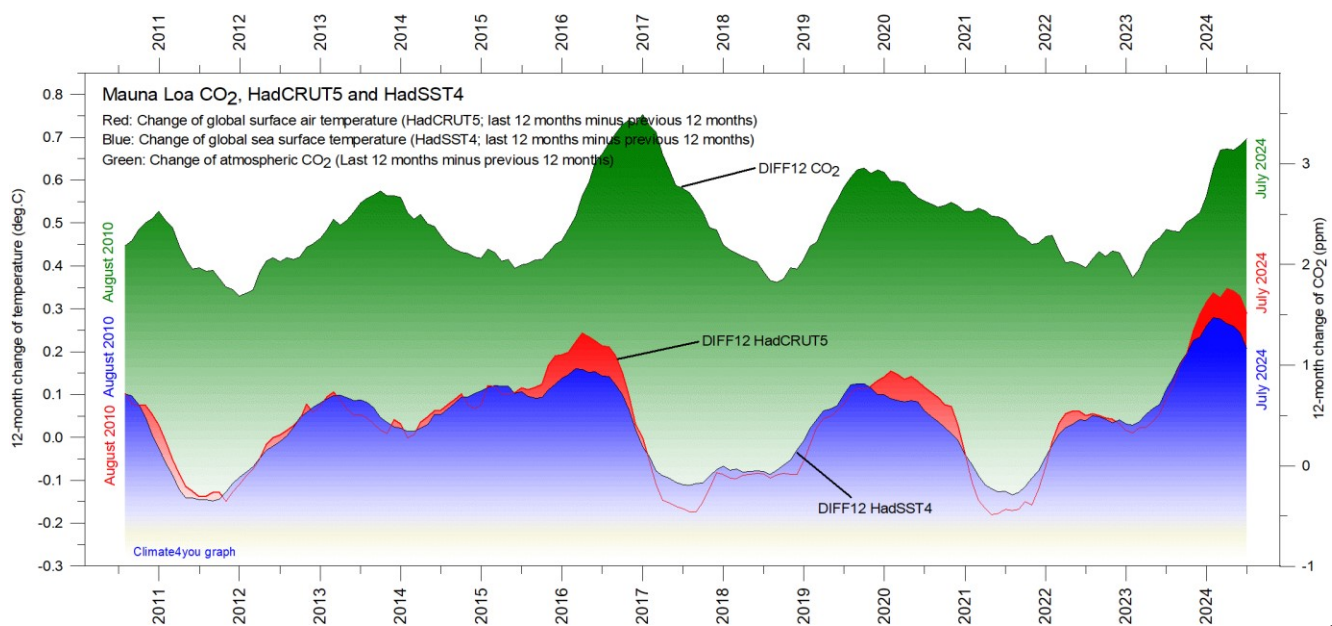
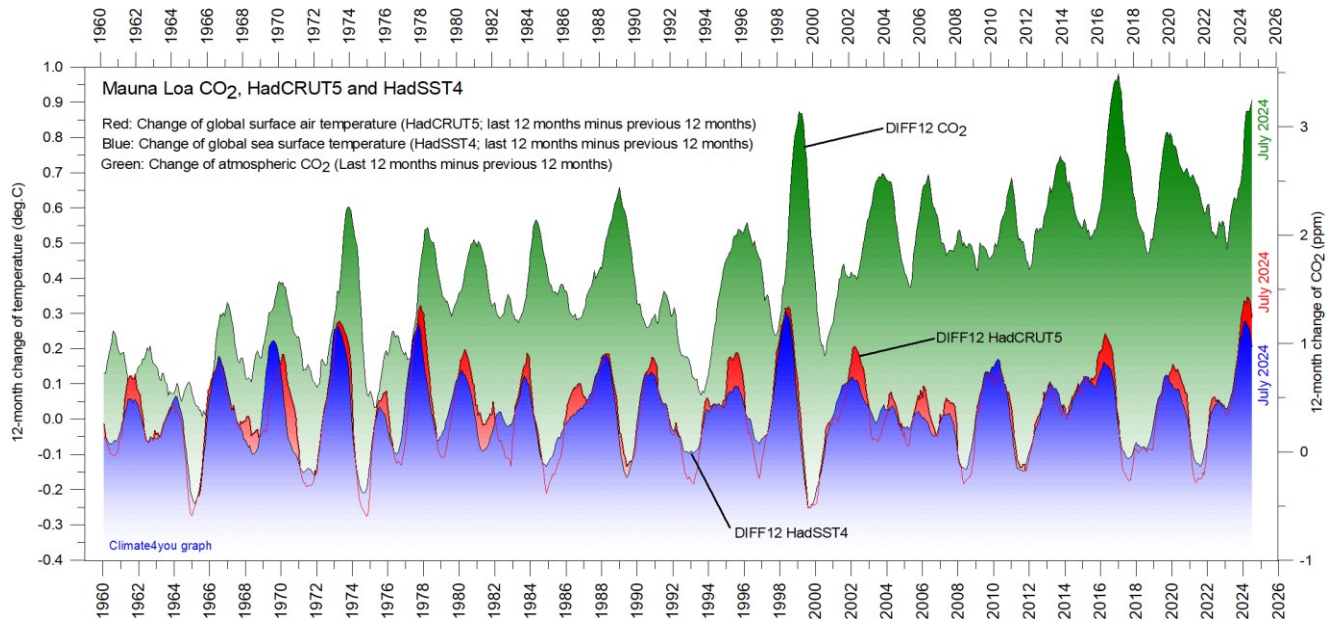
Modern political initiatives usually assume the human influence (mainly the burning of fossil fuels) to represent

the core reason for the observed increase in atmospheric CO₂ since 1958 (diagrams on page 47).

The coronavirus pandemic since January 2020 resulted in a marked reduction in the global consumption of fossil fuels. It is therefore enlightening to follow the effect of this reduction on the amount of atmospheric CO₂.

However, there is still no clear effect to be seen of the above reduction in release of CO₂ from fossil fuels. Presumably, the main explanation for this is that the human contribution is too small compared to the numerous natural sources and sinks for atmospheric CO₂ to appear in diagrams showing the amount of atmospheric CO₂.

The phase relation between atmospheric CO₂ and global temperature, updated to July 2024



12-month change of global atmospheric CO₂ concentration ([Mauna Loa](#); green), global sea surface temperature ([HadSST4](#); blue) and global surface air temperature ([HadCRUT5](#); red dotted). Entire data series since 1958 in upper figure, and last 15 years in lower figure, to enhance modern dynamics. All graphs are showing monthly values of DIFF12, the difference between the average of the last 12 month and the average for the previous 12 months for each data series.

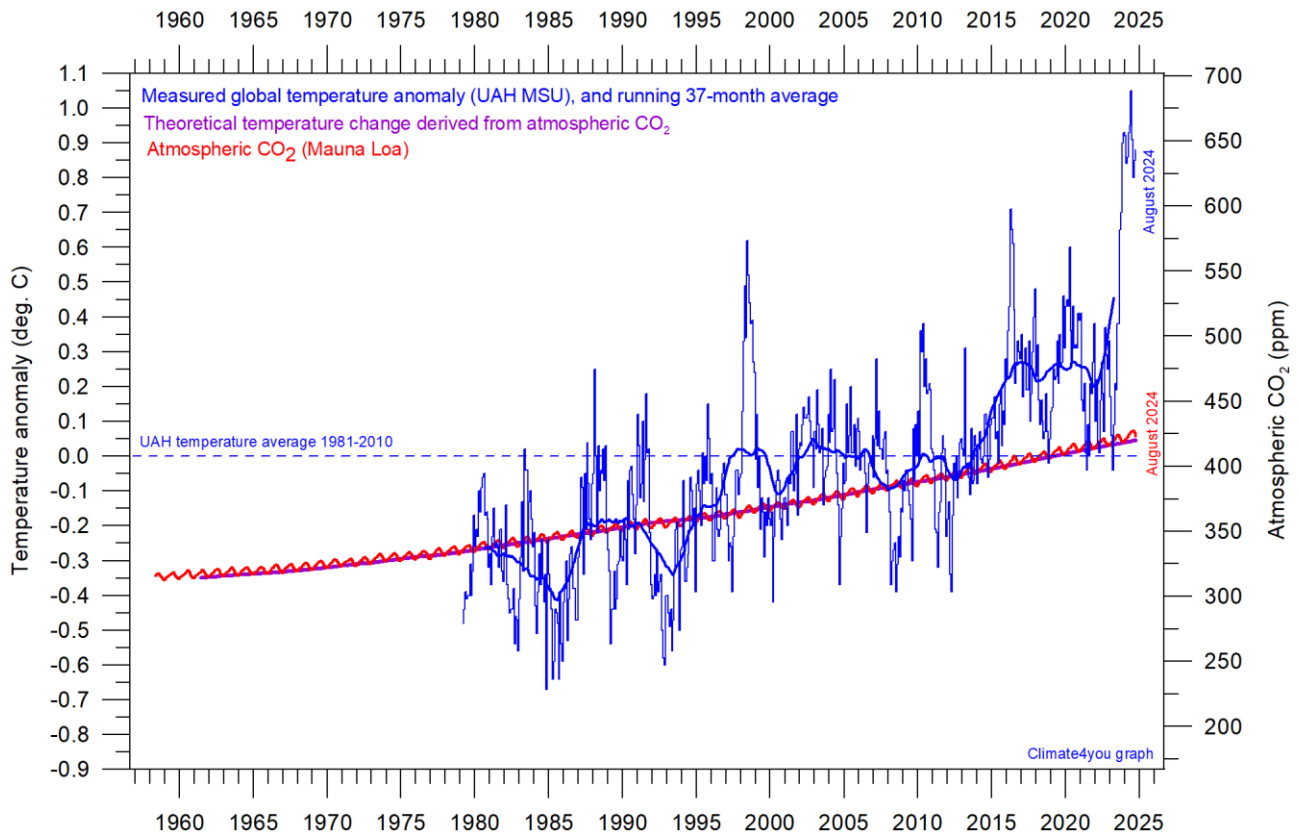
The typical sequence of events is seen to be that changes in the global atmospheric CO₂ follow changes in global surface air temperature, which again follow changes in global ocean surface temperatures. Thus, changes in global

atmospheric CO₂ usually are lagging 9.5–10 months behind changes in global air surface temperature, and 11–12 months behind changes in global sea surface temperature.

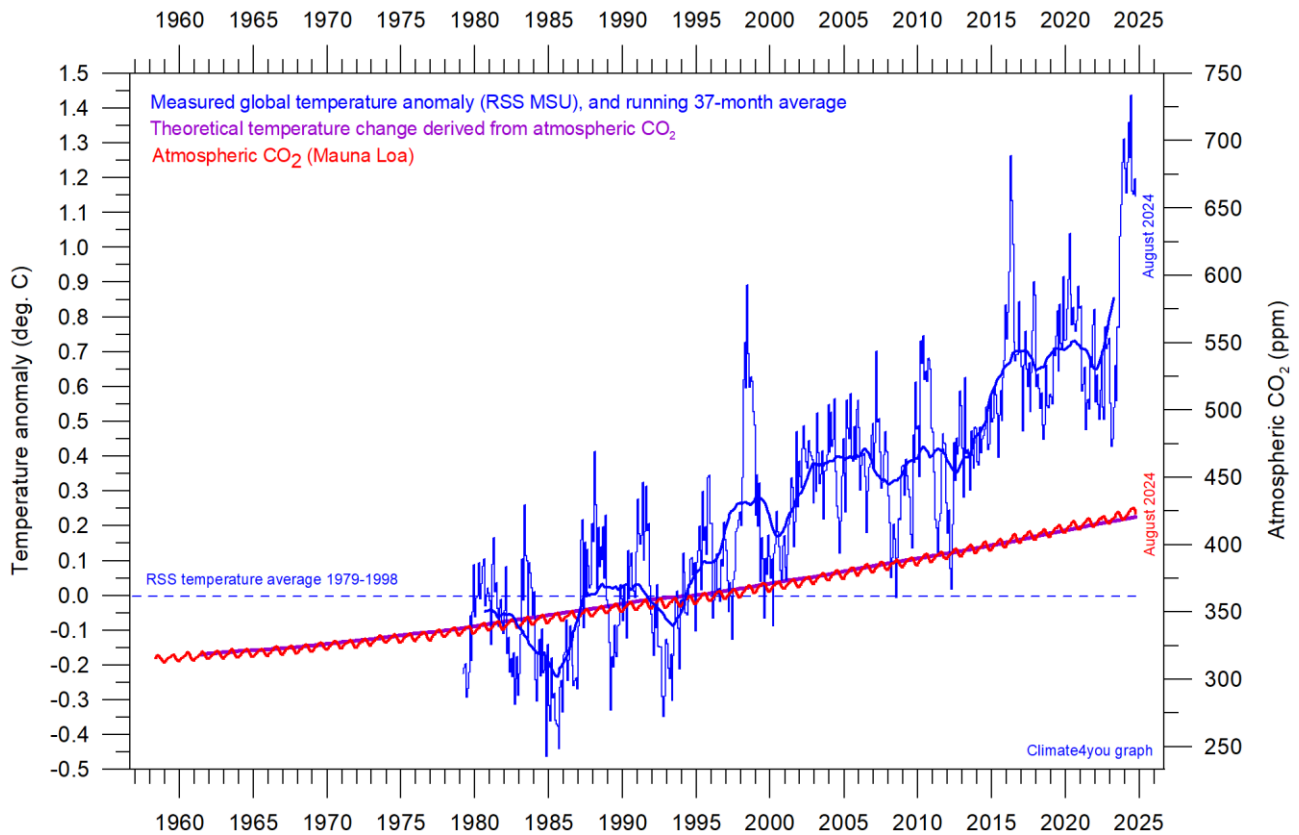
Reference: Humlum, O., Stordahl, K. and Solheim, J-E. 2012. The phase relation between atmospheric carbon dioxide and global temperature. *Global and Planetary Change*, August 30, 2012.

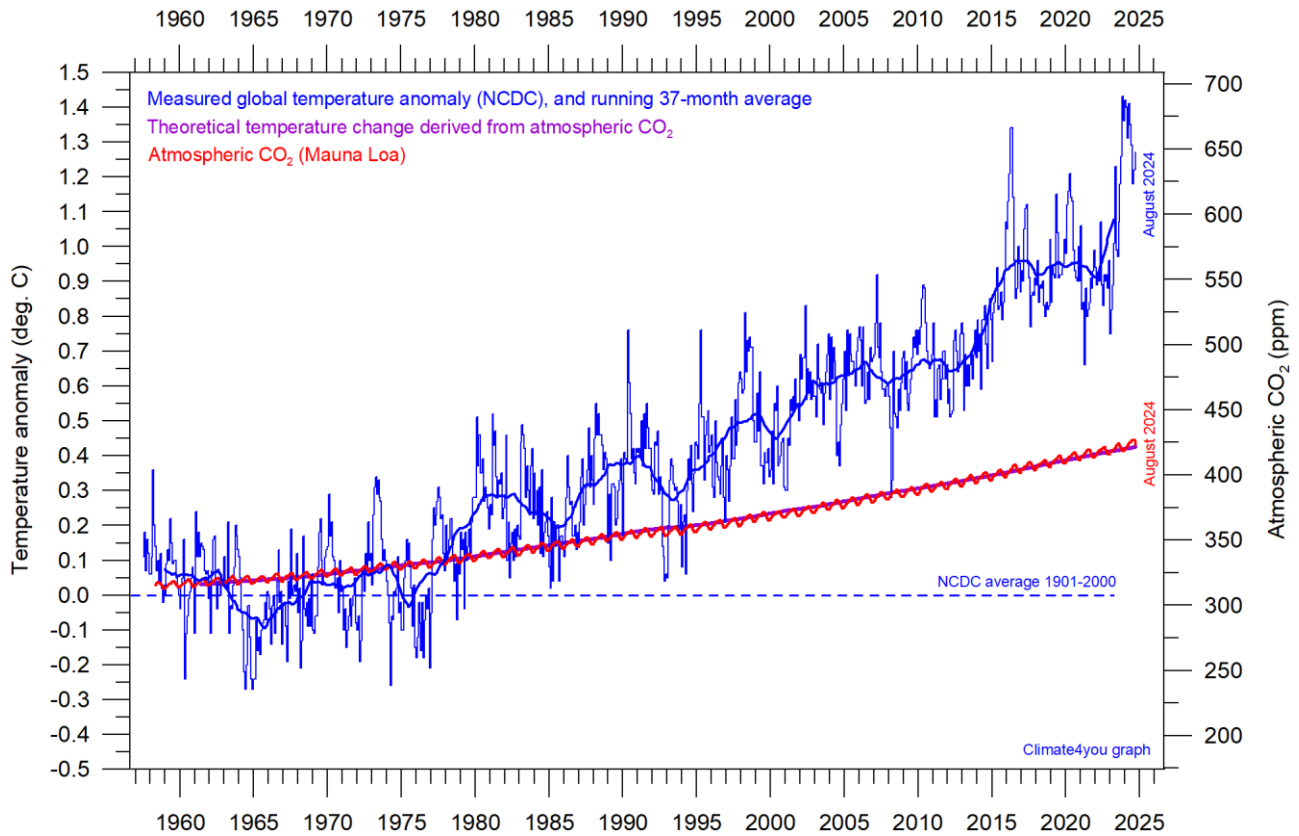
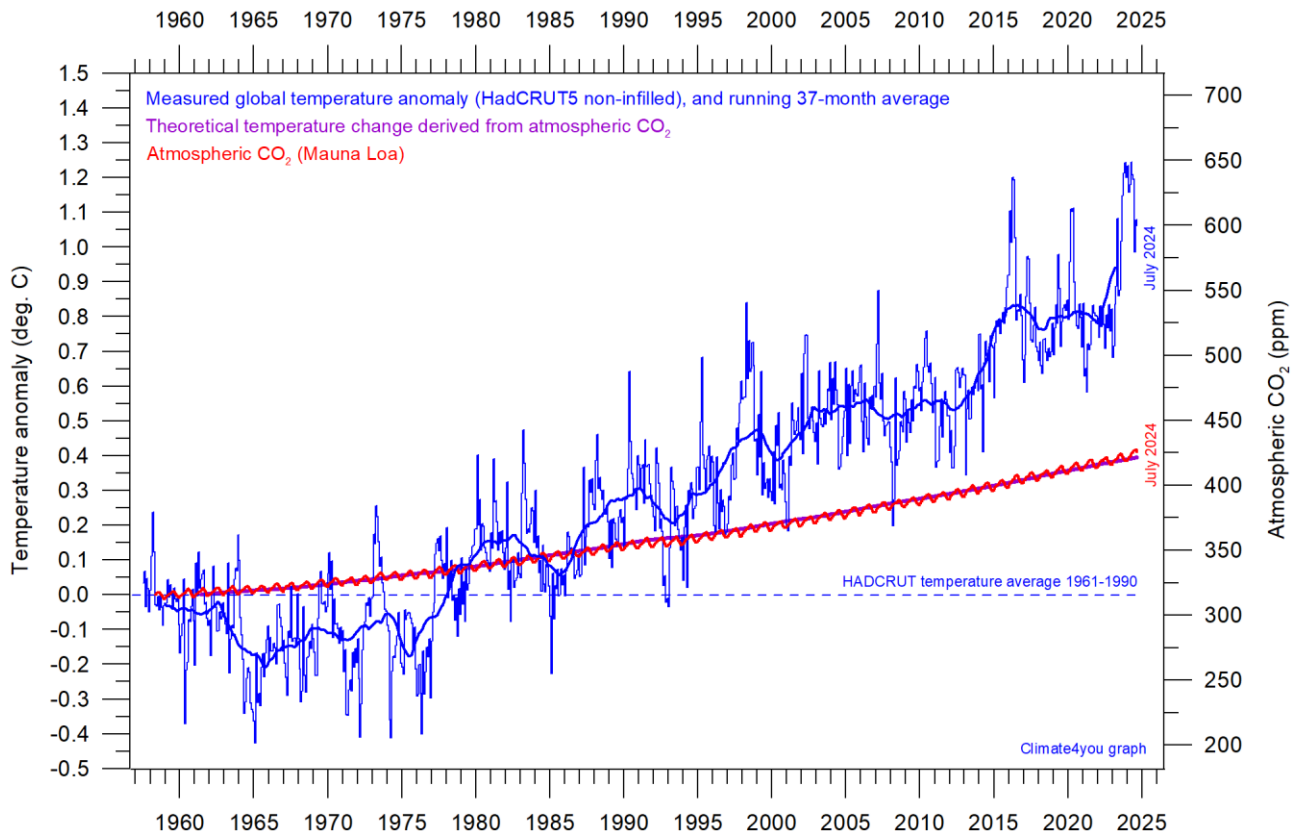
<http://www.sciencedirect.com/science/article/pii/S0921818112001658?v=s5>

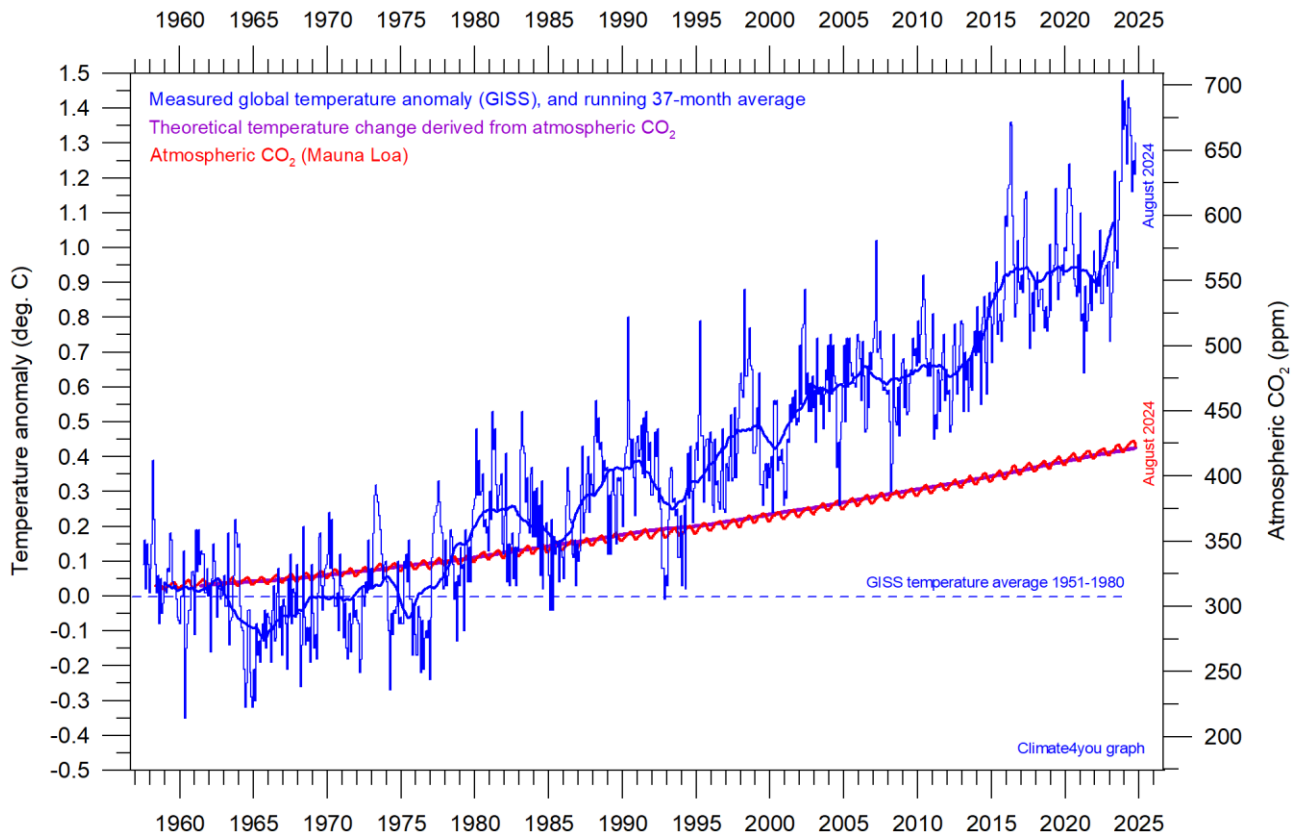
Global air temperature and atmospheric CO₂, updated to August 2024



52







Diagrams showing UAH, RSS, HadCRUT5, NCDC and GISS monthly global air temperature estimates (blue) and the monthly atmospheric CO₂ content (red) according to the [Mauna Loa Observatory](#), Hawaii. Purple line (running along red CO₂ curve) shows theoretical temperature change due to changing atmospheric CO₂. The Mauna Loa data series begins in March 1958, and 1958 was therefore chosen as starting year for all diagrams above. Reconstructions of past atmospheric CO₂ concentrations (before 1958) are not incorporated in this diagram, as such past CO₂ values are derived by other means (ice cores, stomata, or older measurements using different methodology), and therefore are not directly comparable with direct atmospheric measurements.

From a theoretical point of view, it is generally agreed that the atmospheric temperature effect ΔT of increasing atmospheric CO₂ may be expressed as (see, e.g. Myhre et al. 1998 and IPCC Third Assessment Report, section 6.1):

$$\Delta T = \Delta F * \lambda$$

where $\Delta F = 5,35 \ln(C1/Co)$ W/m², and where Co and C1 indicates the concentration of atmospheric CO₂ at the beginning and end of the time interval considered. The factor λ is a so-called climate sensitivity parameter (expressing the global mean surface temperature response to the imposed radiative CO₂ forcing). This factor has been determined to about 0,26°CW⁻¹m². The relation shows that as the concentration of atmospheric CO₂ increases, its

theoretical greenhouse effect increases in a logarithmic fashion, not linear. Therefore, for each increase in CO₂ concentration, the effect on temperature is smaller and smaller.

If all other effects in the real world are ignored, the above relation shows that any doubling of atmospheric CO₂ concentration produces a temperature increase of nearly 1°C (0.96°C), no matter how high the initial concentration of CO₂.

The purple line in the above diagrams (p.50-52) is calculated using the observed concentration of atmospheric CO₂ since March 1958. The axis for CO₂ is adjusted to show overlap between CO₂ (red) and the

calculated accumulated temperature effect (purple). In all graphs, the temperature anomaly axis has been adjusted to position the initial calculated effect of CO₂ roughly at the average for the beginning of the observed temperature graph (blue). This is done to make it possible to compare the theoretical CO₂ temperature development (purple) with the observed development (blue).

All these diagrams show the observed temperature development to be much more complicated than the theoretical development from atmospheric CO₂ alone. With exception of the UAH diagram, the overall observed temperature increases since 1958 is much larger than calculated from CO₂ alone. In addition, the observed temperature development is characterised by recurrent intervals characterised by increasing and decreasing temperatures, respectively, a development extremely different from the calculated temperature (purple graph). Clearly many other factors than only CO₂ is in control of the real-world atmospheric temperature.

At today's CO₂ atmospheric concentration (about 426 parts per million; see diagram on p.49), CO₂ has little ability to absorb additional heat and is therefore only a weak greenhouse gas. Previously, at lower atmospheric concentrations CO₂ was a stronger greenhouse gas, relative to other greenhouse gasses. At today's concentration, however, its ability to warm the planet at higher concentration levels is small. Thus, the often-cited assumption that carbon dioxide is the main driver of climate change is not correct in year 2024.

Nevertheless, in contrast to the above real-world observations, climate models are programmed to give the greenhouse gas carbon dioxide CO₂ a leading role on control on the global air temperature. The fact that the observed real-world temperature has been changing much more than expected just from CO₂, is usually ascribed to an added greenhouse effect of atmospheric water vapour in the upper Troposphere, the concentration of which by the models is expected to increase along with CO₂ (see, e.g. Schneider et. al. 1999).

However, measurements of water vapour in the upper Troposphere apparently show this assumption to be mistaken (see, e.g., diagrams on p.47-48). Therefore, the quite substantial difference between modelled and observed atmospheric temperature must be caused by other factors (see, e.g., Koutsoyiannis and Vournas 2023). In addition, the very dynamic change pattern displayed by the observed temperature also needs to be explained before a sound understanding of global climate dynamics can be claimed.

All temperature-CO₂ diagrams (p.52-54) shows both atmospheric temperature and atmospheric CO₂ to be increasing since 1959. However, this fact does not demonstrate that temperature is controlled by CO₂. In fact, it might just as well demonstrate the opposite relation (temperature controlling CO₂), or, that both temperature and CO₂ is controlled by a third factor. See also diagrams on page 51.

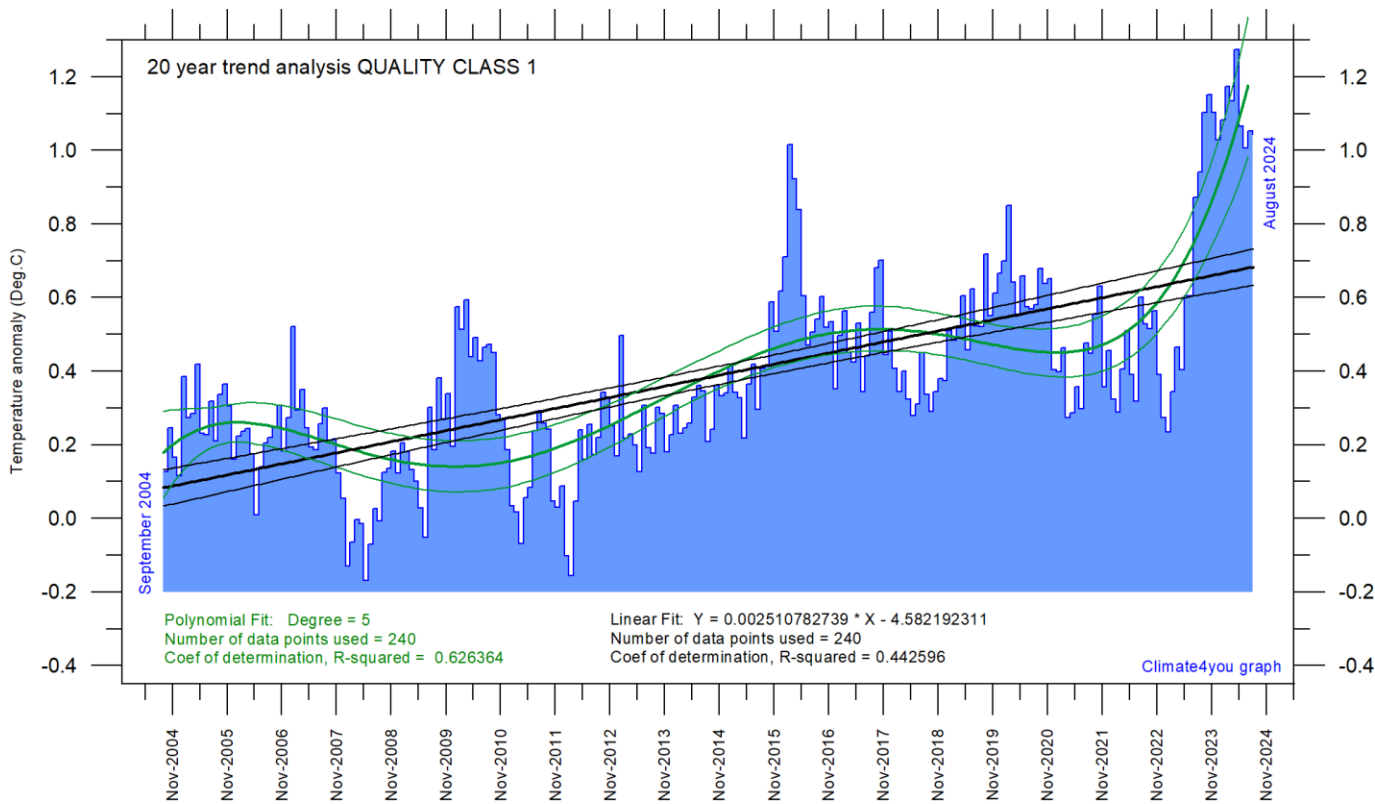
Litterature:

Demetris Koutsoyiannis & Christos Vournas 2023. *Revisiting the greenhouse effect – a hydrological perspective*. Hydrological Sciences Journal, doi: 10.1080/02626667.2023.2287047

Myhre, G., E. Highwood, K. Shine, and F. Stordal 1998. *New estimates of radiative forcing due to well mixed greenhouse gases*, Geophys. Res. Lett., 25(14), 2715–2718, doi:10.1029/98GL0190

Schneider, E.K., Kirtman, B.P., and Lindzen, R.S. 1999. *Tropospheric Water Vapor and Climate Sensitivity*. Journal of the Atmospheric Sciences, 56, 1649-1658.

Latest 20-year QC1 global monthly air temperature changes, updated to August 2024



Last 20 years' global monthly average air temperature according to Quality Class 1 (UAH and RSS; see p.6 and 9) global monthly temperature estimates. The thin blue line represents the monthly values. The thick black line is the linear fit, with 95% confidence intervals indicated by the two thin black lines. The thick green line represents a 5-degree polynomial fit, with 95% confidence intervals indicated by the two thin green lines. A few key statistics are given in the lower part of the diagram (please note that the linear trend is the monthly trend).

In the enduring scientific climate debate, the following question is often put forward: Is the surface air temperature still increasing or has it basically remained without significant changes during the last 15-16 years?

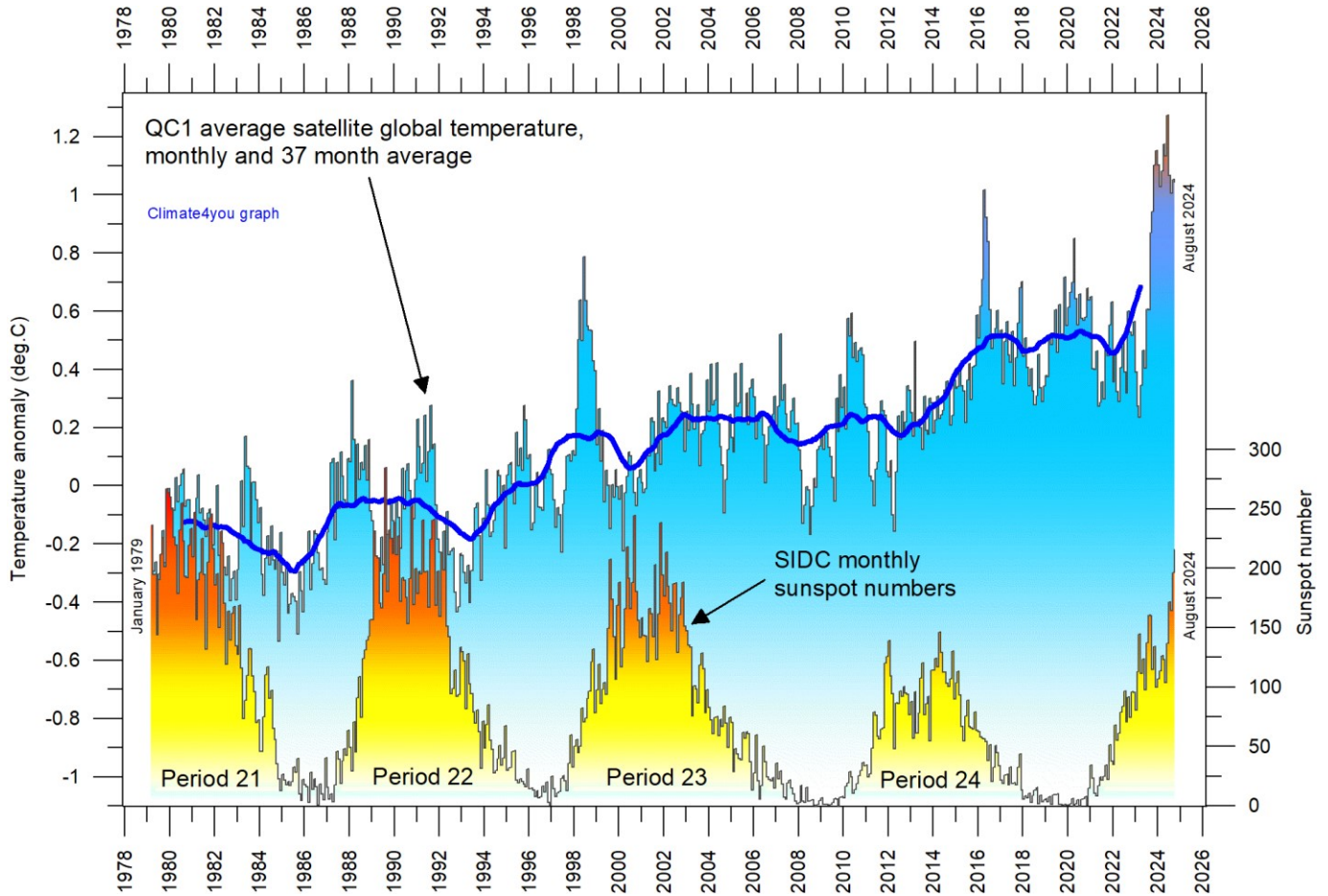
The diagram above may be useful in this context and demonstrates the differences between two often used statistical approaches to determine recent temperature trends. Please also note that such fits only attempt to describe the past, and usually have small, if any, predictive power.

In addition, before using any linear trend (or other) analysis of time series a proper statistical model should be chosen, based on statistical justification.

For global temperature time series, there is no *a priori* physical reason why the long-term trend should be linear in time. In fact, climatic time series often have trends for which a straight line is not a good approximation, as is clearly demonstrated by several of the diagrams shown in the present report.

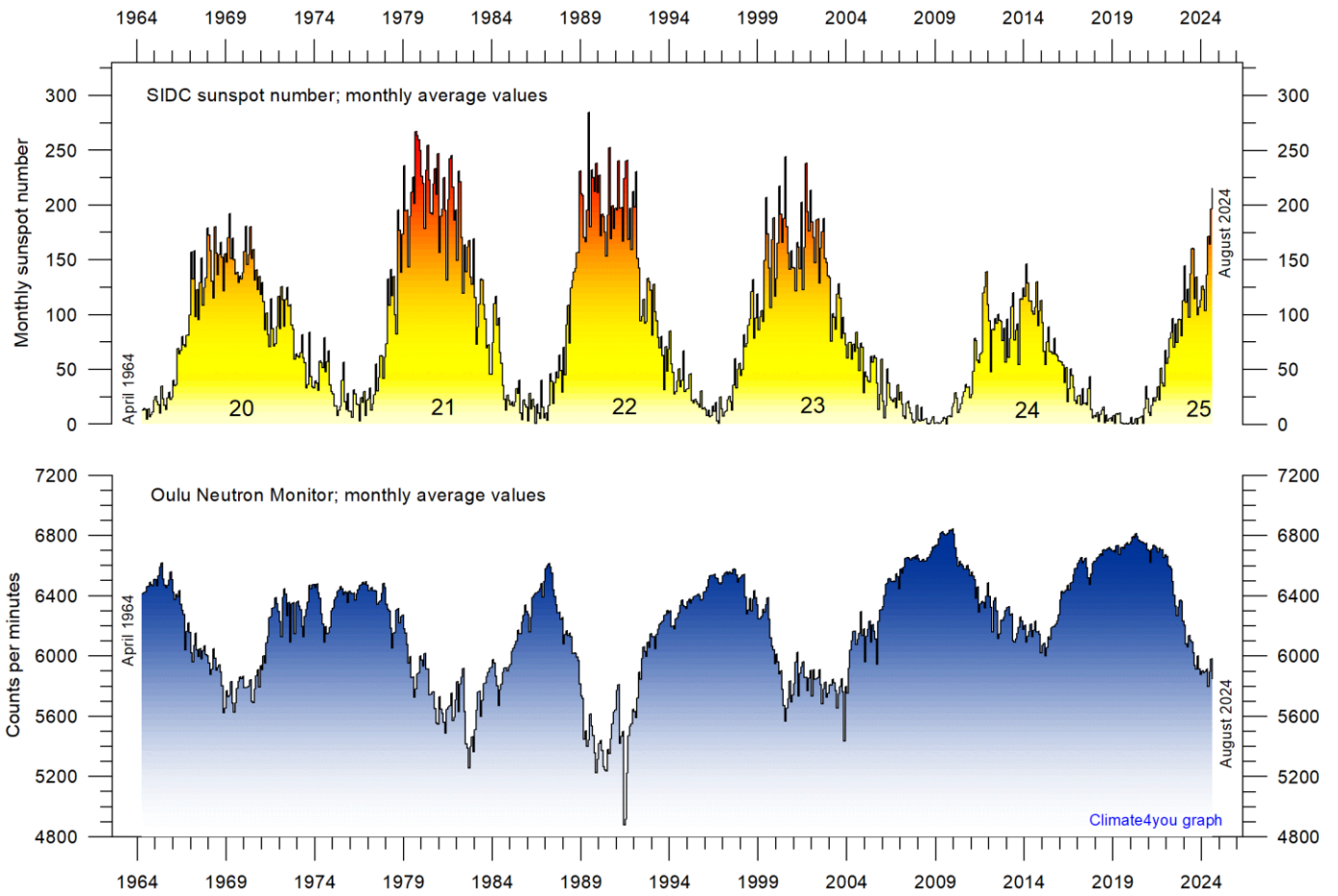
For an commendable description of problems often encountered by analyses of temperature time series analyses, please see [Keenan, D.J. 2014: Statistical Analyses of Surface Temperatures in the IPCC Fifth Assessment Report.](#)

Sunspot activity (SIDC) and QC1 average satellite global air temperature, updated to August 2024



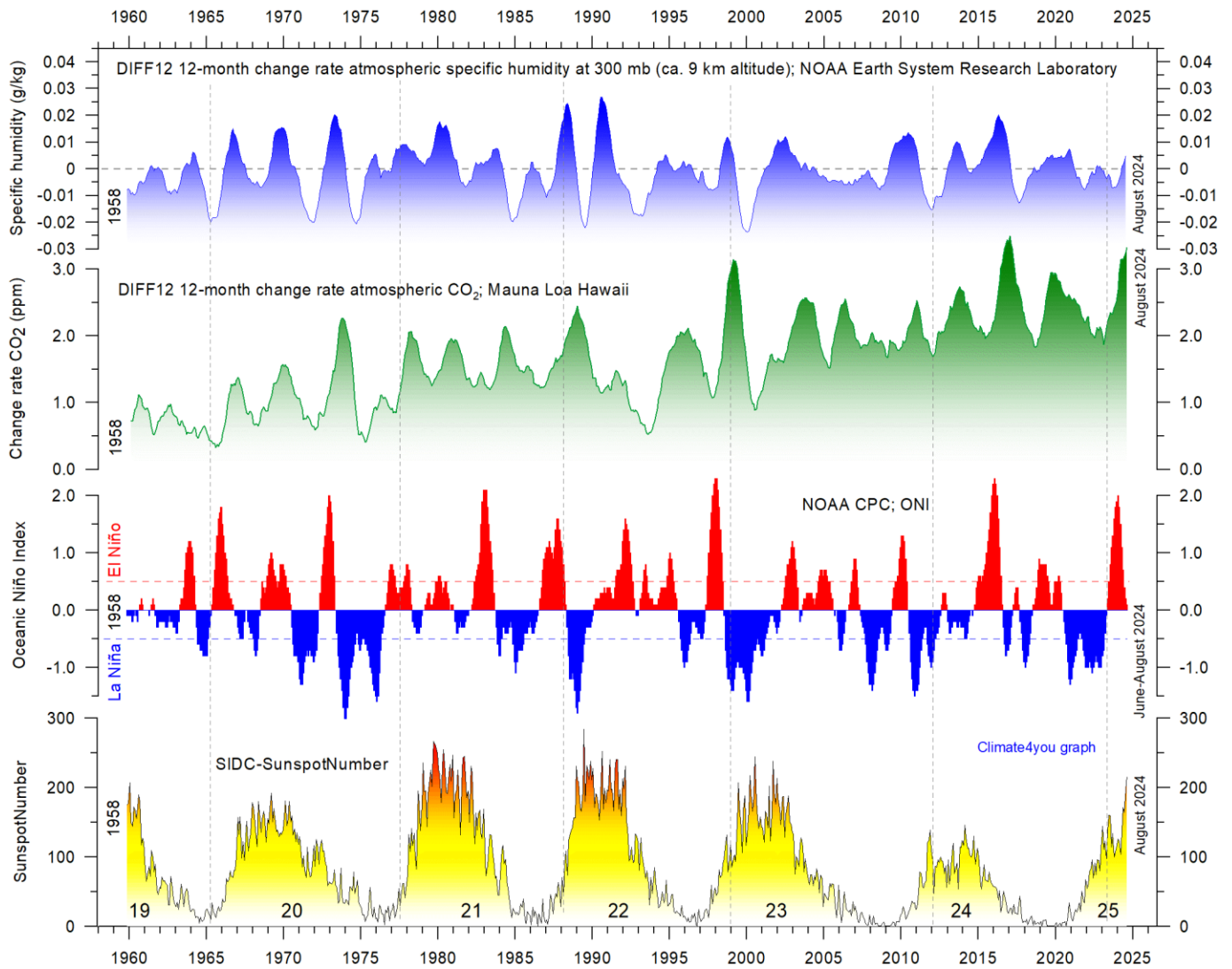
Variation of global monthly air temperature according to Quality Class 1 (UAH and RSS; see p.4) and observed sunspot number as provided by the Solar Influences Data Analysis Center (SIDC), since 1979. The thin lines represent the monthly values, while the thick line is the simple running 37-month average, nearly corresponding to a running 3-year average. The asymmetrical temperature 'bump' around 1998 is influenced by the oceanographic El Niño phenomenon in 1998, as is the case also for 2015-16. Temperatures in year 2019-20 was influenced by a moderate El Niño. In summer 2023 a new El Niño episode has begun (see diagram on p.25).

Monthly sunspot activity (SIDC) and average neutron counts (Oulu, Finland), updated to August 2024



Observed monthly sunspot number (Solar Influences Data Analysis Center (SIDC) since April 1964, and (lower panel) monthly average counts of the Oulu (Finland) neutron monitor, adjusted for barometric pressure and efficiency.

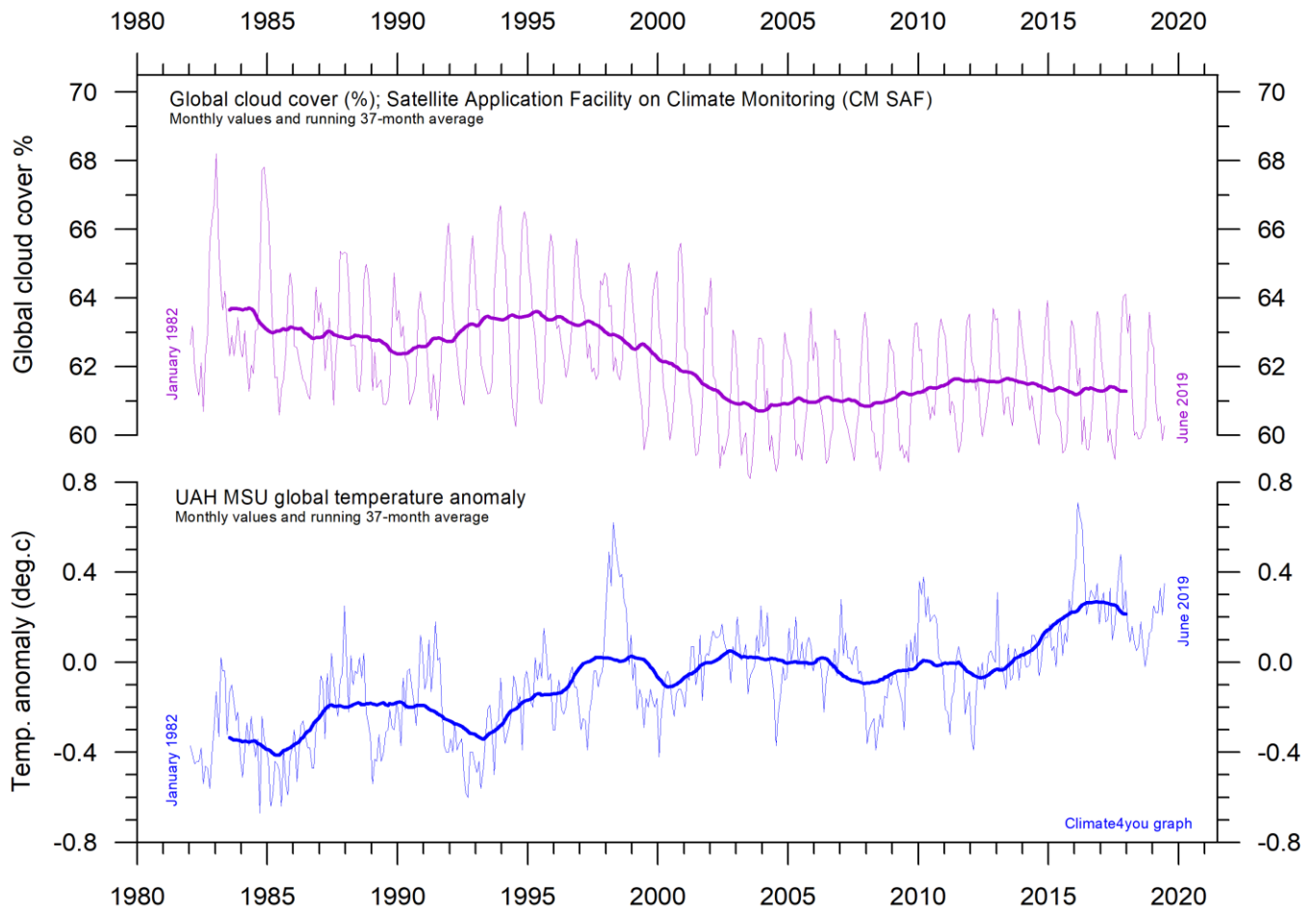
Monthly sunspot activity (SIDC), Oceanic Niño Index (ONI), and change rates of atmospheric CO₂ and specific humidity, updated to August 2024



Visual association since 1958 between (from bottom to top) Sunspot Number, Oceanic Niño Index (ONI) and annual change rate of atmospheric CO₂ and specific humidity at 300 mb (ca. 9 km altitude). Upper two panels: Annual (12 month) change rate of atmospheric CO₂ and specific humidity at 300 mb since 1959, calculated as the average amount of atmospheric CO₂/humidity during the last 12 months, minus the average for the preceding 12 months (see also diagrams on page 43+44). Niño index panel: Warm (>+0.5°C) and cold (<0.5°C) episodes for the Oceanic Niño Index (ONI), defined as 3 month running mean of ERSSTv4 SST anomalies in the Niño 3.4 region (5°N-5°S, 120°-170°W)]. For historical purposes cold and warm episodes are defined when the threshold is met for a minimum of 5 consecutive over-lapping seasons. Anomalies are centred on 30-yr base periods updated every 5 years. Thin vertical stippled lines indicate the visually estimated timing of sunspot minima. The typically sequence following a sunspot minimum appears to be a warm El Niño episode followed by a cold La Niña episode. Effects on change rates of atmospheric CO₂ and atmospheric specific humidity are visually apparent, with ONI variations being followed by changes in first humidity, and then (last) by CO₂.

The above diagram is inspired by the Leamon et al. 2021 publication: Robert J. Leamon, Scott W. McIntosh, Daniel R. Marsh. Termination of Solar Cycles and Correlated Tropospheric Variability. Earth and Space Science, 2021; 8 (4) DOI: [10.1029/2020EA001223](https://doi.org/10.1029/2020EA001223)

Monthly lower troposphere temperature (UAH) and global cloud cover, updated to April 2021

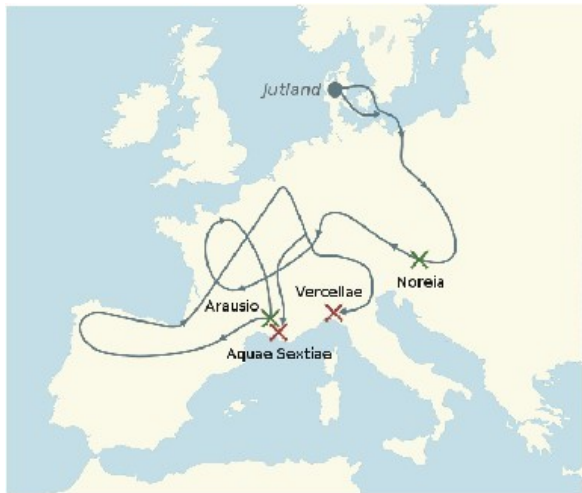


Lower tropospheric air temperature and global cloud cover. Upper panel: Global cloud cover according to Satellite Application Facility on Climate Monitoring. Lower panel: Global monthly average lower troposphere temperature (thin line) since 1979 according to [University of Alabama](https://climate4you.com/) at Huntsville, USA. The thick lines represent the simple running 37-month average. Reference period for UAH is 1991-2020.

Cloud cover data citation: Karlsson, Karl-Göran; Anttila, Kati; Trentmann, Jörg; Stengel, Martin; Solodovnik, Irina; Meirink, Jan Fokke; Devasthale, Abhay; Kothe, Steffen; Jääskeläinen, Emmihenna; Sedlar, Joseph; Benas, Nikos; van Zadelhoff, Gerd-Jan; Stein, Diana; Finkensieper, Stephan; Håkansson, Nina; Hollmann, Rainer; Kaiser, Johannes; Werscheck, Martin (2020): CLARA-A2.1: CM SAF cLOUD, Albedo and surface RADIATION dataset from AVHRR data - Edition 2.1, Satellite Application Facility on Climate Monitoring, DOI:10.5676/EUM_SAF_CM/CLARA_AVHRR/V002_01, https://doi.org/10.5676/EUM_SAF_CM/CLARA_AVHRR/V002_01.

Climate and history; one example among many

120-114 BC: The Cimbrian flood and the Cimbrian war 113-101 BC



The migrations of the Cimbri and the Teutons between 113 and 101 BC (left diagram), with places of major battles with Roman forces indicated. Drawing showing Cimbrian people during their European journey (right).

61

The Cimbrian flood (or Cymbrian flood) was a large-scale incursion of the North Sea in the region of the [Jutland](#) peninsula (Denmark) in the period 120 to 114 BC, resulting in a permanent change of coastline with much land lost. The flood was caused by one or several very strong storm(s). A high number of people living in the affected area of Jutland drowned, and the flooding apparently set off a migration of the Cimbri tribes previously settled there (Lamb 1991). Most likely the Cimbrian flood was the result of the gradual flooding of the present North Sea since the end of the last (Weichselian) glaciation, in combination with a stormy period, presumably influenced by a period of global cooling (see below).

The Cimbri were a tribe from Northern Europe, who, together with the [Proto-Germanic Teutones](#) and the [Ambrones](#) threatened the [Roman Republic](#) in the late 2nd century BC. Most ancient sources categorize the Cimbri as a [Germanic](#) tribe, but some authors include the Cimbri among the Celts

(<http://en.wikipedia.org/wiki/Celts>). Old sources located their original home in Jutland, which was referred to as the Cimbrian peninsula throughout early historical times. For example, on the map of [Ptolemy](#), the "Kimbroi" are placed in the northernmost part of the Jutland peninsula, in the modern Danish region Himmerland, shortly south of the sound Limfjorden. The modern [Vendsyssel-Thy](#) region of Denmark north of Limfjorden was at that time still mainly a group of islands. *Himmerland* (Old Danish *Himbersysel*) is generally thought to refer to the name Cimbri. However, the precise origin of the name *Cimbri* is unknown.

Some time before 100 BC many of the Cimbri, as well as the Teutons and Ambrones migrated south-east. After several unsuccessful battles with the Boii and other [Celtic tribes](#), they appeared ca 113 BC on the [Danube](#), in [Noricum](#), where they invaded the lands of one of Rome's allies, the Taurisci. On the request of the Roman consul Gnaeus Papirius Carbo, sent to defend the Taurisci, they retreated, but only to find

themselves deceived and attacked by Roman forces at the [Battle of Noreia](#). Here they nevertheless defeated the Roman army seriously. Only a storm, which separated the armies, saved the Roman forces from complete annihilation.

However, Rome was however finally victorious in the Cimbrian war, and the Cimbri-Teutonic forces - who had inflicted on the Roman armies the heaviest losses that they had suffered since the [Second Punic War](#) with victories at the battles of Arsusio and

Noreia – were almost completely annihilated, during the battles at Aquae Sextiae and Vercellae.

The timing of the war had a great effect on the internal politics of Rome, and the organization of its military. The war contributed greatly to the political career of [Gaius Marius](#), whose [consulships](#) and political conflicts challenged many of the Roman republic's political institutions and customs of the time. The Cimbrian threat, along with the [Jugurthine War](#), inspired the landmark [Marian reforms](#) of the [Roman legions](#).



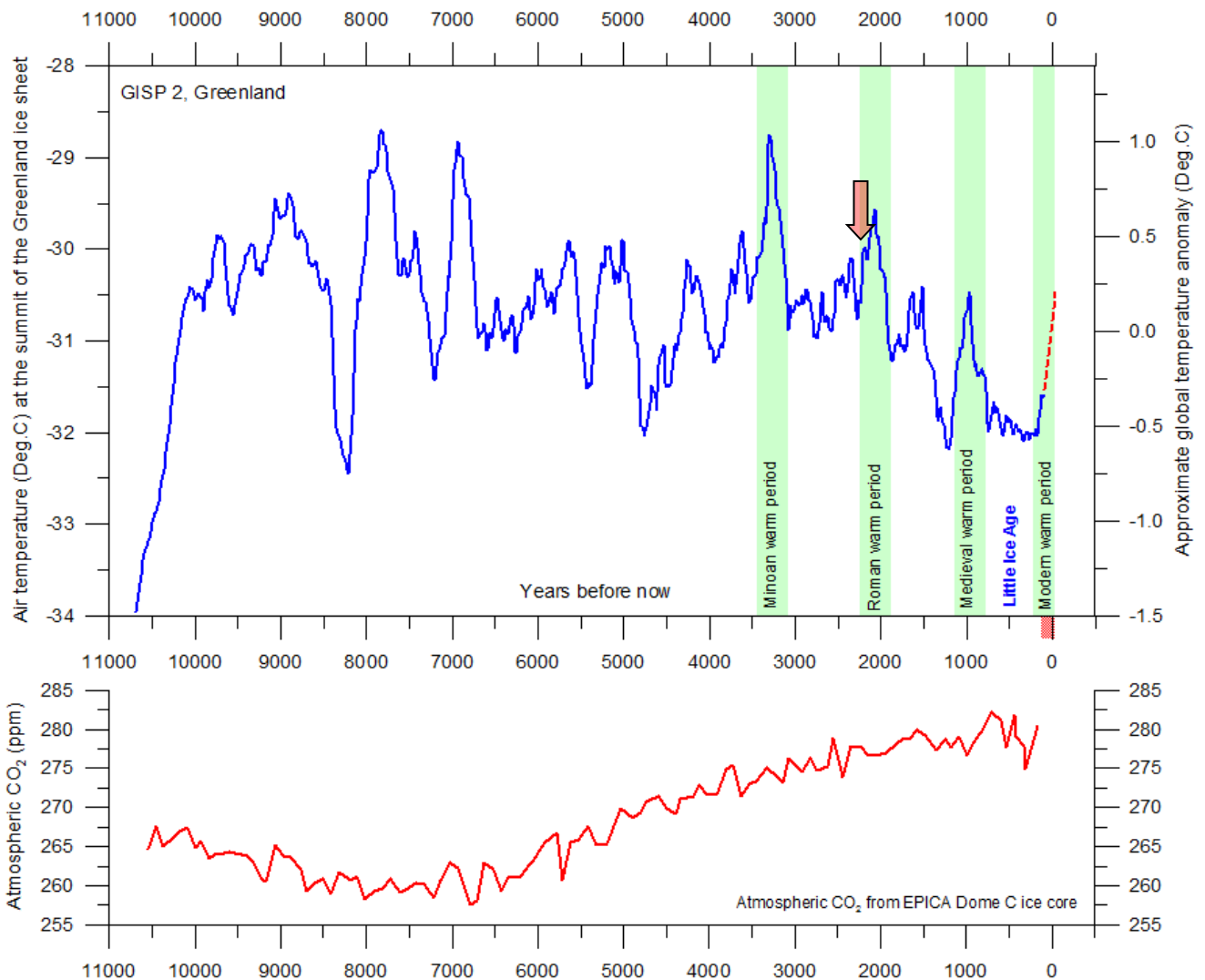
Gundestrup cauldron (left). Plate E from the Gundestrup Cauldron (right), showing Roman warriors.

The [Gundestrup Cauldron](#) is the largest known example of European Iron Age silverwork. It is 69 cm in diameter and 42 cm in height and weighs almost 9 kg. It has been dated to the period between 130 BC and 1 BC. The cauldron is made up from 13 separate plates - 5 long rectangular plates that form the interior; 7 short rectangular plates that form the exterior; and one round base plate, together with the shallow, curved, undecorated base. The cauldron was found in Himmerland on May 28, 1891, by peat cutters working in a small peat bog called Rævemose, near Gundestrup.

This unique piece of artwork suggests that there was contact between Jutland and southeastern Europe, but it is uncertain if this contact can be directly

associated with the Cimbrian migration. Neither has archaeologists found any clear indications of a mass migration from Jutland around this time, and presumably it was only the tribes living in the areas directly affected by the flood and subsequent sand drifting which decided to move south, out of Jutland.

Part of the explanation for the Cimbrian Flood might perhaps be sought in the diagram below, showing the Cimbrian flood to occur in the latter part of a relatively cold period shortly before the Roman Warm Period.



The upper panel shows the air temperature at the summit of the Greenland Ice Sheet, reconstructed by [Alley \(2000\)](#) from [GISP2 ice core data](#). The approximate timing of the Cimbrian Flood (arrow) is in the latter part of the cold period before the Roman Warm Period. The time scale shows years before modern time, which is shown at the right hand side of the diagram. The rapid temperature rise to the left indicate the final part of the even more pronounced temperature increase following the last ice age. The temperature scale at the right hand side of the upper panel suggests a very approximate comparison with the global average temperature (see comment below). The GISP2 record ends around 1855, and the red dotted line indicate the approximate temperature increase since then. The lower panel shows the past atmospheric CO₂ content, as found from the [EPICA Dome C Ice Core](#) in the Antarctic ([Monnin et al. 2004](#)). The Dome C atmospheric CO₂ record ends in the year 1777.

Whenever the planet cools, the cooling is especially pronounced near the poles and smaller near the Equator. The planetary cooling thereby produces an enhanced thermal contrast between equatorial regions and the poles. In the northern hemisphere,

this thermal contrast tends to develop especially in latitudes between about 50 and 65°N, in the so-called zone of westerlies. Global cooling and the strengthened north-south thermal gradient is typically the basis for development of stronger

cyclonic storms over oceans in the zone of westerlies, leading to increasing flood frequency

and damage for adjoining coasts and land areas, especially around the North Sea.

References:

Lamb, H. 1991. *Historical Storms of the North Sea, British Isles and Northwest Europe*. Cambridge University press, Cambridge, 204 pp.

All diagrams in this report, along with any supplementary information, including links to data sources and previous issues of this newsletter, are freely available for download on www.climate4you.com

Yours sincerely,

Ole Humlum (Ole.Humlum@gmail.com)

Arctic Historical Evaluation and Research Organisation, Longyearbyen, Svalbard

20 September 2024.

Planned publication of next newsletter: around 26 October 2024.